

Acquisitions and Bibliographic Services Branch

395 Wellington Street Ottawa, Ontario K1A 0N4 Bibliothèque nationale du Canada

Direction des acquisitions et des services bibliographiques

395, rue Wellington Ottawa (Ontano) K1A 0N4

Your file Votre reference

Our life. Notice reference

# NOTICE

The quality of this microform is heavily dependent upon the quality of the original thesis submitted for microfilming. Every effort has been made to ensure the highest quality of reproduction possible.

If pages are missing, contact the university which granted the degree.

Some pages may have indistinct print especially if the original pages were typed with a poor typewriter ribbon or if the university sent us an inferior photocopy.

Reproduction in full or in part of this microform is governed by the Canadian Copyright Act, R.S.C. 1970, c. C-30, and subsequent amendments.

# **AVIS**

La qualité de cette microforme dépend grandement de la qualité de la thèse soumise au microfilmage. Nous avons tout fait pour assurer une qualité supérieure de reproduction.

S'il manque des pages, veuillez communiquer avec l'université qui a conféré le grade.

La qualité d'impression de certaines pages peut laisser à désirer, surtout si les pages originales ont été dactylographiées à l'aide d'un ruban usé ou si l'université nous a fait parvenir une photocopie de qualité inférieure.

La reproduction, même partielle, de cette microforme est soumise à la Loi canadienne sur le droit d'auteur, SRC 1970, c. C-30, et ses amendements subséquents.

# **Canadä**

# ENERGY UTILISATION IN COMMINUTION AND ITS APPLICATION TO ROCK BLASTING

ру

Umesh Prasad, B. Tech.

Department of Mining and Metallurgical Engineering McGill University

Montreal

August 1994

A Thesis submitted to the Faculty of Graduate studies and Research in partial fulfilment of the requirements of the degree of Master of Engineering

(c) Umesh Prasad



Acquisitions and Bibliographic Services Branch

395 Wellington Street Ottawa, Ontario K1A 0N4 Bibliothèque nationale du Canada

Direction des acquisitions et des services bibliographiques

395, rue Wellington Ottawa (Ontario) K1A 0N4

Your Ne Votre référence

Our file. Notre référence

THE AUTHOR HAS GRANTED AN IRREVOCABLE NON-EXCLUSIVE LICENCE ALLOWING THE NATIONAL LIBRARY OF CANADA TO REPRODUCE, LOAN, DISTRIBUTE OR SELL COPIES OF HIS/HER THESIS BY ANY MEANS AND IN ANY FORM OR FORMAT, MAKING THIS THESIS AVAILABLE TO INTERESTED PERSONS.

L'AUTEUR A ACCORDE UNE LICENCE IRREVOCABLE ET NON EXCLUSIVE PERMETTANT A LA BIBLIOTHEQUE NATIONALE DU CANADA DE REPRODUIRE, PRETER, DISTRIBUER OU VENDRE DES COPIES DE SA THESE DE QUELQUE MANIERE ET SOUS QUELQUE FORME QUE CE SOIT POUR METTRE DES EXEMPLAIRES DE CETTE THESE A LA DISPOSITION DES PERSONNE INTERESSEES.

THE AUTHOR RETAINS OWNERSHIP OF THE COPYRIGHT IN HIS/HER THESIS. NEITHER THE THESIS NOR SUBSTANTIAL EXTRACTS FROM IT MAY BE PRINTED OR OTHERWISE REPRODUCED WITHOUT HIS/HER PERMISSION.

L'AUTEUR CONSERVE LA PROPRIETE DU DROIT D'AUTEUR QUI PROTEGE SA THESE. NI LA THESE NI DES EXTRAITS SUBSTANTIELS DE CELLE-CI NE DOIVENT ETRE IMPRIMES OU AUTREMENT REPRODUITS SANS SON AUTORISATION.

ISBN 0-315-99977-2



# ABSTRACT

Since blasting is a comminution process, the feasibility of establishing a correlation between the Bond rod mill work index (kWh/t) and some easily measurable physico-mechanical properties relevant to blasting was investigated. Further, the concept of operating blast work index and its potential applications were explored. Four different rock types and a well documented case study of two blasts were selected for this study.

The work index is found to be uncorrelated with the density and unconfined compressive strength, slightly related with tensile strength, and well correlated with dynamic rock properties, especially the P-wave velocity and the bulk modulus. The standard deviation in measured compressive and tensile strength values is found to be very high, compared to their seismic and dynamic elastic properties.

The case study encompassed two blasts with identical blast-patterns and rock type consuming almost the same amount of explosive (kg/t) but with very different specific blast energies (MJ/t). The agreement between operating work index of the two blasts (13.4 kWh/t vs. 13.1 kWh/t) and laboratory work index (17.0 kWh/t) was modest (within 30 %). The operating work index corresponding to either blasts has been used to predict the product size  $(P_{E})$  of the other. The choice of feed size  $(F_{E})$  was discussed; whereas the previous researchers had used the theoretical value of infinity, the use of much smaller value, the average of effective burden and spacing, was proposed. This concept is used in a proposed method to estimate blasting energy requirements as a function of blast geometry, rock type and desired product size. Future test work that would provide a data base and validation for this concept is described.

<u>Key words</u>: blasting, work index, physico-mechanical properties, feed size, product size, explosive energy.

# RÉSUMÉ

Le sautage étant une forme de comminution, nous avons essayé d'établir un lien entre l'indice de broyabilité de Bond (celui du broyeur à barres) et certaines des propriétés physico-mécaniques faciles à mesurer et utilisées dans les études de dynamitage. Nous avons également étudié de façon préliminaire le concept d'indice de broyabilité opérationnel de dynamitage. Nos efforts se sont penchés sur quatre types rocheux (calcaire, gneiss, granite et marbre) et une étude de cas de deux dynamitages bien documentés.

Nous n'avons pas trouvé de corrélation entre l'indice de broyabilité et la densité ou la résistance à la compression non-confinée. L'indice de broyabilité était légèrement correlé avec la résistance en tension, et bien correlé avec certaines propriétés dynamiques, soit la vélocité des ondes P et le module (bulk modulus). L'écart-type des résistances en compression et tension était beaucoup plus élevé que celui des propriétés élastiques de nature séismique et dynamique.

Les deux sautage de l'étude de cas avaient été faits dans le même type de roche, avec des patrons de forage identiques, et presque la même charge d'explosifs (en kg/t) mais pas la même énergie spécifique de dynamitage (exprimée en MJ/t). L'indice opérationnel de broyabilité des deux dynamitages était presqu'identique (13.4 kWh/t vs. 13.1 kWh/t), inférieur de 30% à l'indice de broyabilité mesuré en laboratoire (17.0 kWh/t). Nous avons discuté de la valeur du  $F_{80}$  à utiliser, soit une valeur infinie (ce que les autres chercheurs ont toujours fait), soit une valeur qui reflèterait le patron de forage. Nous avons proposé la moyenne mathématique du fardeau réel et de la distance entre les trous de forage. Nous proposons, à l'aide de ce concept, une méthode de prédiction de l'énergie requise pour le dynamitage basée sur le patron de forage, le type de roche et le produit désiré. Nous décrivons le programme expérimental qui serait nécessaire à l'élaboration d'une base de données et la validation de ladite méthode.

# ACKNOWLEDGEMENTS

It is a pleasure to acknowledge my sincere gratitude to my research supervisor, Dr. B. Mohanty and co-supervisor Dr. A. R. Laplante of the Department of Mining and Metallurgical Engineering, for their invaluable advice, guidance and encouragement during the course of this research.

The help and encouragement provided by the staff and colleagues of the Department of Mining and Metallurgical Engineering in McGill University are also gratefully acknowledged. Special thanks go to Dr. M. Momayez for initiating the writer in the operation of the RDP-2000 servo-controlled hydraulic press.

The writer would also like to acknowledge separately, the technicians G. Marc and M. Leroux for their help in setting up the laboratory experiments.

Financial support received through NSERC grant during the course of this study is also gratefully acknowledged.

Finally, the author expresses his deepest appreciation to his parents and family members, without whose love, constant encouragement and support, this thesis would never have been completed.

# TABLE OF CONTENTS

Page	ı
ABSTRACTS	
RESUME	
ACKNOWLEDGEMENTS	
TABLE OF CONTENTS	
LIST OF FIGURES	L
LIST OF TABLES	L
LIST OF ACRONYMS	C
INTRODUCTION	l
1.1 BACKGROUND	1
1.2 OBJECTIVES	1
1.3 THESIS STRUCTURE	5
PRINCIPLES OF BLASTING	5
2.1 INTRODUCTION	6
2.2 REVIEW OF BLASTING PRACTICES	6
2.3 MECHANICS OF BLASTING PROCESS	1
2.4 PHYSICAL PROPERTIES OF ROCK	2
	_
PRINCIPLES OF COMMINUTION	و
3.1 INTRODUCTION	9
3.2 COMMINUTION PROCESSES	
3.3 ENERGY-SIZE RELATIONSHIP	
3.4 WORK INDEX	
3.5 POPULATION BALANCE MODELS	5
MATERIALS AND METRODS	4
4.1 MATERIALS USED	4
4.2 ESTIMATION OF THE WORK INDEX	4

	4.3	PH	YSI	.CO-	ME	:CH	AN:	LCA	AT.	TE	:57	rs	•	•	•	•	•	•	٠	٠	•	•	•	•	•	•	•	•	•	48
RESULT	cs .	•		•	•	-		• •					•	•	•	•	•	•	•	•	•	•	•	•	•	•		•	•	55
	5.1	WO	RK	INI	DEX	:							•		•	٠		•		•	•					•	-			55
	5.2	PH	YSI	co-	-ME	CH	AN:	IC	ΑŢ	PF	ROI	PEF	TI	ES	•	•	-	•	•	-	•	•	•	•	•	•	-	•	٠	65
DISCUS	SIO	SI .		•	•	•	•								•	•	•	-	-	•	-	-	-	-	•	-		•	-	77
	6.1	WO	RK	INI	DEX	:	-						•		•		•	•	•		•	•	•	•	•	•		•	٠	77
	6.2	PH	YSI	co-	ME	CH	AN:	[C	Т	PF	ROI	PEF	TI	ES				٠			•	-		-	•		•			79
	6.3	FR	AGM	ENT	C A	ND	Eì	NEF	RG?	? Ţ	T	ILI	:SA	TI	ON	I	N I	BL	AS.	rin	1G	•	•	•	•	•	•	-	•	86
CONCLU	SIO	as.		•	٠.	•							•	•	•	•	•	•	•	•	•	•	•	•	•	•	•	•	3	L02
FUTURE	: WOI	RK		•	•	•		• •					•	•	•	•	•	•	•	•	•	•	•	•	•	•	•	•	3	L04
REFERE	INCE:	5		•	•	•								•	•	•	•	•	•	•	•	-	•	•	-	•	•	•	3	L06
APPENI	X	_			_	_								_	_	_					_	_							7	113

# LIST OF FIGURES

Page	æ
2.1: A typical open-pit blast pattern	9
2.2: Firing pattern in tunnelling	0
2.3: Sequence of blasting events	3
2.4: Different loading geometries for modulus of elasticity 1	6
3.1: General view of rod and ball mill	1
3.2: Specific energy in a size reduction process	4
3.3: Composite energy-size relationship	9
3.4: Size distribution and 80% passing size	0
3.5: Size distribution and energy-size relationship	1
3.6: Mass remaining in the top size class	8
3.7: Selection function and particle size	2
4.1: Approximate lithology of rock samples	5
4.2: Steps involved in work index determination	7
4.3: General layout of compressive strength test 4	9
4.4: Schematic diagram showing Brazilian test	il
4.5: A typical wave train in an ultrasonic test	2
5.1: Selection function during work index determination	8
5.2: Selection function vs. size classes at steady state	9
5.3: Normalised sel. func. vs. size classes at steady state 6	0
5.4: Work index and non-normalised selection function 6	;3
5.5: Work index and normalised selection function	;4
5.6: Work index and compressive strength	57
5.7: Work index and tensile strength	58
5.8: Work index and bulk density	59
5.9: Work index and 'P' wave velocity	70
5.10: Work index and 'S' wave velocity	71
5.11: Work index and dynamic Young's modulus	72

5.12	: Work index and bulk modulus	73
5.13	: Work index and Compressibility	74
5.14	: Work index and shear modulus	75
5.15	: Work index and Poisson's ratio	76
5.1:	Typical blast pattern of the case study	89
6.2:	Profile of the muckpile after the blasts	89
6.3:	Fragmentation characteristics from the test blasts	90
5.4:	Explosive energy simulation with respect to feed and	
	product size	98

# LIST OF TABLES

Table	e
5.1: Summary of the work indices of four different rock type $\dots$ 5.5.	5
5.2: Summary of the work indices of limestone rock type 5	6
5.3: Regression output of size-sel. func. correlationship 6	1
5.4: Regression output of ln(WI)-ln(SF) correlationship 6	2
5.5: Regression output of WI-ln(SF) correlationship 6	5
5.6: Summary of the properties of rock 6	6
6.1: Regression output of WI-compressive strength	0
6.2: Regression output of WI-tensile strength	1
6.3: Regression output of WI-density correlationship 8	2
6.4: Regression output of WI-P wave velocity correlationship 8	2
6.5: Regression output of WI-S wave velocity correlationship 8	3
6.6: Regression output of WI-dynamic Young's modulus 8	3
6.7: Regression output of WI-dynamic bulk modulus 8	4
6.8: Regression output of WI-dynamic shear modulus 8	5
6.9: Regression output of WI-dynamic Poisson's ratio 8	6
6.10: Parameters showing explosive properties 8	7
6.11: Parameters showing blast results of the case study 8	8
6.12: Calculated parameters based on the present work 9	)1
6.13: Prediction of fragment size using operating work index 9	)5
6.14: Explosive energy for different product size for limestone 9	)6
6.15: Explosive energy for different feed size	7
6.16: Explosive energy calculation for different rock type 9	9
6.17: Error Propagation for Fm	)1

# APPENDIX

A1:	Work inde	x of Sta	nstead	d gra	anite					•	•	-	•	•	•	•	•	A1
A2:	Work inde	x of gne	iss	• •														A2
A3:	Work inde	x of mar	ble	<b></b> .									-	•	-			АЗ
A4:	Selection	functio	n of (	each	cycle	for	gra	nite	: .	•			-					<b>A</b> 4
A5:	Selection	functio	n of (	each	cycle	for	gne	iss		-			•		•			A5
× c -	Coloraian	£				£		<b>L.</b> 7										

# LIST OF ACRONYMS

- PBM Population Balance Model.
- SAG Semi-Autogenous Grinding.
- ANFO Ammonium Nitrate Fuel Oil.
- ASTM American Standards for Testing of Materials.
- ISRM Internation Society of Rock mechanics.
- VOD Velocity of Detonation (m/s).
- AWS Absolute Weight Strength (Cal/g).
- ABS Absolute Bulk Strength (Cal/cc).
- RWS Relative Weight Strength (with respect to AWS of ANFO).
- RBS Relative Bulk Strength (with respect to ABS of ANFO).

#### 1.0 INTRODUCTION

#### 1.1 BACKGROUND

Breaking of rock has been one of the earliest occupations of mankind. For countless years this work was entirely manual, first with rock implements (a first form of autogenous comminution), then with metallic tools. The industrial revolution introduced mechanical energy which replaced human labour, first with very low capacity units such as stamp mills, then with basic comminution units which have survived for over one hundred years with little change, such as jaw crushers (invented in 1858 by Eli Whitney Blake [1]), rod and ball mills. The past twenty-five years have signalled a second, more modest revolution in mechanical comminution machines, with the arrival of entirely new devices such as tower and vibrating mill or pressure rolls [2], and the emerging dominance of the semi-autogenous mill to replace secondary and tertiary crushing and rod milling in nearly all new applications.

The use of chemical energy for comminution actually predates that of mechanical energy. The first use of drilling and blasting has been reported at the Oberbeiberstollen mine of Hungary in 1627 [3]. It is likely that the Chinese, who mastered explosives centuries before, used them for blasting as well. Lower power explosives have been replaced today by many other chemicals, such as dynamites, slurry, ANFO (ammonium nitrate/fuel oil), emulsions etc.. Primary comminution today is still largely achieved by blasting, except for softer ores such as halite, potash and coal, which are extracted mechanically. Continuous miners are also being used for harder materials for tunnelling, where applicable, because a more regular tunnel profile can be achieved whilst protecting the integrity of the remaining rock structure.

With the dominance of chemical energy sources for primary breakage and virtual monopoly of mechanical energy for secondary breakage, the two

engineering fields have diverged and use of the term 'comminution' was progressively restricted to mechanical breakage. Thus, AIME's two relatively recent monographs on comminution [4.5] exclude blasting, albeit only implicitly. The two now distinct fields have evolved separately, that of crushing and grinding focusing much more research effort, both fundamental and applied. In all fairness to blasting practitioners, crushing and grinding systems are easier to study, and of those, the easiest one, ball milling, has by far attracted more interest.

One of the first benefits of the studies of comminution was the derivation of a reliable methodology to estimate energy requirements in crushing, rod and ball milling [6]. The methodology is based on calibrated pendulum, rod and ball mills, named after the designer of the method, Fred Bond [7]. Energy requirements are correlated to the feed and product size, and the ability to achieve a certain grinding rate. Bond's methodology is not so relevant to semi-autogenous milling, which requires large scale testing (typically with a pilot mill, 1.5 m in diameter), but oddly enough, recent efforts to derive a simpler methodology for SAG mill scale-up and parameters for reliable simulation use data derived from a pendulum very similar to that Bond created to estimate energy requirements for crushers. Bond himself was confident that his approach could be applied to large scale comminution, and even tried to apply his equation to blasting [8]. In fact, the derivation of Bond's equation implicitly starts with blasting feed --i.e. a material with an 'infinite'  $F_m$  (the 80% passing size of the feed).

The above is a brief and somewhat selective history of comminution engineering. Bond's theory has evolved little since the early forties. Population balance models (PBM) have, over the past 25 years, become the focus of more fundamental research, especially in academic circles. Applications are manifold, but of interest to this work is the proposition that PBM can be used for mill scale-up and plant design. PBM will be briefly reviewed in this work, as they could be suitable for modelling of

blasting, to assist ultimately in assessing energy requirements.

Blasting, as a branch of engineering, has developed along a different path, limited to the large scale fragmentation of insitu rock mass. The progress in blasting practice had been until recently focussed towards the optimization of the process. During the last two decades the focus has shifted towards a more fundamental understanding of explosiverock interaction and quantitative prediction of blast results. developments have been slow however, due to the dynamic nature of blasting (the whole process lasting only a few milliseconds) and its complexity. The complexity is due to the interaction of various branches of science such as chemistry (of the explosive), physics (of energy transfer from explosive to rock), and rock mechanics (of deformation and fracture of The usual inhomogeneity, anisotropy and the macro- and rock). microstructure of the rock mass are major contributors to the complexity. Although the recent advances in experimental techniques and in computer equipment have made predictions of blast results a practical reality, much remains to be known about energy utilization in rock fragmentation. Some work has been reported dealing with energy-size relationship of blasting, albeit, more or less on an empirical basis (Kuznetsov [9]; Cunningham [10]; Just [11]; and Da Gamma [12]), but much fewer studies have dealt with the subject at the fundamental level.

The properties of explosives and rocks play an important role in the blasting process. Much of the explosive properties are reliably known and are reproducible. However, current knowledge of the properties of rock, due to its inhomogeneity and anisotropic nature, are insufficient to explain its behaviour during blasting. The relevant properties of rock during the blasting process can be grouped under physical and mechanical properties. The physical properties consist of density (resistance against mass movement); modulus of elasticity (stiffness against deformation); and seismic wave propagation in rock (energy transfer and its attenuation). The mechanical properties (behaviour against applied

load) consists of static compressive, tensile and shear strength. In the present work the static and dynamic physico-mechanical properties of the selected rock types, such as density, compressive and tensile strength, seismic wave propagation in rocks, and the dynamic modulus of elasticity have been determined, along with their work indices, with a view in establishing quantitative correlations.

The divergent routes chosen by comminution and blasting engineers may in fact lead to the same end i.e. estimating and minimizing energy spent in the process of size reduction. Seeking a correlation of easily measurable physico-mechanical properties of rocks and their Bond work indices, therefore, appears to be a logical objective. This thesis will attempt, albeit in a very modest and exploratory way, the reconciliation of these two approaches --i.e. comminution and blasting.

# 1.2 OBJECTIVES

The objectives of the investigation are the following:

- \* A review of pertinent information in blasting, blast related physico-mechanical rock properties and comminution (in the classical sense) will be completed. Potential links will be suggested.
- \* For four different rock types (limestone, gneiss, granite and marble), the rod mill work index and basic physico-mechanical properties will be measured. An attempt will be made to correlate the various fundamental properties to the work index.
- \* Results will be interpreted in light of available data in literature and testing methodology that incorporate both approaches.

#### 1.3 THESIS STRUCTURE

Chapter two presents comminution from a blasting point-of-view. The basics of blasting practices in both underground and open-pit, mechanics of rock blasting and the relevant rock properties are outlined.

In the third chapter, a review of some salient aspects of comminution is presented. Basic comminution units are first described, then, classical energy-size relationships are presented and discussed. This section focuses on Bond's theory and work index, whose measurement for crushers, rod and ball mills is described. Finally, population balance models are presented. Their link to the estimation of energy requirements in comminution is discussed.

Chapter four identifies the rock types used for this work. The methodology of the specific measurements performed is described.

Chapter five presents experimental results; these are discussed in depth in chapter six. Finally, chapter 7 concludes this essay; salient findings are reviewed and suggestions are made as to how this initial venture can be pursued and further quantified.

. . . . .

# 2.0 PRINCIPLES OF BLASTING

#### 2.1 INTRODUCTION

Blasting is one of the most economical methods of comminution. In this process, an explosive, a chemical compound, capable of producing sudden outburst of energy at high pressure and temperature, is emplaced in blast holes and detonated. The rock surrounding the charge is fragmented and displaced due to the sudden release of the energy of the explosive. The important factors contributing to the fragmentation process can be grouped under the headings of a) rock properties consisting physicomechanical, geological and seismic properties; b) explosive properties consisting of shock energy, gas energy, density, velocity of detonation, initiation system; c) rock-explosive interactive properties consisting explosive distribution, blast geometry, and energy transfer from explosive to rock.

# 2.2 REVIEW OF BLASTING PRACTICES

There is a wide variety of conditions and factors that determine the proper use of explosive in blasting. These factors include the mining methods, the equipment selected, geotechnical characteristics of the rock, properties of the explosives and their accessories, blast geometry and environmental constraints. The type of explosive selected should be such that it results in the desired fragmentation and rock movement for the minimum overall cost. Blasting practice should also aim to minimize flyrock, air and ground vibration, and backbreak.

2.2.1 ENERGY FACTOR: Competent rock requires explosives of high energy for optimum fragmentation. For a specific blast configuration and explosive type, this high energy translates into higher powder factor (kg of explosive per cubic meter of material blasted) or more explosive per

unit burden for the same type of the explosive. It should be noted that a kilogram of dynamite, ANFO, or emulsion yields different energy outputs. However, the explosive loads in a blast may be comprised of ANFO, dynamites, slurries and emulsions in different boreholes or in combination in the same borehole, all with different energies. This situation warrants the development of an "energy factor" approach rather than the traditional "powder factor" approach.

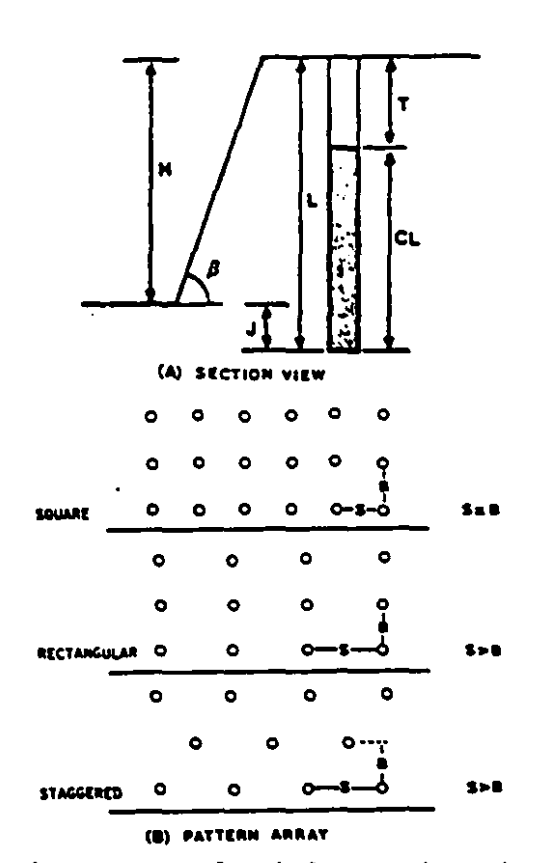
The energy, strength or power of an explosive in the explosive industry is used to rate the commercial explosives. The explosive energy is associated with total release of energy, rate of release of energy and the efficiency with which it is transmitted to the rock. All these factors pose difficulties in defining energy of an explosive with a single Moreover, most commercial explosives exhibit non-ideal parameter. detonation behaviour (the ideal reaction in commercial explosive is approached in extremely large diameters). By simply varying the charge diameter, the explosive may behave in a very different manner, despite having the same chemical composition. The effect of this non-ideal reaction is most readily evident in the change of velocity of detonation (VOD) as a function of charge diameter. In the case of ANFO approximately 20% decrease in VOD is reported with the decrease of explosive diameter from 150 mm to 75 mm. Factors affecting explosive strength and the explosive rating based on ideal and non-ideal detonation are reviewed thoroughly by Mohanty [13]. The explosive energy is currently calculated by the thermodynamics of the explosion. It is described by the following parameters.

- a. Absolute weight strength, AWS
- b. Absolute bulk strength, ABS
- c. Relative weight strength, RWS
- d. Relative bulk strength, RBS

The AWS or ABS are the absolute amount of available energy (Megajoules) in each kilogram or in each cubic meter of explosive, respectively. The ratio of the AWS and ABS of an explosive to the AWS and ABS of some standard explosive, such as ANFO, is called the relative weight strength and relative bulk strength, respectively.

Some of the important properties of rock with reference to its competency are its density, seismic velocity, modulus of deformation, and compressive, shear and tensile strengths. These properties are discussed toward the end of this chapter. Their influence during blasting is complex. These rock parameters collectively contribute to the blastability (a qualitative term to represent the competence of a rock against blasting, or lack of it) of the rock i.e. the ease of blasting. The blastability of a rock mass becomes complex in nature in the presence of textural and structural variations. The complex nature of blastability is further complicated under confinement and dynamic loading as is encountered in blasting.

2.2.2 OPEN PIT BLASTING: Blast diameters range from 50 mm to 450 mm, and powder factors vary on an average from 0.3 to 0.6 kg/m³ [13]. The bench height and the diameter of borehole are fixed for day-to-day production blasts. The first and foremost parameter to be selected for the blast design is the burden (the distance of first blasthole from the free face). It depends on various parameters such as bench height, pit width, explosive and the initiation system employed. A booster or a detonator is placed at the bottom and the rest of the explosive is loaded on top of it. The explosive column may be continuous or in the form of decks with inert material filling the space in-between. The explosive is usually topped with stemming, made from drill cuttings. The spacing, subgrade drilling, decking and stemming are selected on the basis of rock type and the explosive to be used. A typical open-pit blast hole and blast pattern are shown in Figure 2.1 [14].



- B: Burden
- S: Spacing
- H: Bench height
- L: Drilled length
- T: Stemming length
- J: Subgrade drilling
- CL: Charge length
- ß: Bench slope angle

Figure 2.1: Blasthole section view (A) showing terminology used in design and (B) pattern array for layout of holes [14]

Empirical relations have been proposed by Ash [15], Pugliese [16], Van Ormer [17], Hagan [18], Dick et al. [19] and many others for the design of blast geometries. Delay intervals between holes and rows are designed to provide a free face for succeeding blastholes. This sequential blast improves the fragmentation and throw of the blasted mass. Sequential blasting also helps to control height of the muckpile, overbreak and vibrations.

2.2.3 UNDERGROUND BLASTING: The details of underground blast design are discussed by Langefors and Kihlstrom [20], and Dick et al. [19] Excavation in underground works is accomplished in two phases. The first phase consists of the development phase such as shaft-sinking, tunnelling,

raising etc. The second phase deals with the actual production of ore. Due to the limited number of headings and free faces underground, blasting is more complicated. Different methodologies of development mining are associated with different drilling patterns. A typical firing pattern in tunnelling is shown in Figure 2.2 [21]. The blasthole diameter can

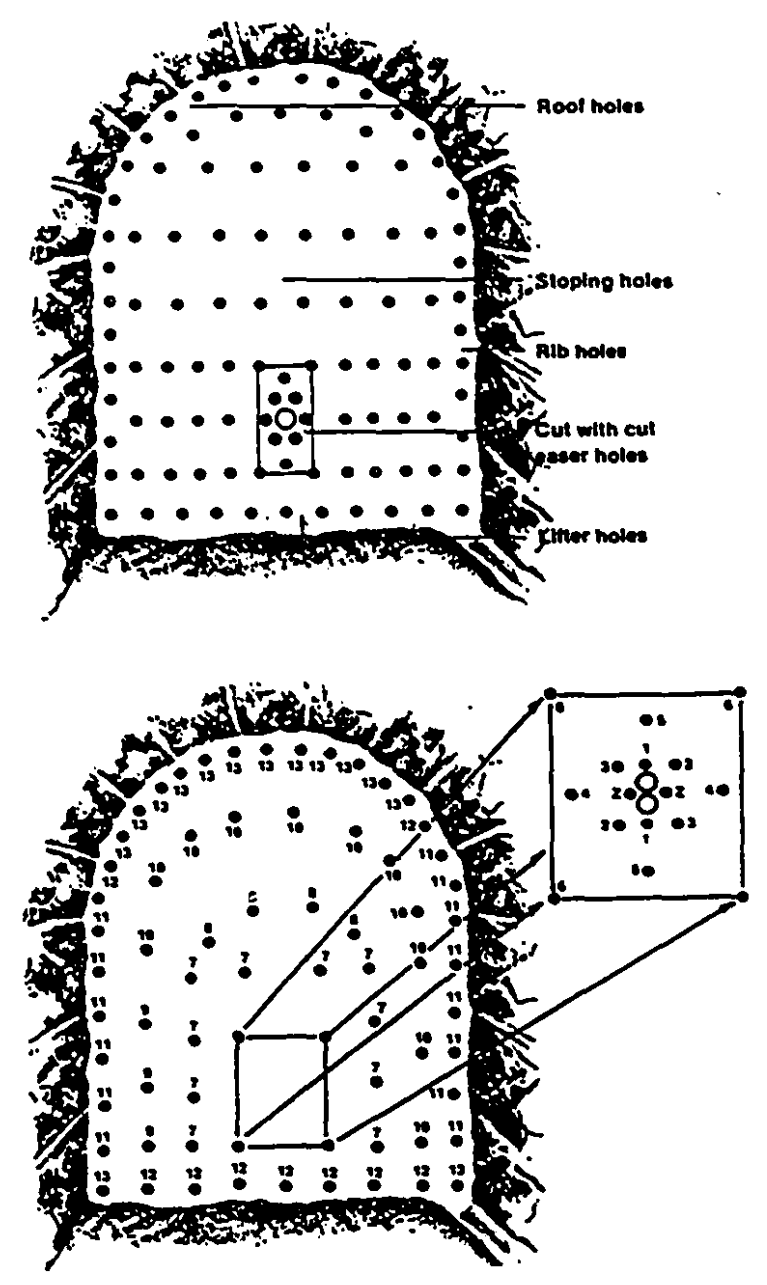


Figure 2.2: Firing pattern in tunnelling [21].

range from 32 mm to 75 mm, with 45 mm being the most common. Explosive loading and firing methods vary with methods of development and mining. Some of the holes are charged with explosive, whereas, other act as free space. The type of explosive varies from dynamite to ANFO. For production blasting, inert material in the form of cartridges is used for stemming if necessary (but never for development rounds). Deck charging is not necessary due to the small length of borehole. Electric or non-electric blasting caps with delays of 25 milliseconds to 10 seconds are used for firing. For underground coal mines only the explosives permitted by local regulatory board are used. Fume characteristics of the explosive are very important in selecting particular type of explosive. A wide range of explosives with powder factor ranging from 0.9 to 6 kg/m³ are used to meet the many different conditions in an underground mine.

#### 2.3 MECHANICS OF BLASTING PROCESS

Explosives, when initiated, produce a chemical reaction propagating at high velocity in the explosive column. The completion of the reaction of all the explosive results in gaseous products in the borehole at very high pressures (10 GPa) and high temperatures (3000° K) [20]. The original detonation reaction in the explosive generates shock waves in the surrounding rock. These waves propagates in the rock in a spherical, conical or cylindrical front depending upon the shape of the explosive. Radial and tangential stresses are generated in the rock which cause primary cracking. In the vicinity of the explosive, the rock is crushed with very high expenditure of explosion energy. The crushed zone extends to about 2-4 times the borehole radius. A zone of around 5-10 times the borehole radius is affected due to radial cracking. If the explosion is near a free face, the radial compressive stress waves are reflected from the free face as tensile stress waves, thus causing spalling. The energy transfer from shock wave to rock mass depends on the respective acoustic impedances of rock (product of stress wave velocity and density of the medium). The radial compressive stress, the reflected tensile stress and the tangential stress and shear stress are all causes of primary breakage. Following stress waves, highly pressurised gas expands into the pre-existing cracks or the cracks created in the primary breakage stage. This is called the secondary breakage stage during which heaving of the rock is initiated. The energy responsible for primary breakage can be attributed to shock energy. The effect of shock wave during blasting has been explained in detail by Kutter and Fairhurst [22], Rinehart [23] and Mohanty [24]. The effect of gas expansion energy is discussed by Porter and Fairhurst [25], and Langefors and Kihlstorm [20]. Tertiary breakage is also observed due to in-flight collision of the rocks as discussed by Hagan [26] and Chiapetta [27]. The sequence of blasting events is shown in Figure 2.3 [14].

# 2.4 PHYSICAL PROPERTIES OF ROCK

The behaviour of rock while blasting is dependent upon several factors such as location, mineralogy, and macro- and micro-structures. Minerals are the building blocks of rocks. The mineral grains are interlocked by cementing material consisting of other minerals, cohesive granular aggregates, and moisture. The structure of grain network, unlike that of crystal lattice, is rarely homogenous and periodic. The mineral matter is pervaded by microfractures such as cracks, pores etc. In larger units, the rock is cut by macrostructures such as parting, joints, bedding planes, faults etc. The spacing and orientation of these micro and macro structures are rarely uniform [28]. The properties of rock analyzed in this investigation are density, strength, elastic modulus, and seismic velocities.

# 2.4.1 DENSITY

It is a characteristic property of mineralogy and packing density of the grains only and is not affected as much by the presence of

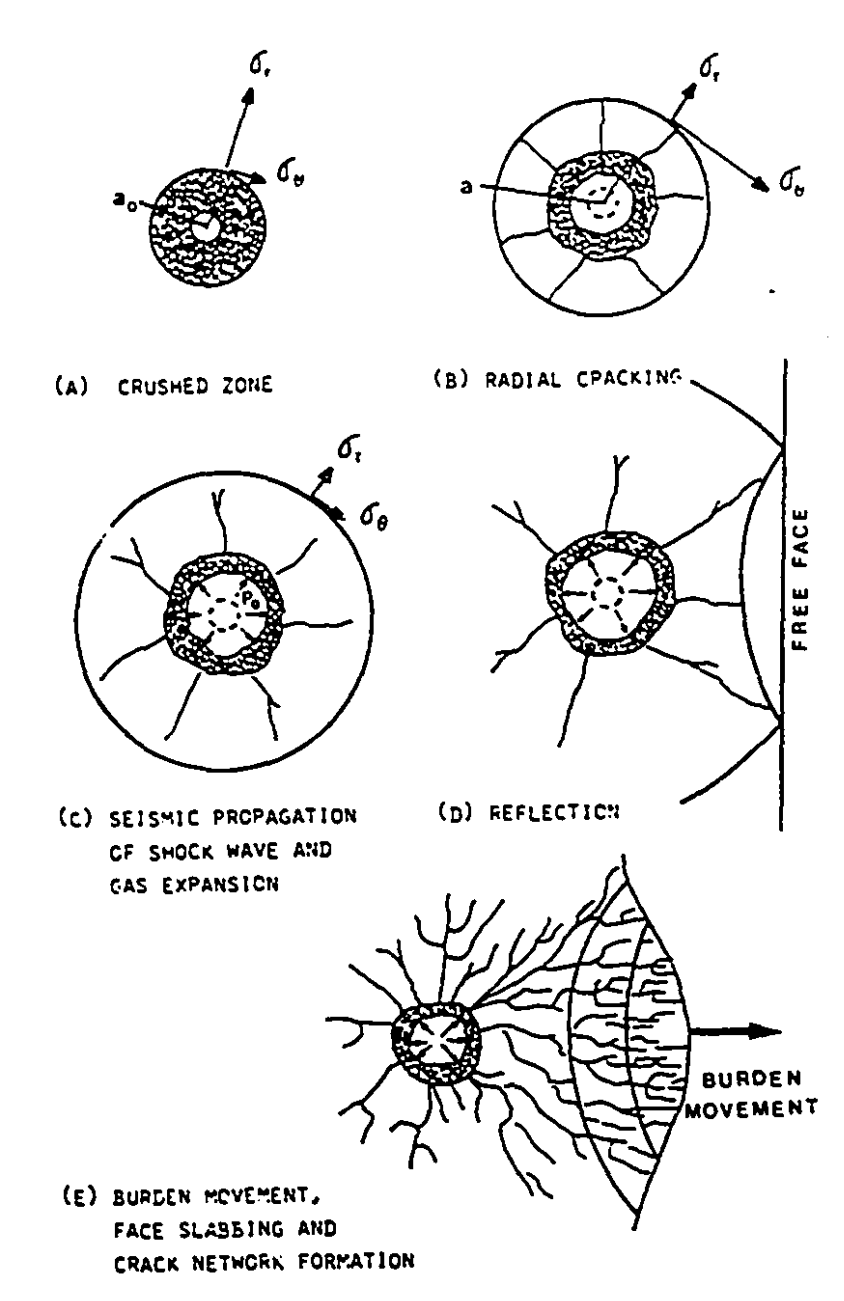


Figure 2.3: Generalised plan view through detonating borehole showing sequence of events occurring in the rock mass, where 'a0' and 'a' are charge radius and expanded borehole radius, respectively,  $P_{z}$  is borehole pressure  $\sigma_{z}$  and  $\sigma_{z}$  are tangential and radial stress components, respectively [14].

discontinuities and other crack systems. It is a function of temperature, pressure and the amount and type of fluid saturation. The weight of water and the air present in the void is not considered in the unit weight  $(kg/m^3)$ , whereas bulk density (also  $kg/m^3$ ) takes into account of pores and water present therein. Density in situ is usually lower than that measured in an intact laboratory sample.

Dry density=W<sub>s</sub>/V<sub>b</sub>

Bulk density=(W<sub>s</sub>+W<sub>w</sub>)/V<sub>b</sub>

where  $W_{a}$  is the weight of grain (kg),  $W_{w}$  is the weight of pore fluid (kg), and  $V_{b}$  (m<sup>3</sup>) is the bulk sample volume.

#### 2.4.2 STRENGTH OF ROCK

Strength is the resistance to deformation of a material against the applied force. The strength of rock depends largely on the nature of the micro-structure and less on its the mineral composition. It can be defined only when all the strength factors such as the intensity and duration of load, the size of the rock samples, confining pressure and temperature, moisture and pore water pressure and the failure criteria are known. The strength of a rock increases with increasing rate of loading and confinement, however, it decreases with increasing moisture content and temperature. Compressive, tensile and shear strengths are three types of rock strengths which can be measured in a variety of ways under static and dynamic conditions. Generally, rocks have very low tensile strength, moderate shear strength and high compressive strength.

The characteristic phenomenon of high compressive strength is that a lot of energy is wasted in friction or plastic deformation. Particles broken are of smaller sizes with a large number of pieces. The continuous cracks present after failure still remain intact. In tension, failure takes place at the weakest part of the material. There is no friction

involved among the grains. Only cohesion comes into the picture. This may be the reason for the much lower tensile strength compared to compressive strength.

#### 2.4.3 ELASTIC MODULUS

The principles of linear elasticity can be applied to many rocks over some specified range of stress level. They are used in engineering applications when departure from linearity is not significant. The modulus of elasticity is a general term defined as the ratio of stress to corresponding strain within elastic limit. Different loading geometries as shown in Figure 2.4, each defining a different elastic modulus. Young's modulus (E) is defined as the ratio of stress to strain in simple compression or tension. If a body is compressed equally from all direction, its original volume will be decreased. The ratio of fractional change in volume to the applied stress is defined as the bulk modulus (K). The reverse of the bulk modulus is described as compressibility. The shear modulus or modulus of rigidity  $(\mu)$  is defined as the ratio of shear strain to shear stress. Weathered and fractured rocks have low moduli of elasticity.

#### 2.4.4 POISSON'S RATIO

It is defined as the ratio of transverse strain to the corresponding axial strain when loaded axially within its elastic limit. It can also be calculated from the stress wave velocities.

$$v = \frac{(C_p^2 - 2C_s^2)}{2(C_p^2 - C_s^2)}$$
 2.1

where  $C_p$  and  $C_s$  are the longitudinal and shear wave velocities, respectively (m/s).

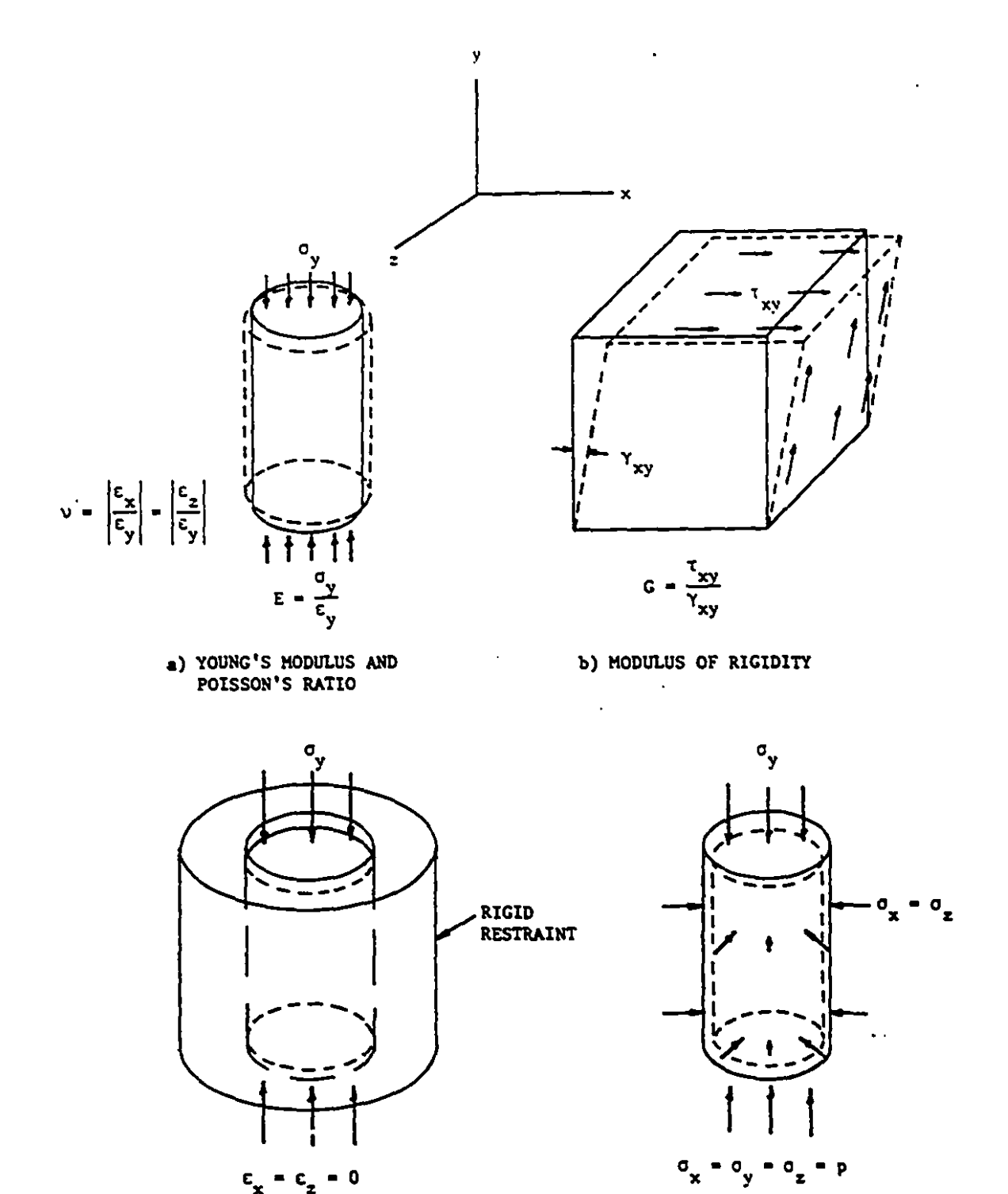


Figure 2.4: Loading geometries to define elastic moduli [28].

d) BULK MODULUS

c) CONSTRAINED MODULUS

# 2.4.5 STRESS WAVES

Several types of waves are generated when an elastic material is suddenly deformed by explosive action. If the direction of particle motion is parallel to the direction of propagation, the wave is called longitudinal. The particles in the path of these waves move backward and forward along the line of propagation. This compressional or dilational motion is also called primary or P wave. The speed of propagation of the longitudinal waves is higher than that of the other waves. It is given by following:

$$C_{p} = \left(\frac{\lambda + \mu}{\rho}\right)^{\frac{1}{2}}$$
 2.2

 $C_p$  is the velocity of the P wave (m/s),  $\rho$  is density of rock (kg/m³).  $\lambda$  and  $\mu$  are Lame's constants (GPa) from which moduli of elasticity can also be calculated. The Lame's constant,  $\mu$  is same as the shear modulus or the modulus of rigidity.

If the direction of particle motion is normal to the direction of propagation, the wave is called transverse. These waves are also called distortional, shear or S waves. Transverse waves tend to change the shape of material while also compressing it. P and S waves are called body waves, because they travel through the body of solid material. The velocity of propagation of the S wave, C, is lower than that of the P wave, C, and it is equal to:

$$C_s = \sqrt{(\mu/\rho)}$$
 2.3

# 2.4.6 DYNAMIC ELASTIC MODULI

The elastic properties such as Young's modulus (Y), Bulk modulus (K), Shear modulus  $(\mu)$  as explained above can be measured under both static and dynamic loading condition. Presence of moisture or liquid results in lower static elastic properties, however, it causes increase in

dynamic elastic properties (wave energy is transferred more efficiently). The P and S waves measured are proportional to the stress applied in the rock sample to some extent. The dynamic modulus is, therefore, also dependent on the stress applied. The dynamic constants increase with a decrease in porosity while Poisson's ratio remains more or less unaffected [29].

For homogeneous isotropic elastic materials with bulk density (p), compressional  $(C_p)$  and shear  $(C_s)$  wave velocity, the elastic moduli are related by following equations.

$$Y = \frac{\rho \cdot C_s^2 (3C_p^2 - 4C_s^2)}{(C_p^2 - C_s^2)}$$
 2.4

$$K = \rho \left( C_p^2 - \frac{4}{3} C_s^2 \right)$$
 2.5

$$\mu = \rho.C_s^2 \qquad \qquad 2.6$$

$$C_{p} = \sqrt{\frac{K + \frac{4}{3}\mu}{\rho}}$$

The specific tests employed to obtain these properties are described in more detail in chapter 4.

#### 3.0 PRINCIPLES OF COMMINUTION

#### 3.1 INTRODUCTION

Whereas a loose definition of comminution would include a variety of energy sources, a strictus sensu definition (restricted to mineral processing) would deal solely with mechanical stress, resulting in scraping, sawing, impacting, crushing, pulling, cutting, bending or twisting processes [30]. In many respects, comminution is perhaps the most important operation in mineral processing, for two very fundamental First, the size distribution of the products, extent of reasons. liberation and the amount of fines produced are determined in these processes. These in turn will determine the efficiency of the subsequent separation processes. Second, comminution circuits often represent the largest capital and operating costs [31]. This would not be surmised from a theoretical analysis of the energy required for breakage, but the efficiency of most comminution steps is surprisingly low (some estimates are as low as 0.6% in ball mill [32]), resulting in very large energy requirements, much of it wasted in form of heat and vibration.

# 3.2 COMMINUTION PROCESSES

Comminution processes may be grouped into crushing and grinding depending upon the initial size of the feed and the extent of size reduction achieved. The conventional machines used in these processes are jaw, gyratory and cone crushers (used to process feeds from 2 m down to 2 cm), rod and ball mills (for grinding material from 2 cm down to below 100  $\mu$ m), and roll crushers (used for breaking materials in the intermediate sizes). Traditionally, comminution was thus effected by crushers down to 1 to 2 cm, and then by mills down to final product size. The past twenty five years have seen changes that challenge this simple classification, with grinding mills (mostly semi-autogenous mills, SAGs) handling coarser

feeds and crushers (Gyradisc, Waterflush') handling finer feeds. These innovations have even produced a comminution approach that inverts the traditional rank of crushers and tumbling mills: in ABC or SABC circuits, an autogenous, and more recently a SAG mill, yields a product whose coarsest particles are usually 4-5 cm, and are crushed prior to recycling to the SAG. The fine fraction of the SAG product, below about 1-2 mm, is directed to a ball mill and ground to final size.

In crushing, the size reduction is achieved by applying slow compression. The force is applied to the material by a moving iron plate against another fixed or moving iron plate. The size distribution of the product depends on the opening of the outlet of the crusher. In grinding, material is broken by impact and abrasion, dry or in water suspension. Grinding is usually conducted in rotating cylindrical vessels known as tumbling mills. The mill is charged with a grinding medium consisting of steel balls in ball mills, rods in rod mills, large balls and coarse ore in SAGs, and ore or pebbles in autogenous mills. Typical rod and ball mills are shown in Figure 3.1 [33]. The classification action of rod mills (the result of the fanning of the rods at the feed end) limits fines production, and yields a product more uniform in size (than a ball mill). Rod mills are used for coarse grinding of feeds with a top size of 10 to 20 mm [34]; the product, with a top size of 1-3 mm, is usually fed to a ball mill. However, ball mills can accommodate much coarser feed sizes, nearly as coarse as rod mill feeds, provided ball size is increased accordingly. This normally results in a loss of efficiency, as the diameter of balls and rock particles is then poorly matched. milling is used for fine grinding-- i.e. to achieve an average size range of 10 to 300  $\mu m$  [35]. Since fines provide an undesirable rheological effect for the grinding process, they must be removed as rapidly as possible. This is achieved by operating most ball mills in closed circuit with classifiers, usually hydrocyclones. In recent years, very few rod mills have been commissioned, as the trend towards simpler circuits (hence

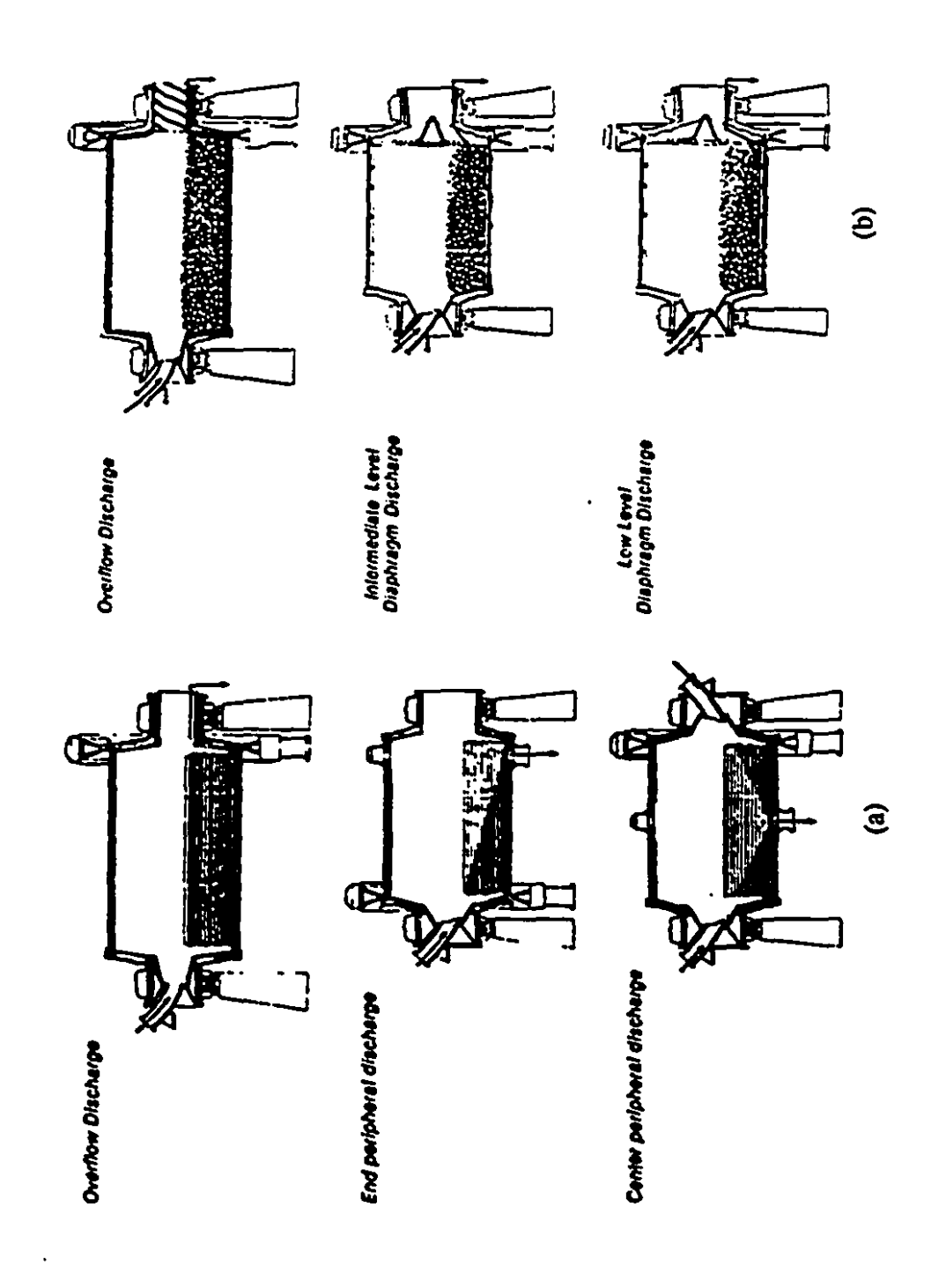


Fig. 3.1: General view of (a) Rod mills and (b) Ball mills [33].

fewer units) has resulted in the replacement of secondary and tertiary crushers (and the attached screening step) and rod mills with SAGs or, more recently high pressure rolls. This has resulted in a drop of capital and operating costs of approximately 25% for comminution. SAGs incorporate large diameter balls to the coarse component of the ore (typically up to 15-20 cm) to act as grinding medium. High pressure rolls with large D/L (diameter to length) ratios apply very large pressures to the ore to produce a large number of microcracks in the material. As a result the specific energy consumed in the following processes is reduced considerably [36].

Recent research in comminution is focused toward inter-granular fracture rather than trans-granular fracture for adequate liberation of minerals [37]. Thermally assisted liberation of quartz has been reported by Wills [38]. Electrical and thermal energy has also been used to modify the physical properties and related texture and structure of heterogenous rock and ore. Generation of hairline crack along the grain boundaries and their propagation using electric shock and ultrasonic energy has been demonstrated by Parekh [39] and Andres [40]. Pretreatment of minerals with microwave radiation has also been studied by Chen [41] and Walkiewicz [42]. However, these new techniques are still very much at the experimental stage, and show no signs of ever replacing crushing and milling. If anything, this work has served to illustrate that existing technology, though not energy efficient, represents a forceful compromise between the theoretical limits of particulate breakage and the practical constraints of processing well in excess of a billion tonnes yearly.

# 3.3 ENERGY-SIZE RELATIONSHIP

The breakage energy associated with any comminution process can be explained by two approaches, stress and energy based. The stress approach is used to explain the strength of the rock or material on macroscopic

scale such as compressive, shear or tensile strength. The fracture stress or the strength (in MPa) depends on many factors such as macro- and microstructure of the material, extent and rate of stress and the method of stress application. Due to the lack of ability to quantify the strength of a heterogenous and anisotropic material, stress criteria are often lumped into an energy criterion. The energy approach is also a macroscopic representation of fracture strength but it takes into account the crack size present in the material (the Griffith theory). knowledge of the strain energy (energy absorbed under stress application) and surface energy (work done in creating unit surface area), the minimum work required in a comminution process can be estimated (alternately, if the actual energy used is measured, one can estimate how efficiently it is used). The macro- and micro-structural and physico-mechanical properties of material can be lumped into one term known as grindability (ease of grinding). Grindability is quantified in terms of an amount of undersize (with respect to a specified size) produced in a specified machine, from a known starting size, and for a given energy input (e.g. per revolution of a calibrated rod or ball mill). The grindability of the material is widely used in comminution engineering to determine energy requirements and scale-up equipment. The specific energy consumed in a size reduction process increases continuously with decreasing product size (see Figure 3.2 [43]). The amount of energy expended in the process of size reduction depends on the following factors:

- i) initial size and reduction ratio intended
- ii) stiffness, density and structure of the rock
- iii) temperature and moisture content
- iv) extent and rate of stress applied
- v) machinery and its operating conditions.

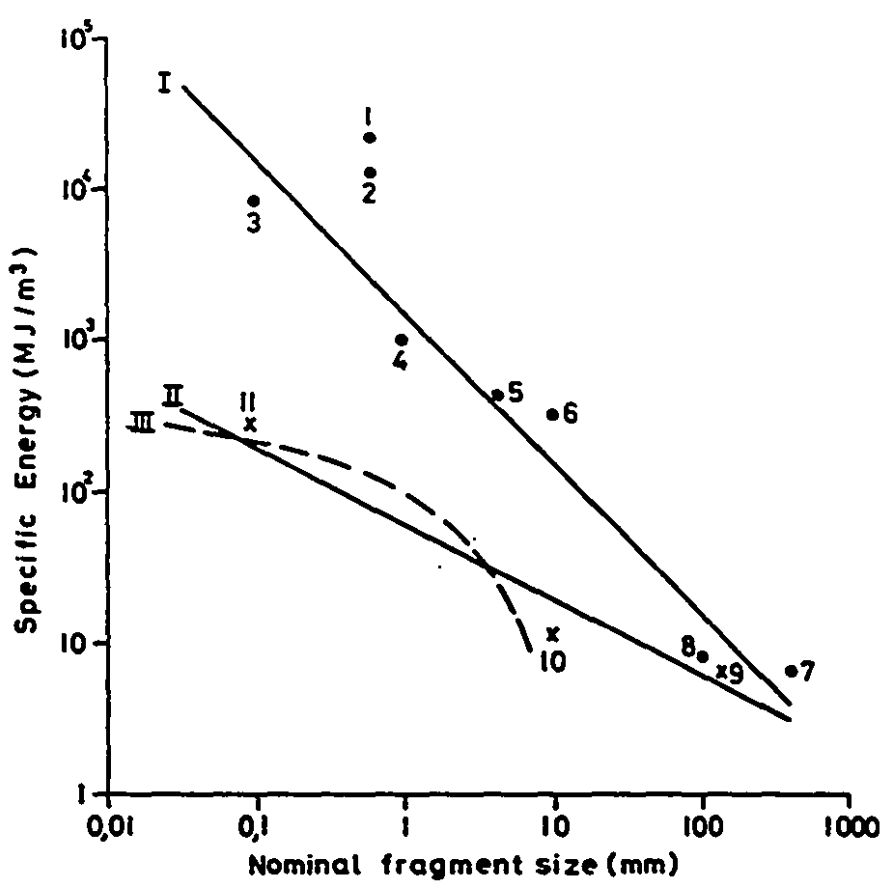


Figure 3.2: Specific energies as a function of nominal particle size for different methods of breaking hard rock with a uniaxial compressive strength of about 200 MPa (after Cook and Joughin, 1970). (1) Flame jet piercing; (2) Water erosion jet; (3) Diamond cutting or drilling; (4) Percussive drilling; (5) Drag bit cutting; (6) Roller bit boring; (7) Impact-driven wedge; (8) Explosive blasting; (9) Jaw-crusher; (10) Gyratory crusher; (11) Milling. Line I, for methods of excavation, corresponds to Rittinger's hypothesis using an effective surface energy of 0,27 MJ/m<sup>2</sup>; line II for methods of comminution corresponds to Bond's relationship using a work index of 200 MJ/m<sup>2</sup> or about 25 kWh/ton, and line III to Kick's hypothesis using a strength of 100 MJ/m<sup>2</sup> or 100 MPa [43]

Energy consumption in blasting is of the order of 0.4-0.6 kWh/t, whereas in case of crushing and grinding it is 3-6 kWh/t and 10-30 kWh/t, respectively. This difference is due to the differences in product size, reduction ratio and discontinuous nature of boundary layers or cracks. Discontinuities are present at both macro- and micro-scale, and at both scales decreasing particle size generally reduces their relative density, as breakage takes place preferentially along the discontinuities. Formal estimation of the energy spent in a process of size reduction, for a specific reduction ratio, dates from the previous century. The classical energy-size relationships, empirically derived for a comminution process, will now be described briefly.

## 3.3.1 RITTINGER'S LAW

The first theory of comminution was postulated by Rittinger (1867). It is also known as the surface theory. It states that the specific energy consumed in the process of size reduction is directly proportional to the new surface area produced and hence inversely proportional to product diameter. This theory is based on intuitive grounds; neither mathematical nor experimental proof is available. The basic drawback of this theory is that it does not consider deformation done during breakage. Actual work done may be considered as the product of force and deformation. The force required for breakage is proportional to the surface area over which it acts; this is the basis of Rittinger's law. The deformation can be considered as shape change or change in strain energy and is not considered. To understand the breakage mechanism, a knowledge of stress applied and strain induced is necessary. Austin [44] modified it for aggregate rock mass as:

$$E = K^R \left( \frac{1}{X_p} - \frac{1}{X_r} \right)$$
 3.1

where  $K^R$  is a constant, E is the specific energy expended to change the feed from a size of  $X_t$  to a product of size  $X_p$ . For an aggregate rock mass

the size may be defined as 50 or 80 percent passing size through a square woven screen (usually the latter).

#### 3.3.2 KICK'S LAW

Kick (1885) postulated the second theory of comminution, also known as the volume theory. It is based on a stress-strain model. It states that the specific energy consumed or work done in a comminution process is proportional to reduction in the volume of the particle. The work done is the same for the same reduction ratio irrespective of the size range. The drawback with this theory is that it takes into account only strain energy, which is correct only before fracture propagation takes place. When it does, the surface energy has to be taken into account. Mathematically it can be represented by:

$$E = K^K \log \left(\frac{X_f}{X_p}\right)$$
 3.2

where E is the strain energy per unit mass to reduce a feed size  $X_r$  to a product size  $X_p$ .  $K^K$  is strain energy per unit mass to produce ten fold reduction in size, incorporating the efficiency of comminution process as well. Kick also assumed the rock mass to be homogenous, which is rarely the case. Rock is characterized by flaws, dislocations, joints, etc, which cause the material to break below its elastic limit.

#### 3.3.3 BOND'S LAW

The above two theories met with many difficulties in explaining size reduction processes over the full size range of comminution. Therefore a third theory of comminution known as Bond's law [45] was developed. Bond summarised the three comminution principles as follows [7]: a) it may be assumed that the energy content of a particle is inversely proportional to the square root of its size. The required energy in the course of size reduction is added to the initial energy content of the feed to produce the energy content of the product. Therefore the net

energy required is the difference between the energy content of feed and product; b) the second principle states that the useful work in the size reduction process is proportional to the length of new crack produced. In ordinary comminution processes, particles absorb strain energy and are deformed under compression or shear until the weakest flaw in the particle fails with the formation of a crack. The slight deformation causes other crack tips to develop at other flaw sites, and particles break thereby releasing strain energy as heat. The strain energy required to break is proportional to the length of the crack formed; c) the third principle deals with the relationship of particle flaws to material breakage. A flaw is defined as any structural weakness which develops as a crack under strain. Flaws are always present in brittle material and may cause wide variations in breaking strength. The weakest flaw in a particle determines its breaking strength in comminution. It also controls the number of fragments produced by breakage.

Though Bond tried to correlate his law with crack theory, in actual sense he did a compromise between the earlier two theories. The concept lies in the fact that the energy consumed is proportional to the initial size of the rock (first theory) till the stage of fracture is reached. Once the stage of fracture is reached the energy consumed further by fracture is proportional to the surface area created (second theory). The total specific energy is thus inversely proportional to the square root of the initial size.

$$E = K^{B} / \sqrt{X_{p}}$$

where  $K^B$  is a proportionality constant.  $X_p$  is the 80 percent passing size of the product passing through a standard square sieve as adopted by Bond. E is the total work done during the size reduction process. Bond generalised the above relationship further, and presented the energy consumed in a size reduction process, E (in kWh/t), from a specific feed

size to a specific product size as follows:

$$E = 10 W_1 \left( \frac{1}{\sqrt{X_p}} - \frac{1}{\sqrt{X_r}} \right)$$
 3.3

where  $W_i$  is the work index (intrinsic property of a material, relating energy input in kWh/st (1 kWh=3.6 MJ), required to break a given material from a theoretically infinite size to 80 % passing 100 micrometers).  $X_r$  is the feed size, and  $X_r$  the product size (both 80% passing).

## 3.3.4 MODIFICATIONS

All of the above theories can be expressed by an empirical equation, which was demonstrated experimentally by Charles [46].

$$dE = -K^c \left(\frac{1}{X^a}\right) dX$$
 3.4

where dE is the infinitesimal change in energy input during a size reduction process to produce a change of product size dX. X is the initial size of the aggregate rock mass. 'n' and 'K' are the constant depending upon the nature of rock broken and the method of rock breakage. The negative sign shows that an energy input decreases particle size.

Hukki [47] suggested that the relationship between energy consumed and particle size is a composite form of the Rittinger, Bond and Kick laws (Figure. 3.3 [47]). The value of the constant varies depending upon the initial size and the breakage mechanism considered. The value of n is equal to 1, 2 and 1.5 for Kick's, Rittinger's and Bond's equations, respectively. Austin [44] pointed out that particles cannot be broken in differential amounts, since the products of breakage must contain small fragments even if the original particle is only slightly broken. The correct equation can be written as

$$dE = -K^c \left(\frac{1}{X_{max}^n}\right) dX$$

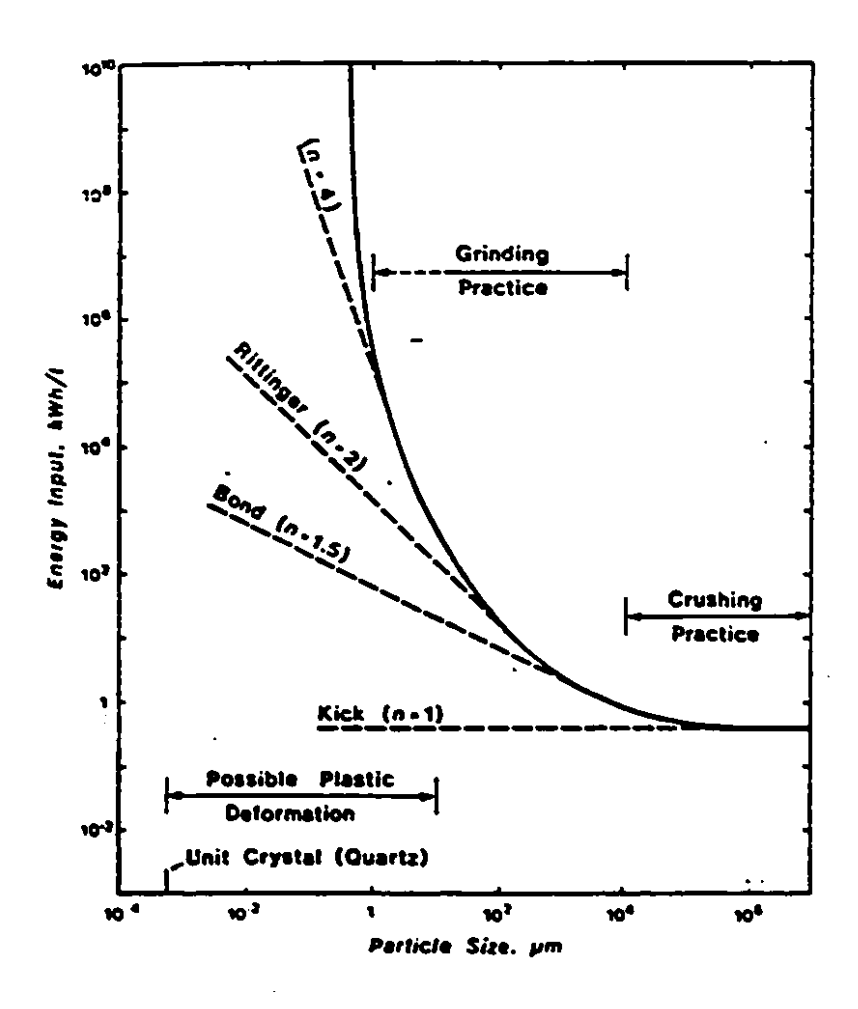


Figure 3.3: Composite energy-size relationship [47].

In all the above size-energy theories, only size, mean size or 80 % passing size is discussed. In actual practice, the full size range cannot be represented by one parameter (see Figure 3.4 [48]).

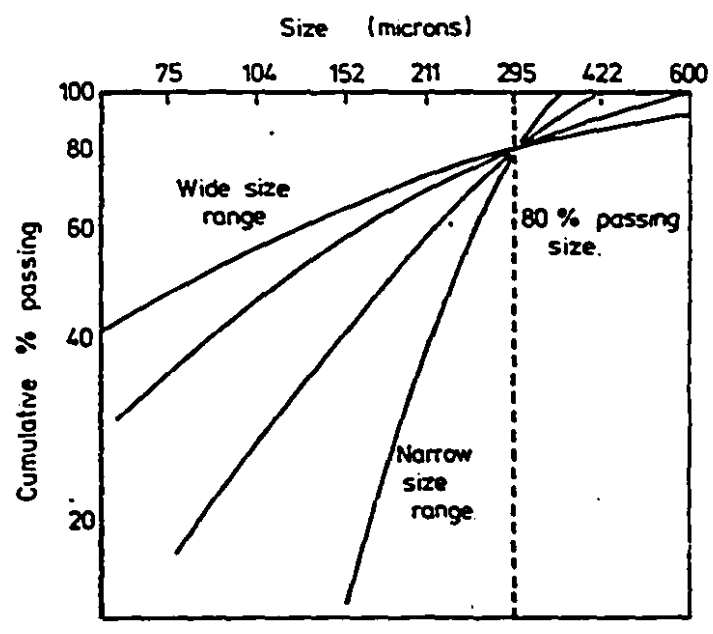


Figure 3.4: Size distribution and 80% passing size [48].

At least two parameters, such as a size and distribution moduli, are needed to represent the size distribution. This led to the fourth theory.

Charles [46] combined the famous Gates-Gaudin-Schumann equation (G-S-S), a statistical size distribution equation to represent fragment size distribution, with the generalised size-energy relation, and pointed out that the size modulus  $(K_c)$  of the Schumann size distribution plot varies with the specific grinding energy (proportional to grinding time) according to relation

$$E = \frac{c}{(m-1)(n-m+1)} \cdot K_c^{1-m}$$

where C is a constant specific to the size reduction process used and is very difficult to estimate, as c is also unknown. 'm' and 'n' are the exponents of the G-G-S equation and that of the generalised energy-size relationship, respectively. If the size distribution of the product of a comminution process follows the G-S-S equation with a slope 'n' then the energy size relation plot on log-log plot will follow the same slope, but with the opposite sign, as shown in Figure 3.5 [46].

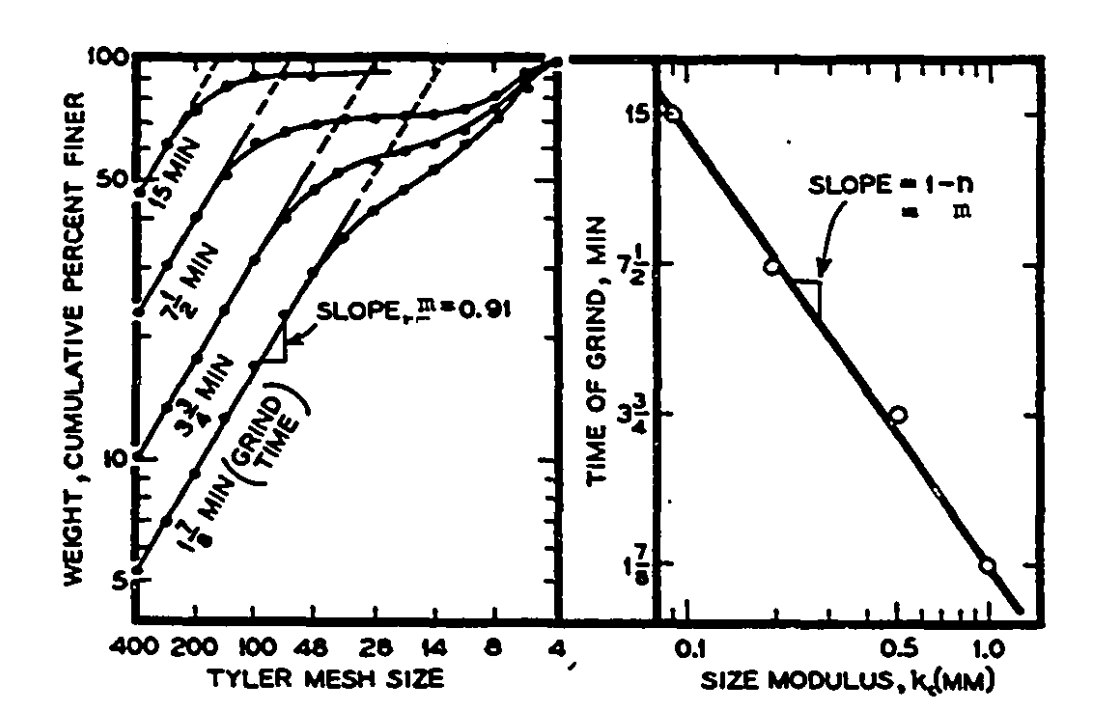


Figure 3.5: Size distribution and energy-size relationship [46].

## 3.4 WORK INDEX

The work index (WI), as discussed earlier, originates from the third theory of comminution. It is the proportionality constant of the Bond's law and takes into account material characteristics, the method of size

reduction and the efficiency of the operation. Bond [45] used this index to model grinding circuits by assuming that an almost negligible change occurs in work index during grinding. Thus, the energy requirement for a material in a standard grinding mill (2.44 meter inner diameter overflow mill operating under a given set of standard conditions) can be predicted for a specified feed and product size. The efficiency of any grinding mill or circuits can also be evaluated using populance balance model [49].

Bond made use of separate bench-scale laboratory tests both for rod and ball mills. He determined the lab-scale work index  $(W_i)$  by equating the work applied in the 2.44 meter mill to the number of revolutions to obtain the same size reduction. On the other hand the work index calculated from the mill based on the power draw from the motor and the feed and product size is known as operating work index!  $(W_{io})$ . The ratio of operating work index,  $W_{io}$  to lab-scale work index,  $W_{i}$  is called the efficiency factor of the size reduction process [51].

Presently the laboratory scale work index determination in its modified form (with a smaller calibrated mill) is used to estimate the grinding energy required in the standard mill (inner diameter of 2.44 meter size) for a specified feed and product size. The work index (WI) is also used to represent the relative resistance of breakage of different materials. In the present work the work index (WI) is used in the latter form i.e. as a relative breakage behaviour. The work index measured takes into account, at least implicitly, strain energy (elastic and plastic energy), surface energy, kinetic energy (some of the kinetic energy is translated into heat, material and machine vibration, sound, electricity and light generation) and finally material-material and material-machine friction. The work index is thus a measure of breakage performance in a defined piece of equipment according to a strict procedure. The different

<sup>&</sup>lt;sup>1</sup> The operating work index during blasting is calculated by the explosive energy (kWh/t) spent in getting a desired product size (80% passing in  $\mu$ m) with the assumption of feed size to be infinity [8,50].

friction. The work index is thus a measure of breakage performance in a defined piece of equipment according to a strict procedure. The different work indices measured by different lab units are outlined as follows:

3.4.1 <u>Hardgrove Index</u>: The Hardgrove Index (HGI) is generally used to represent the softness of coal. The machine consists of a top rotating ring with eight one inch diameter balls which roll on a bottom stationary ring cavity [52]. About 50 grams of material of one size range is selected for grinding for 60 revolutions. The weight (g) passing through 200 ASTM sieve size, W, is measured to calculate the Hardgrove index, by an empirical formula:

HGI = 13 + 6.93 W

The HGI varies in an opposite direction to the Bond work index (the higher the HGI, the lower is the work index). The use of the HGI is normally restricted to coal.

3.4.2 Bond Ball Mill Test: The work index determination by this method consists of a standard ball mill of internal diameter and length equal to 30.5 cm (12") [7]. The grinding medium consists of 285 steel balls weighing in total 20.125 kg. The size of the ball vary between 3.68 cm (1.45") and 1.55 cm (0.61") in diameter, out of which 120 are over 2.54 cm (1") diameter. The mill is filled with 700 cm³ bulk volume of dry minus 3330  $\mu$ m (6 mesh) material and ground (70 rpm) for 100 revolutions. The mill is dumped, the ball charge is screened and the feed sample is screened on the sieve size tested (at 600  $\mu$ m, 28 mesh, or finer). The oversize is weighed and fresh unsegregated feed is added to make it to the initial volume. This mixture is ground further with same grinding medium to produce the desired undersize to maintain 250 percent circulating load. The process is repeated till steady state of constant undersize is achieved. The work index is determined using a standard formula.

3.4.3 Bond Rod Mill Test: This test is conducted in a standard laboratory batch mill of 30.5 cm (12") diameter and 61 cm (24") long with a wave type internal lining. It can be tilted 5° from horizontal both side to reduce the preferential isolation of the coarse material. The mill is charged with two 4.4 cm (1.75") diameter iron rod weighing 6.5 kg each, and six 3.2 cm (1.25") diameter rod weighing 3.5 kg each. The rod length used is 53.3 cm (21") and the total weight of the system is 33.38 kg. The mill is rotated at a fixed speed of 46 revolutions per minute. The material used for the test should be less than 12.7 mm (1/2") size and the volume of the sample to be 1250 cm3 [7]. Tests can be conducted at all sizes ranging from 4.75 mm to 208  $\mu m$  (4 to 65 mesh). At the end of each cycle the steel rods are taken out and the mill is emptied by rotating it for 30 seconds at a 45° inclination. The product is screened at the screen size tested and the oversize material is mixed with unsegregated original sample to make to initial weight of 1250 cm3. This new mixed sample is placed in the mill and is ground for the estimated number of revolution so as to achieve the 100 percent circulating load. The grindability of the material is calculated keeping the same volume of material in the mill. The average grindability of the last three cycles at steady state is used to calculate the work-index using a standard formula.

3.4.4 <u>Bond Impact Test</u>: Two identical hammers weighing 13.6 kg (30 lbs) are arranged for simultaneous blow by impact or drop test or by pendulum test on a test piece of rock. In the original test [7] the size of the rock selected was of minus 7.6 cm (3") and plus 5.1 cm (2"). A series of test is conducted by giving more energy to the hammer till the rock breaks. The impact crushing strength, I (in kWh per unit of thickness), and the impact work index, W<sub>i</sub>, are calculated as follows:

$$I = \frac{2 M d}{D}$$

$$W_i = 2.59 \frac{I}{\rho}$$

where

M: mass of one hammer (kg)

d: distance between the hammer (m)

D: thickness of rock (m)

p: specific gravity of rock

W.work index (kWh/m)

#### 3.5 POPULATION BALANCE MODELS

Population balance models (PBM) are a relatively new concept in comminution engineering. A PBM can be used to analyze and simulate the size reduction processes in terms of a mass balance [53]. material in any comminution device is assumed to consist of different size classes (e.g. ASTM or Tyler series). The specific breakage rate (selection function) and the primary breakage size distribution (breakage function) of individual size classes are used to quantify the comminution process. The grinding time or the residence time distribution in the process of size reduction are assumed to be divided into number of stages, a concept first given by Epstein [54]2. The product of the first stage may be considered to the input of the second stage and the product of the second stage is used to calculate the input of the third stage and Mathematical models associated with PBMs for batch mili dry so on. grinding will now be briefly reviewed.

The distribution of the fragments after rock breakage is common to all size reduction processes. This is a statistical variable and is referred as 'Breakage Function.' The other phenomenon associated with tumbling mills is the kinetics of breakage; it is normally assumed that first order kinetics apply, and the rate constant was originally termed

<sup>&</sup>lt;sup>2</sup> Alternatively, a continuous residence time distribution, typically that of tanks in series, a well known Weller model can be used [55].

the 'Selection Function.' If breakage is instantaneous (or nearly so, such as in crushers), then the concept of breakage kinetics cannot be used, and is often replaced by that of a 'Classification Function.' This may well be the case of blasting. The difference between the two approaches becomes important when linking PBMs to energy considerations, as will be discussed in section 3.5.5.

#### 3.5.1 BREAKAGE FUNCTION

The breakage function quantifies the size distribution of particles after minimum breakage, often referred to as 'single breakage events.' This breakage distribution is described either continuously (typically with an equation) or discretely (with a vector), the latter being by far the commonest approach. The size distribution is then divided into size classes, typically with Tyler Series. Now consider a particle of original size j being broken once; its fragments will be distributed amongst finer size classes, i=j+1 to n, in a stochastic manner that can be represented by a probability density function. This PDF,  $B_{ij}$ , is the average mass fraction finer than the lower size limit of class i, when broken from size class j. Because in any grinding process, the number of particles being broken is very large, the stochastic nature of the cumulative breakage function,  $B_{ij}$ , is often disregarded; it becomes the proportion of material finer than size i when broken once from size j.

The actual breakage function,  $b_{ij}$ , is defined as the proportion of material which appears anywhere in size class i (i.e. between the lower limit of size classes i and i-1) when broken once from anywhere in size class j. It is calculated easily from  $B_{ij}$ , as:

$$b_{ij} = B_{i+1,j} - B_{ij}$$

From the above definitions one can draw useful conclusions:

1) By definition, we consider that material breaks only if it

leaves its original size class'.

- Quite obviously, B<sub>ii</sub> is equal to 1 if i<j.</li>
- 3) We define size class 1 as the coarsest, and the size class n as the finest, including "the pan".  $B_{ni} = 0$ .

Some of the research work at Julius Kruttschnitt Mineral Research Centre has focused the use of one parameter breakage function  $(T_{10})$  typically useful for impact crusher, SAG mills, and possibly blasting [56]. The breakage function,  $T_{10}$  is defined as the cumulative percent passing one tenth of the geometric mean size of the test particle produced under the specified laboratory pendulum test. It is interesting to note that whereas the breakage function for a given material is considered relatively environment independent when modelling ball mills, it becomes very much energy dependent in the pendulum test. As one would expect, the higher the energy input, the finer the product, and the higher the value of  $T_{10}$ . Such an approach is likely to apply to blasting.

## 3.5.2 ZERO ORDER RULE

This hypothesis states that in a tumbling mill the production rate of fines or material finer than any size class is constant with respect to time. In other words, it is independent of the relative coarse material present therein, at least for some initial, non-negligible grinding period. The zero-order rate constant,  $F_i$  is obtained by linear regression of the mass produced finer than class i versus time, usually from breakage of a single size class (or nearly so). This linearity eventually breaks down as less and less material coarser than the size considered is left for grinding. The breakage function can be determined by a) back calculation from feed and product size distributions, b) Bérubé's method

<sup>&</sup>lt;sup>3</sup> This is arbitrary, since a particle could undergo significant breakage, theoretically up to 1/2.8 of its original mass, and yet remain in the same Tyler series.

[57], c) Herbst and Fuerstenau's method [58]. The latter relies on the zero order rule, and will be used in this project on account of its simplicity and numerical robustness. The cumulative breakage function  $(B_{ij})$  is calculated by dividing the rate constant (of zero order,  $F_i$ ) by selection function of the original class  $(S_j)$ . Both of these constants can be determined graphically or by linear regression (over the linear range).

# 3.5.3 THE SELECTION FUNCTION

This parameter quantifies the kinetics of particle breakage for each size class in a grinding reactor. It can be defined as the rate of disappearance of material in a particular size class per unit mass (same as the specific rate of disappearance or first order kinetics rate constant). In a batch mill, a plot of the mass fraction remaining in the coarsest size class on a vertical logarithmic paper versus time should follow a straight line (Figure 3.6 [59]), if the material broken is

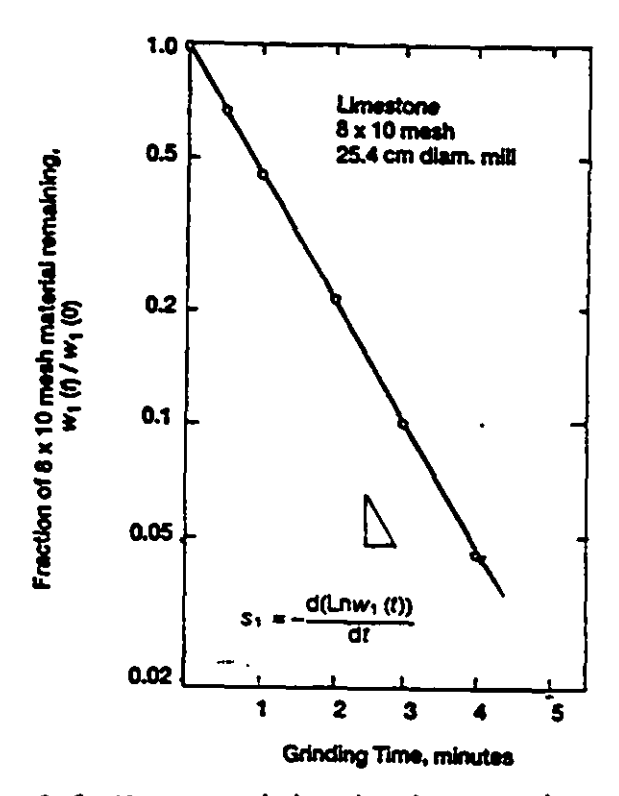


Figure 3.6: Mass remaining in the top size class [59].

reasonably homogenous. The absolute value of the slope is the selection function. For other size classes, this linearity is hidden because material is broken from coarser classes.

The selection function,  $S_i$  (for size class i) is normally determined by retrofit of either one or many data sets<sup>4</sup>. With a single set, an exact solution can normally be found; with multiple sets, a least-square solution is used. The selection function can be estimated for each size class, usually starting with the coarsest, or as a three or four parameter relationship with particle size (in which case a least-square solution is always used).

## 3.5.4 SIZE-MASS BALANCE

The following hypotheses are assumed:

- Rate of disappearance of size class j material = S<sub>j</sub>.M<sub>j</sub>(t)
- Rate of appearance of size i material = Σb<sub>ii</sub>.S<sub>i</sub>.M<sub>i</sub>(t)
- 3) from 1) and 2) the net rate of production of size i material equals the sum of the appearance terms from the breakage of all coarser size classes minus the disappearance term by breakage.

A differential mass balance in terms of  $M_i(t)$ , the mass fraction of particles in the  $i^{th}$  size fraction at time t, would be

$$\frac{dM_i(t)}{dt} = -S_i M_i(t) + \sum b_{ij} S_j M_j(t)$$

The selection function may be dependent on the state of the system, i.e., on the environment of the i<sup>th</sup> size fraction at time t, and the breakage function is assumed to be environment-independent. It is essential that selection and breakage functions be considered average

<sup>&</sup>lt;sup>4</sup> Each data set consists of a feed and product size distribution, to which is associated a breakage function and a grinding time (batch) or residence time distribution (continuous).

values for the particles in the size fraction.

The above equation in the matrix form, as suggested by [60], follows:

$$\frac{dM}{dt} = -(B-I) S M$$

$$M = \begin{bmatrix} m_1 \\ m_2 \\ \vdots \\ m_{n-1} \end{bmatrix}; S = \begin{bmatrix} S_1 & 0 & 0 & \dots & 0 \\ 0 & S_2 & 0 & \dots & 0 \\ \vdots & \vdots & \ddots & \ddots & \vdots \\ 0 & 0 & 0 & \dots & S_{n-1} \end{bmatrix}$$

$$B = \begin{bmatrix} b_{21} & 0 & 0 & \dots & 0 \\ b_{21} & b_{32} & 0 & \dots & 0 \\ \vdots & \vdots & \ddots & \vdots & \ddots & \vdots \\ b_{n-1,1} & b_{n-1,2} & b_{n-1,3} & \dots & 0 \end{bmatrix}$$

where M is a column matrix whose first term is the mass fraction of the first size class and the last, mass in the n-1 class. The selection function matrix is given by the diagonal matrix S, whose elements are rate constants for the first, second, ..., n-1 size classes. The breakage function matrix (B) is represented by a lower triangular matrix, with the terms of the j<sup>th</sup> column describing breakage from size class j and the terms of the i<sup>th</sup> row appearance into size class i. Hence any term  $b_{ij}$  refers to the fraction broken from size class j into class i. I is the identity matrix. The solution of the above equation is obtained by linear transformation, using a matrix "T" such that:

which gives,

$$M(t) = T.e^{-St}.T^{-1}.M(0)$$

where  $\underline{M}(0)$  is the initial size distribution and the columns of T are the eigenvectors of (B-I) S. The matrices T and  $T^1$  can be estimated by a recurrence formula [61]. The only additional assumption made is that  $S_i$   $\star$   $S_i$ : if  $i \star j$ .

# 3.5.5 SCALE-UP USING POPULATION BALANCE MODEL

Population balance modelling has been successfully used in ball mill circuit simulation [62,63]. Similar concepts can be applied in rod mill modelling and its development; however, the work done in this direction is meagre. Use of PBMs in ball milling is outlined here very briefly.

The breakage rate constant (selection function) determined in the laboratory scale batch mill is found to be heavily size dependent (Figure 3.7 [64]) and normally considered to follow power law.

$$S_i = B x_i^{*} Q$$

where  $S_i$  is the selection function of the size class i,  $x_i$  (mm) is its geomean. The above equation shows that  $S_i$  normally increases with increasing particle size. This trend reverses beyond a specific size class (the value of Q equals 1 for smaller sizes and becomes small for large sizes) and is dependent of the mill environment; this is attributed to the difficulty of nipping particles of comparatively larger sizes and the higher energy levels required to break the larger particles. The constant,  $\alpha$ , normally varies between 0.5 and 1.5, a characteristic of the

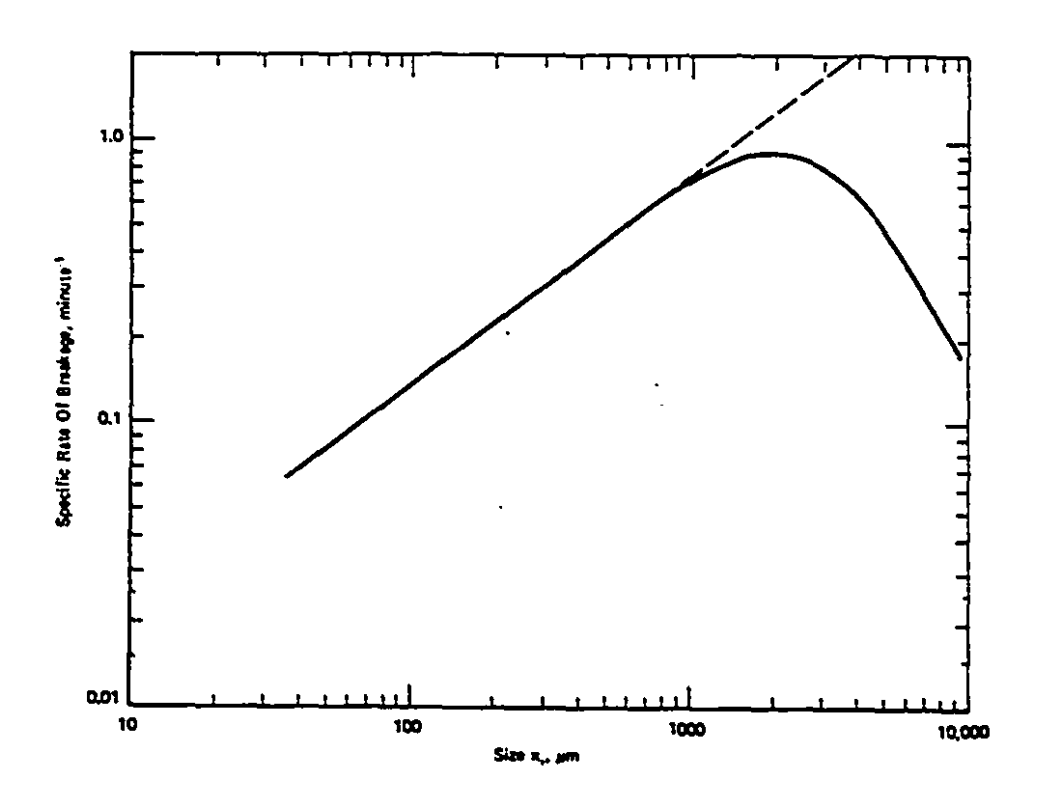


Figure 3.7: Selection function and particle size [64].

material; the value of ß will vary with mill conditions. The selection function S for a plant mill can be estimated by scale-up of laboratory determined data. The necessary corrections applied are due to the combination of mill diameter, ball diameter, ball and material charge of the mill, and the rotational speed of the mill [65]. The overall effect of a mixture of ball sizes on the selection function in the normal breakage region is taken to be the linear weighted sum:

$$\overline{S_i} = \sum S_{i,k} m_k$$

where  $m_k$  is the weight fraction of balls of size interval denoted by k and  $S_{ik}$  is the specific rate of breakage of size i by balls of this size.

The variation in breakage function due to ball and material load and mill speed is still an unresolved issue (that is why the breakage function is usually assumed environment independent for ball mills). Austin [62] applied the necessary correction to get the mean value of  $B_{ij}$  as follows:

$$\overline{B_{i,j}} = \sum \frac{m_k \ S_{j,k} \ B_{i,j,k}}{\overline{S_i}}$$

where  $B_{ijk}$  is the cumulative breakage function for size k balls acting on size j material. In practice, determining  $B_{ijk}$  for a range of particle and ball size requires an inordinate amount of work, which is very seldom performed.

Once the model parameters are known, mill scale-up of grinding circuits can be completed. This also requires a model of classification (ball mills are normally operated in closed-circuit with hydrocyclones); many reliable ones are available in the literature, requiring no additional laboratory test works. The basic difference between the Bond methodology of energy estimation and the PBM approach lies in the fact that the former lumps grinding behaviour in a single parameter, the Work Index, whereas the second phenomenologically describes the breakage of the full size range. Surprisingly, the vast majority of ball and rod mills are still scaled-up using the Bond approach. This can be explained by the universal acceptance the Bond approach has achieved over the past 50 years, largely on account of its robustness and simplicity. No such claim can be made for the determination of blasting energy requirements (there is no established procedure as such), which means that a PBM approach cannot be ruled out.

## 4.0 MATERIALS AND METHODS

#### 4.1 MATERIAL USED

Samples of four rock types, namely, Stanstead granite, gneiss (metasedimentary rock), limestone and marble, were tested. The marble sample was from Mines Gaspé, Québec; the gneiss was from Hemlo Gold Mine, Marathon, Ontario. The Stanstead granite was from the Beebe region, Ouébec, and the limestone from St. Catherines, Ontario.

Figure 4.1 shows the approximate lithology of the four rock types. The Stanstead granite is a coarse grained igneous rock with a slight gneissity. The gneiss is a metamorphic rock with intermediate sized grains having well developed foliation. The limestone is highly anisotropic in nature; a well developed conglomerate of different minerals is present irregularly in this rock type. The marble is fine-grained, with well-defined foliation planes filled with fine grained minerals, including specs of biotite.

# 4.2 ESTIMATION OF THE WORK INDEX

## 4.2.1 CHOICE OF APPARATUS

Since the objective of this work is to correlate an index used to estimate comminution energy requirements to some easily measurable physico-mechanical rock properties, the various apparati used for energy index measurements are compared. The Hardgrove Index, as mentioned in the previous chapter, measures the friability index of soft materials (such as coal), and is, therefore, unsuitable. The Bond ball mill test, on the other hand, is used to measure the work index in finer sizes, 100% -3.36 mm (6 mesh), which is roughly the product of the rod-mill. This size is too small to be well correlated with blasting energy requirements. The rod mill, however, with a feed size of 100 percent passing 13.2 mm, is more suitable, and was our final choice. Bond's pendulum test for

2

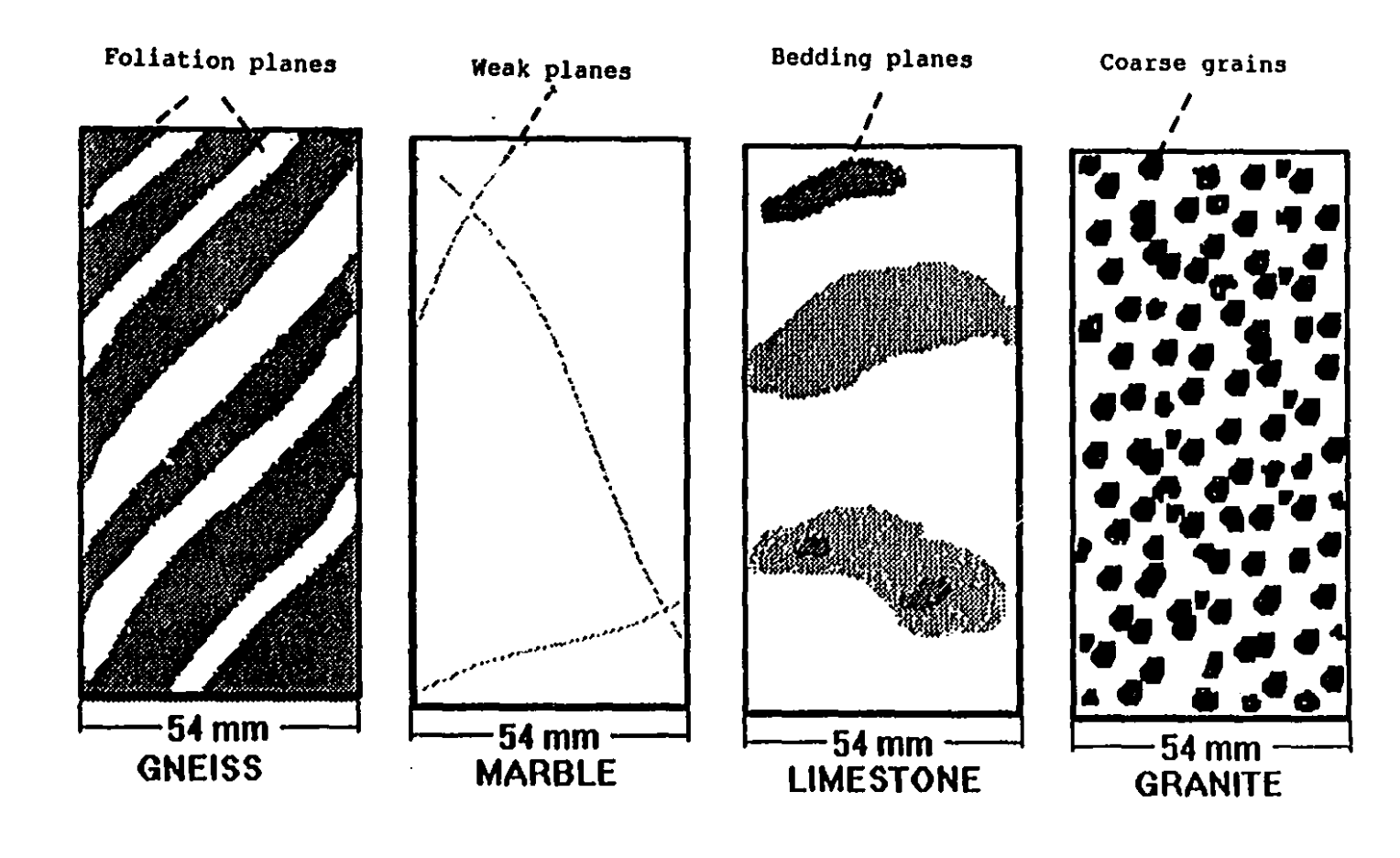


Figure 4.1: APPROXIMATE REPRESENTATION OF THE SAMPLES

crushing energy determination [57], with even coarser feeds (typically -75 mm), would be better suited, but was unavailable at McGill University.

### 4.2.2 DETERMINATION OF THE WORK INDEX

The traditional method of Bond index determination is a locked cycle test which was described in section 3.4.3. The target is to achieve a product with 50% undersize by weight. For this work, a product size of 1180  $\mu$ m, which is a typical value for this test, was used. The required number of revolutions was estimated using a population balance model (PBM)<sup>3</sup>. The breakage function used for all rock types was that of a sample from Baskatong Quartz, Saint-Urbain [66]. The selection function used to predict the required number of mill revolution was updated after each cycle, which provided another basis for determining that steady-state had been reached. The selection function was estimated using the GWBASIC software "BALLMILL" and "BALLDATA", developed at McGill University.

The 80% passing size of the fresh feed,  $F_{\infty}$ , was determined by screening. The grams per revolution (GPR) was determined at steady state, when the desired circulating load, 100%, was achieved; the 80% passing size of the undersize,  $P_{\infty}$ , was determined by screening the product of the last cycle. The work index,  $W_{i}$ , is then calculated from following formula:

$$W_{1}(kWh/t) = \frac{1.102*62.5}{GPR^{0.25} \cdot p^{0.23} \cdot (\frac{1}{\sqrt{P_{80}}} - \frac{1}{\sqrt{F_{80}}})}$$
 4.1

where p is the product size at which  $W_i$  is determined (1180  $\mu m$  in the present tests). The steps of the work index determination are shown in Figure 4.2.

<sup>&</sup>lt;sup>5</sup> The rationale for using the PBM is its ability to converge to the correct number of revolutions more rapidly. This benefit is to no avail if the breakage function of each material tested is to be determined, a very time-consuming task.

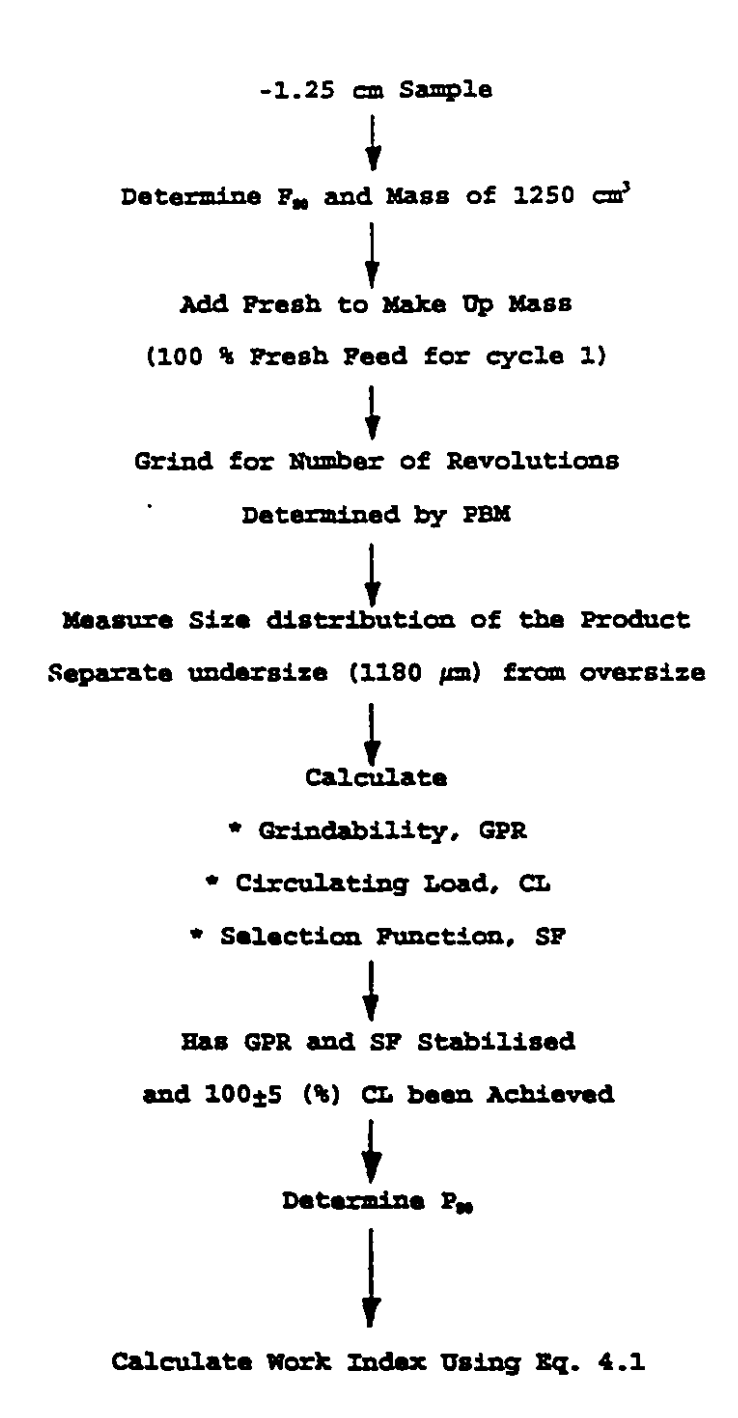


Figure 4.2: Steps followed in rod mill work index determination.

#### 4.3 PHYSICO-MECHANICAL TESTS

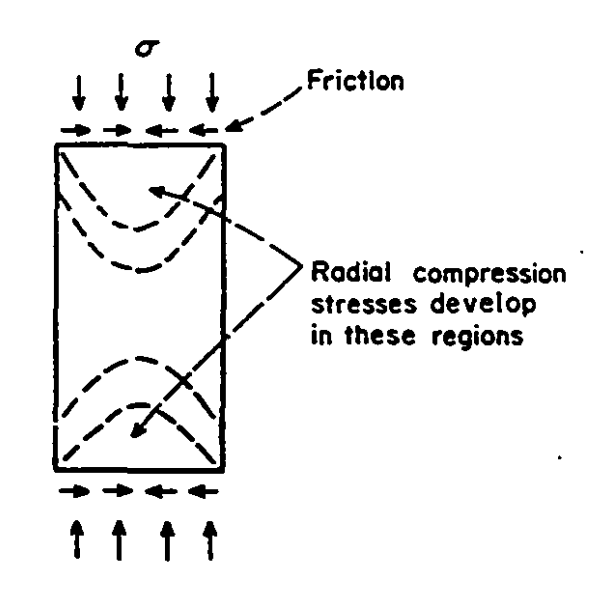
## 4.3.1 STATIC PROPERTIES OF ROCKS

4.3.1.1 UNCONFINED COMPRESSIVE STRENGTH: The compressive strength of a rock as defined by ASTM 2938-86 [67] is the load at failure per unit cross section area of the core sample, provided the sample geometry is according to ASTM or ISRM standards [68]. This is determined in the laboratory by a servo-controlled hydraulic stiff testing machine (RDP-2000). A typical layout is shown in Figure 4.3. A cylindrical sample of rock, with its length to diameter (54 mm) ratio varying between 2 and 2.5, is taken as the standard. The sample ends are maintained flat and perpendicular to the axis with a lapping machine. It is loaded axially using spherical seating at the top under the testing machine. The ultimate compressive stress at failure gives the unconfined compressive strength.

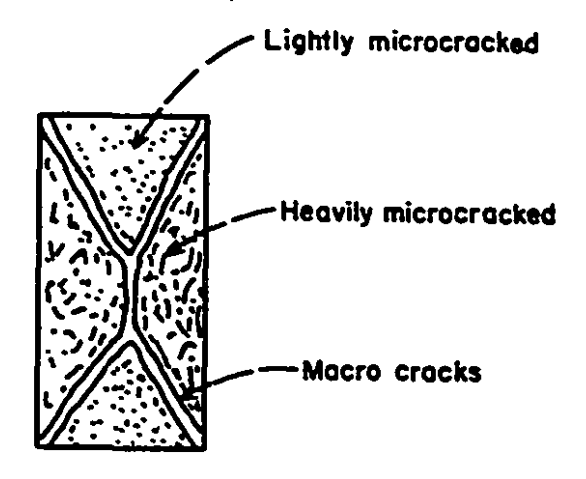
The end effects of the rock sample are not well understood. If high friction is introduced at the end planes, a characteristic shear conical fracture occurs giving high value of strength. However, in case of soft capping or in presence of lubricants between the platens and the specimen, the sample splits in tensile failure with a lower compressive strength. The larger the sample size, the weaker is the strength in compression. This can be explained by weakest link theory [28]. The bigger the sample, the greater is the chance of weak link. Moreover, in the case of a large length to diameter ratio, the sample breaks in bending before the development of shear force. A formula is given by Obert and Duvall [69] to correct the compressive strength  $(\sigma_e)$  for a length (L) to diameter (D) ratio with respect to 1:1 ratio.

$$\sigma_c = \sigma_{c(1:1)} \cdot [0.778 + \frac{0.222}{L/D}]$$

A high rate of loading tends to increase the compressive strength of a material. However, normal rates of loading, such as 0.5-3.0 MPa/s, show



# Stress Pattern



Conical Failure

Figure 4.3: General layout of unconfined compressive strength test [28].

no significant change in compressive strength [70]. The presence of moisture reduces the bonding strength, thereby reducing the compressive strength. Since the extent of strength reduction depends on the rock type and the test condition, moisture should always be reported. present tests, dry samples were used. In the laboratory tests the effect of macro structure on compressive strength can be assumed to be negligible. Micro structure (i.e. the type of grain, grain size and grain packing density) does affect the strength of a rock but its effect is known only qualitatively. The post failure behaviour of rock during compressive strength test is guided by the stiffness of the machine. A soft machine releases all the energy stored at failure which exceeds that required by the rock sample. The failure is therefore violent, due the excess of energy. In a stiff machine, the energy released by the machine is not sufficient in comparison with the energy required by the rock The excess energy available in the rock is used in further deformation of the rock. In the latter case, the post failure curve is studied by 'servocontrolled testing machine.'

4.3.1.2 TENSILE STRENGTH: The tensile strength of the rock samples was determined by the ASTM method, D 3967-86 [71], by the so called 'Brazilian Test' [72]. The rock samples prepared were of approximately same length and diameter (54 mm), as per the ISRM recommendations. The cylindrical rock specimen, lying on its side, is loaded diametrically under compression (Figure 4.4). A vertical fracture develops along the applied load due to the tensile stress. The tensile strength ( $\sigma_0$ ) of the rock in this test is calculated by equation:

$$\sigma_t = \frac{2 \cdot P}{\pi \cdot D \cdot t}$$

where P is maximum load at failure, D is diameter of the specimen, and t is height or thickness of the specimen.

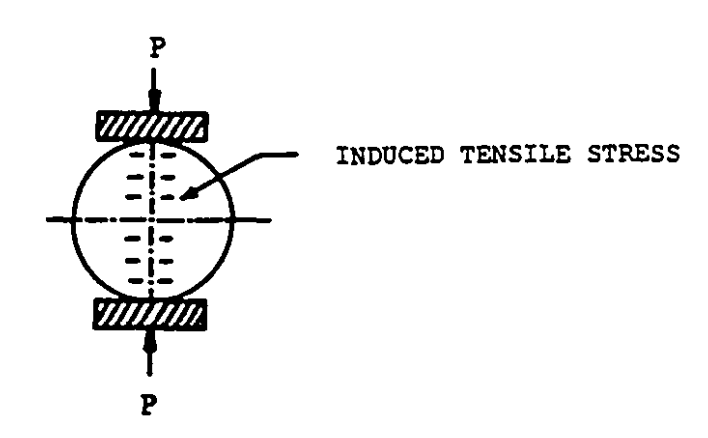


Figure 4.4: Schematic diagram showing Brazilian test [28].

It should be mentioned that the static strength tests conducted for the rock samples were performed at random orientation with respect to the bedding planes (as the core samples drilled from the rock were not consistent with respect to plane of weakness). The load applied was not consistent with reference to the plane of weakness. This resulted in larger than normal scatter in data but it was in keeping with the intention of obtaining 'global' properties rather than that along any specific direction.

4.3.1.3 <u>BULK DENSITY</u>: Since the rock samples used for the tests had regular geometrical shapes, their density was calculated by measuring their volume and mass at room temperature. The effect of moisture present at room temperature in the rock was neglected.

#### 4.3.2 DYNAMIC PROPERTIES OF ROCK

The strength of rock is only one of the physical properties defining its reaction to explosive action. The strength of the rock --e.g. compressive and tensile strengths measured by fracturing the sample-- is valid for static or quasi-static loads. It may not be accurate in

describing the response of rock during blasting, an intensely dynamic process. However, the dynamic properties of rocks, such as the P and S wave velocity and the moduli of elasticity, reflect its strength against rapidly increasing load and vibrations, such as those present during blasting. These dynamic properties were evaluated by non-destructive ultrasonic methods for the present work. The dynamic elastic moduli can be calculated from three independent rock properties, namely the 'P' and 'S' wave velocities in the rock, and its bulk density. These wave velocities are measured by transmitting an ultrasonic pulse through the rock using an electric probe. The outgoing pulse is detected by another probe and the movement of acoustic wave is observed through an oscilloscope connected with the ultrasonic instrument. A typical wave pulse consisting P and S waves is shown in Figure 4.5.

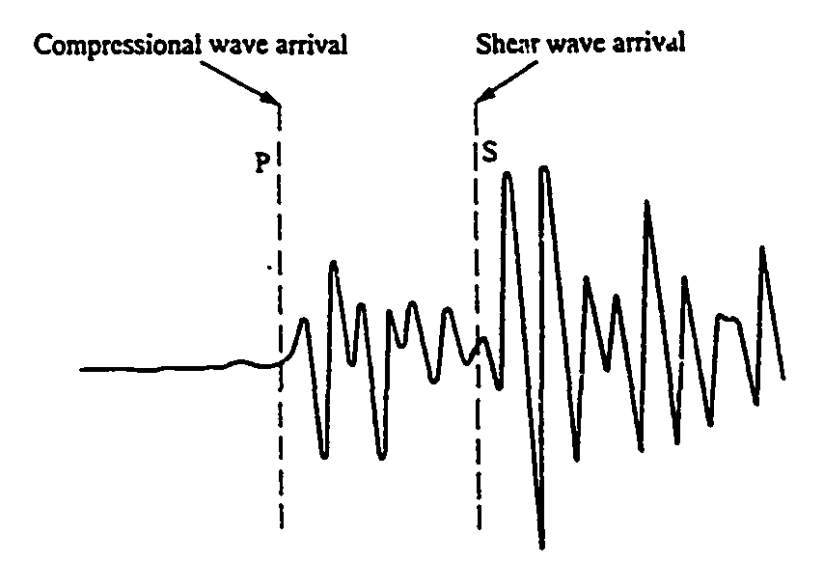


Figure 4.5: A typical wave train in an ultrasonic test.

By measuring the distance, L (m) and the time, T (sec.) required for compressive or shear pulse to travel through the rock, the corresponding longitudinal or shear wave propagation velocity can be determined: The travel time was measured with an oscilloscope having a calibrated sweep rate by initiating the sweep with the driving pulse and recording the arrival of the pulse from the transducer.

$$C_p = \frac{L_p}{T} \quad (m/s)$$

$$C_s = \frac{L_s}{T} \quad (m/s) \tag{4.3}$$

where  $L_p$  and  $L_s$  are the distance traversed by the primary and secondary waves in a time of 'T'.  $C_p$  and  $C_s$  are the 'P' and 'S' wave velocities, respectively. Young's modulus, the bulk and shear moduli, and Poisson's ratio were calculated indirectly by measuring the P and S wave velocities in the rocks and its bulk density. Due to the inhomogeneity and anisotropic nature of the rock the wave velocities were measured along several directions. Moisture content affects the modulus of elasticity; for this work, dry core samples were tested. If the bulk density of the rock is  $\rho$ , then the Young's modulus of elasticity (E), the bulk modulus (K), the shear modulus ( $\mu$ ) and the Poison ratio ( $\nu$ ) are given by following formulae:

$$Y = \frac{p \cdot C_g^2 \cdot (3C_p^2 - 4C_g^2)}{C_p^2 - C_g^2}$$
 4.4

$$K (GPa) = \rho (C_p^2 - \frac{4}{3}C_s^2)$$
 4.5

$$\mu (GPa) = \rho.C_s^2$$
 4.6

$$v = \frac{C_p^2 - 2C_s^2}{2(C_p^2 - C_s^2)}$$
 4.7

These elastic constants are determined without any externally applied load. In the presence of axial load or confinement, their value would increase. Details of the experimental procedure can be found in the ASTM designation D 2845-83 [73].

# 5.0 RESULTS

# 5.1 WORK INDEX

A summary of the important variables --grindability (grams per revolution, GPR), feed and product size,  $F_{80}$  and  $P_{80}$ -- and the work indices of the four rock samples is shown in Table 5.1.

TABLE 5.1

	SUMMARY OF TH	HE WORK INDEX	OF TEST ROCK	TYPES
Rock type	GPR	P <sub>so</sub>	F <sub>80</sub>	Work Index
Unit	(g/rev.)	(mm)	(mm)	(kWh/t)
Granite	25.30	0.93	9.74	7.8
Gneiss	· 14.31	0.84	8.46	10.8
Limestone	7.82	0.96	9.20	17.0
Marble	6.03	0.91	9.20	19.2

Details of the work index determination of the limestone sample are shown in Table 5.2 (similar tables for the other three samples are shown in Appendices A1-A3). These include the original size distribution of the sample and that of the product of all cycles, the selection function of each cycle (used to calculate the number of revolutions needed for the following cycle), the GPR of all cycles and the size distribution of the product of the last cycle (to calculate the  $P_{\rm m}$ ).

TABLE 5.2: Details of work index determination for limestone

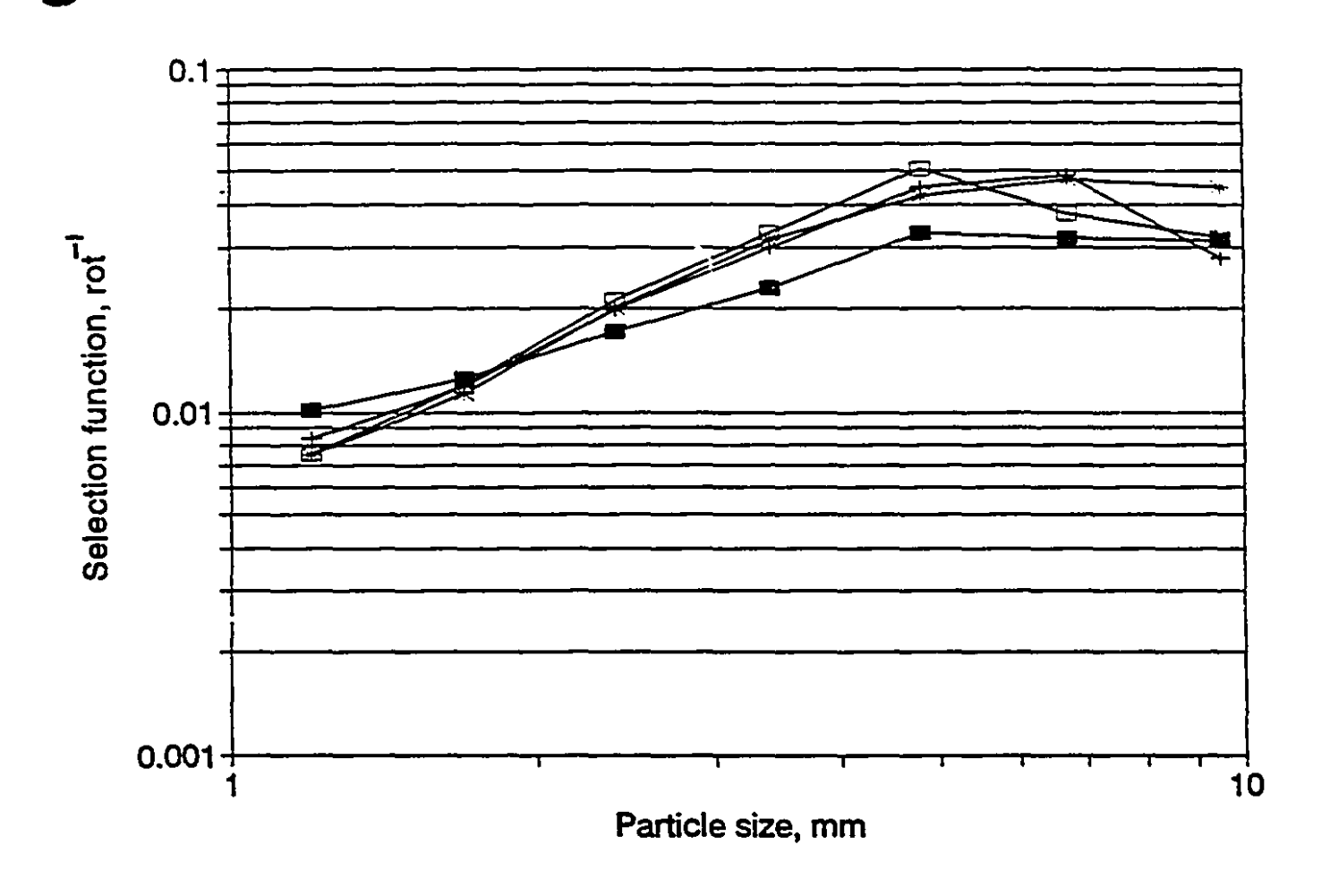
(mm) Rev. 120 120 99 104	
9.5 17.84 0.40 0.35 0.12 0.31	
6.7 20.00 1.30 0.29 0.38 0.66 Limestone	
4.8 14.70 2.30 0.58 1.01 0.68	
3.4 10.66 5.90 2.15 2.71 2.05 F80: 9200 micrometre	
2.4 7.71 9.72 6.39 6.99 5.71 P80: 960 micrometre	
1.7 6.63 12.85 14.84 16.06 14.36 GRP: 7.82 grammes per	rev.
1.2 5.26 13.05 20.02 24.00 25.23 P: 1180 micron.etre	
-1.2 17.20 54.48 55.38 48.75 50.69 WI: 17 kWh/t	
Mass: 1920 grammes	
Tot. 100.00 100.00 100.00 99.99	
grammes per rev. 5.97 7.37 7.62 7.82	
Product size	
Diam. selec. selec. selec.	
(mm) funct. funct. funct. Diam. Passing passing	
(mm) grammes %	
9.5 0.0316 0.0280 0.0449 0.0322	
6.7 0.0321 0.0488 0.0475 0.0379 0.9 133.3 27.84	
4.8 0.0332 0.0448 0.0426 0.0510 0.6 79.9 16.69	
3.4 0.0228 0.0300 0.0318 0.0332 0.4 58.71 12.26	
2.4 0.0170 0.0198 0.0200 0.0210 0.3 43.56 9.10	
1.7 0.0125 0.0118 0.0113 0.0119 -0.3 163.33 34.11	
1.2 0.0101 0.0084 0.0075 0.0076 Total 478.8 100	

The selection function of each cycle for the limestone sample is shown in Figure 5.1, as a function of particle size, on a log-log scale. It eventually converges to a constant curve for cycle 4, except for the two coarsest size classes, where the limited mass of material in the product (0.3-0.6%) makes its determination inaccurate. Similar plots for the other rock types are shown in Appendices A4-A6. Figure 5.2 compares the absolute selection functions (in revolution) of the last cycle for the four rock types. Because different masses were used, the selection functions (SFs) were normalized for a mass of 1920 g (used for the limestone sample):

$$SF_{monthsd} = SF \times (actual mass/1920 g)$$

5.1

The normalized selection function of the four rock types (last cycle) is shown in Figure 5.3. As expected, the selection function particle size relationship was found to be a) size dependent and approximately linear, b) material specific (SF line for granite is at higher level than that of marble) of similar slope, with no obvious correlation with the work index itself. Further there is little difference between the absolute and normalized selection function plots, presumably because all four materials have a similar density, hence similar masses for the Bond test. The regression output obtained from ln(size) and ln(selection function) plot for both absolute and normalized selection function is shown in Table 5.3.



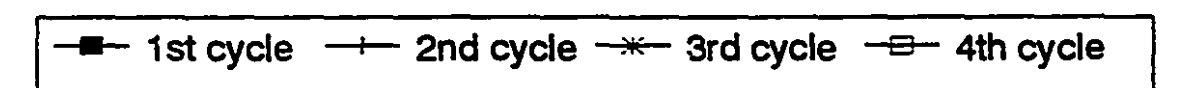


Figure 5.1: Selection functions vs. size classes determined during the work index test of limestone rock type.

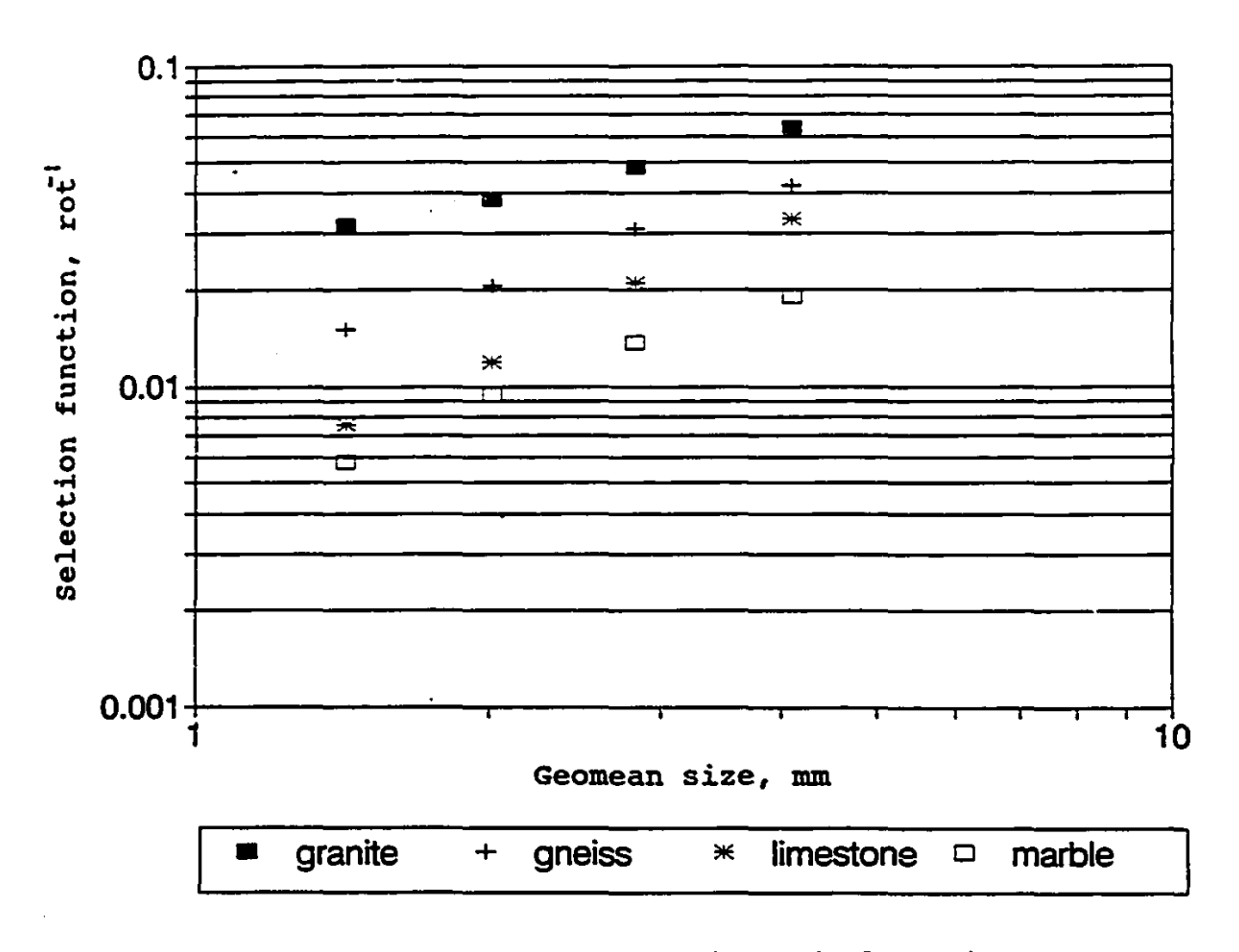


Figure 5.2: Absolute selection function of the four rock types with respect to geomean size of the four lower size classes.

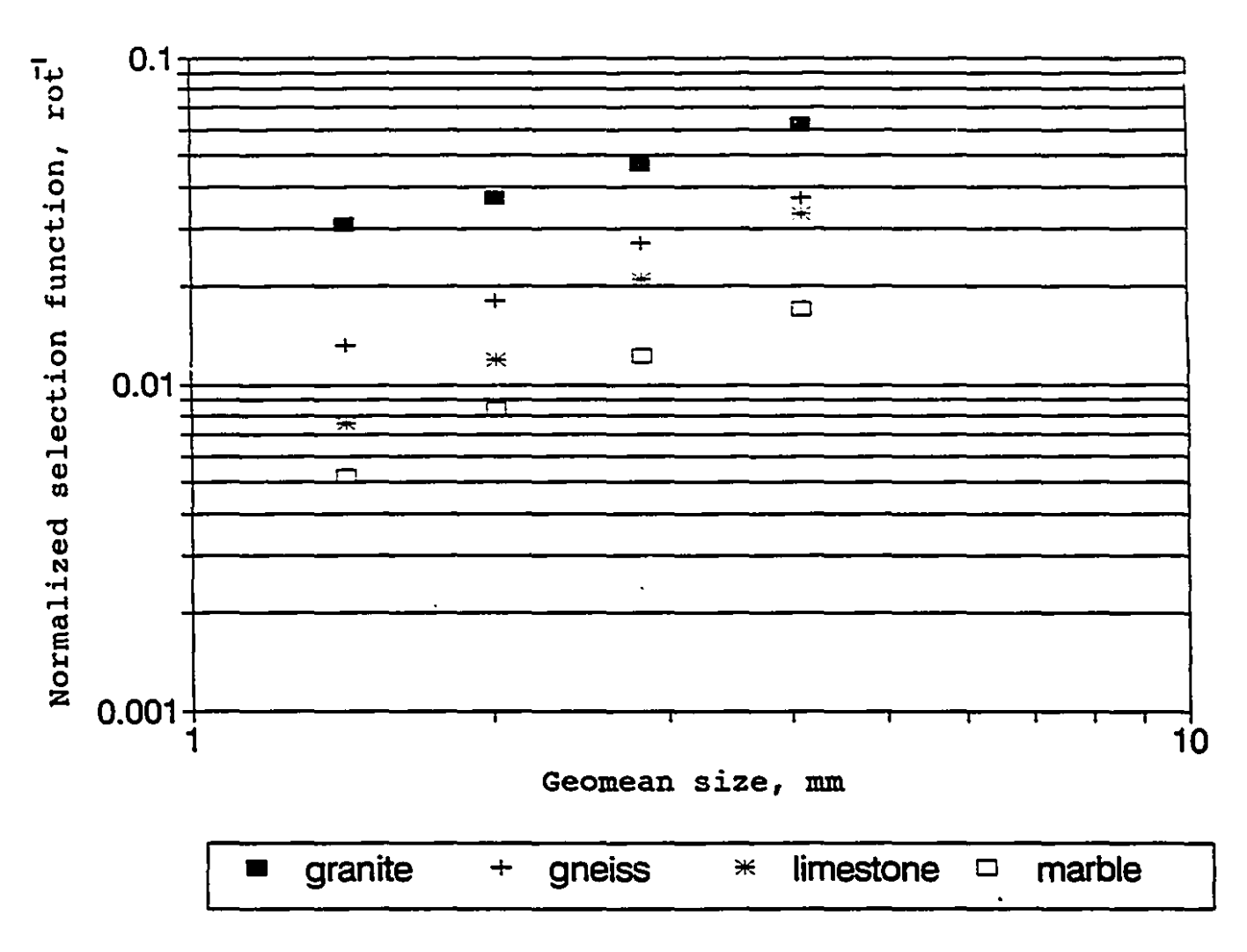


Figure 5.3: Normalized selection function of the four rock types as a function of particle size (geomean of the four finest size classes).

Table 5.3 Regression output of ln (size) and ln (SF) relationship.

	Size vs. Absolute selection function								
ROCK	Constant	X coeff.	r²	Err. of Y	Err. of Const.				
Granite	-3.599	0.673	0.994	0.028	0.036				
Gneiss	-4.383	0.994	0.996	0.037	0.047				
Limestone	-5.147	1.422	0.996	0.047	0.061				
Marble	-5:308	1.122	0.989	0.064	0.082				
	Size vs	. Normalize	d select	ion function	- <del></del>				
Granite	-3.630	0.673	0.994	0.028	0.036				
Gneiss	-4.514	0.994	0.996	0.037	0.047				
Limestone	-5.148	1.423	0.996	0.475	0.061				
Marble	-5.421	1.122	0.989	0.064	0.082				

Limestone has the highest slope (significantly higher than the other three rock type). It is difficult to assess the origin of the higher slope, but the WI appears better correlated with the SF of the 1.2-1.7 mm than the 3.4-4.8 mm. This suggests a fissure or intergranular network that assists the breakage of the coarser size class. To investigate further this correlation, the work indices of the four rock type were plotted with respect to the selection function (both absolute and normalized as per Eq. 5.1) and are shown in Figures 5.4 and 5.5. The work index and its natural logarithm were regressed against the logarithm of the selection function. The regression out put are shown in Table 5.4.

Table 5.4 Regression output of logarithm (WI) and logarithm (SF).

	Work index vs. Absolute selection function									
Size	Constant	X coeff.	r²	Err. of Y	Err. of Const.					
1.2 mm	0.253	-1.828	0.991	0.088	0.123					
1.7 mm	-0.233	-1.499	0.988	0.082	0.114					
2.4 mm	-0.416	-1.272	0.954	0.142	0.198					
3.4 mm	-0.377	-1.152	0.881	0.214	0.299					
	Work index	vs. Normal	ized sel	ection funct	ion					
1.2 mm	0.213	-1.840	0.971	0.160	0.223					
1.7 mm	-0,272	-1.511	0.961	0.155	0.216					
2.4 mm	-0.455	-1.283	0.904	0.213	0.296					
3.4 ೯-೧	-0.416	-1.164	0.814	0.282	0.393					

The logarithm of the WI, rather than the WI itself (regression output of work index and logarithm of selection function relationship is shown in Table 5.5), is better correlated with the selection function, normalized or not for the two finer size classes. There are no significant differences for correlation for the two coarsest size classes. Surprisingly, correlation is slightly better for the non-normalised SF, for either the WI or ln (WI) regressions of all four size classes. The most significant difference in correlation is associated with particle size: correlation clearly improves with decreasing particle size. This yields the highest slopes for the finest size class, with close to the smallest standard deviation. For example, for regression of the type  $\ln(SF) = b_0 + b_1 \cdot \ln(WI)$ ,  $b_1 = -1.828 \pm 0.123$  (a relative error of 6.7 %)

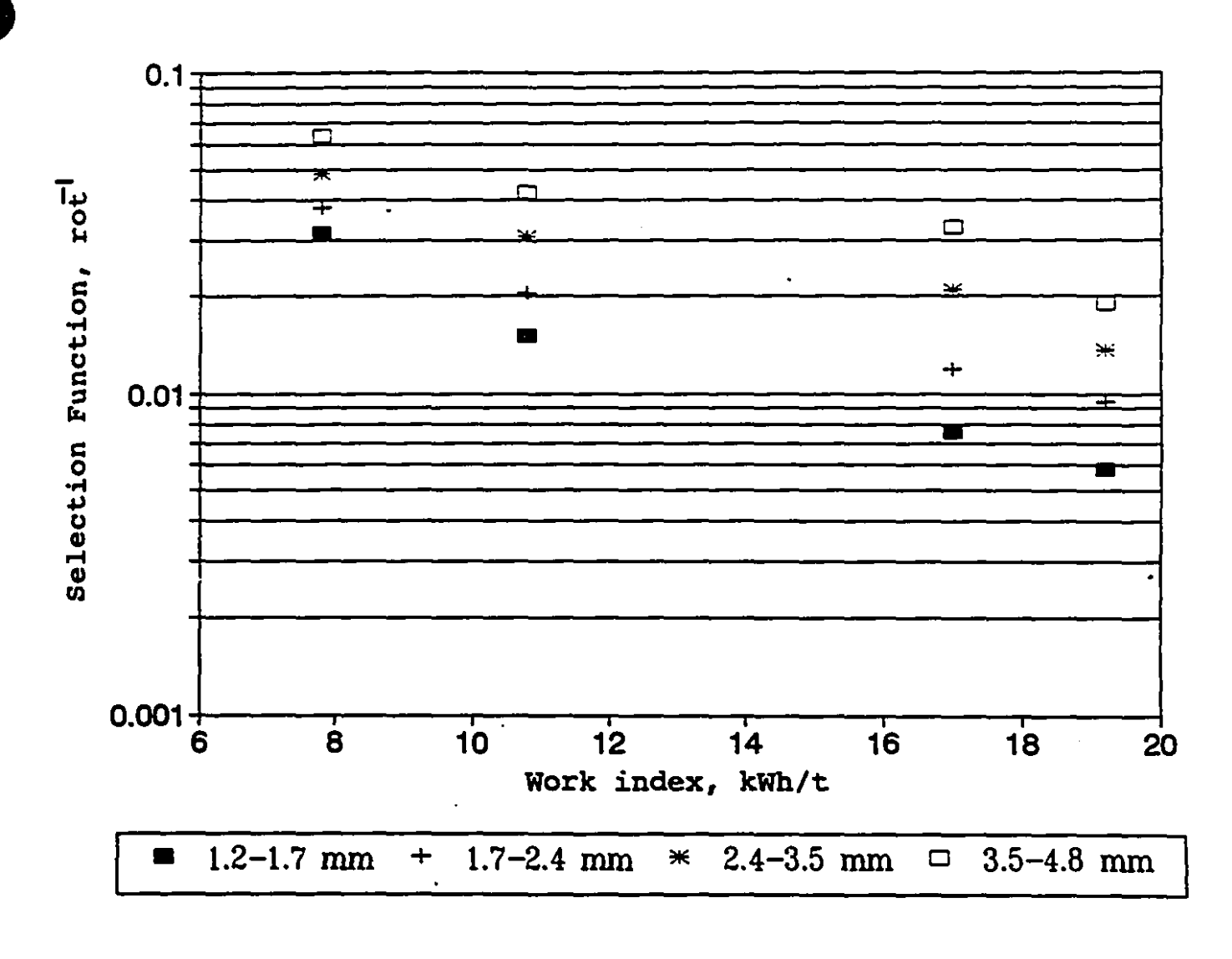


Figure 5.4: Absolute selection function of the four lower size classes and the work index of the four rock types

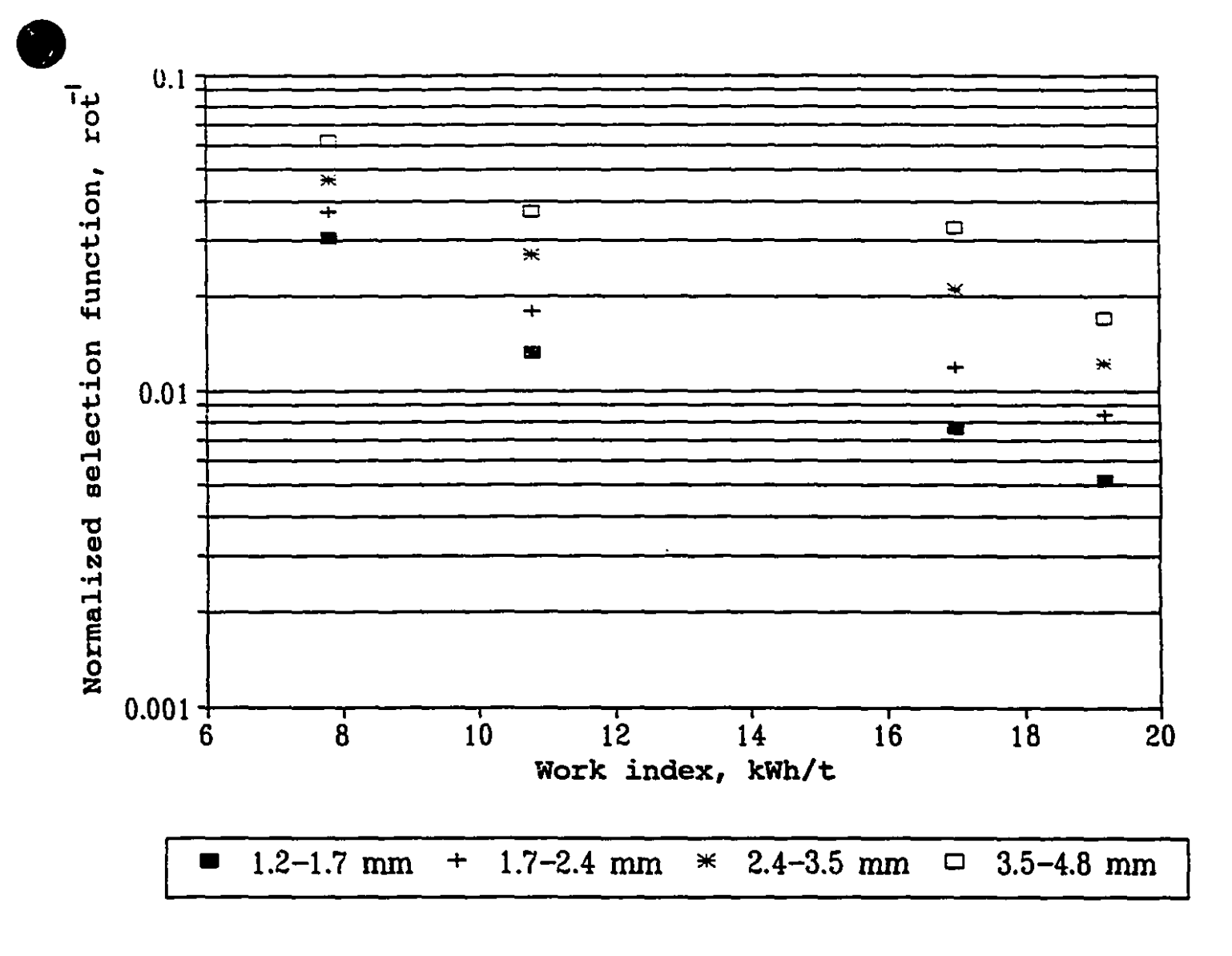


Figure 5.5: Normalized selection function of the four lower size classes and the work index of the four rock types.

€:

Table 5.5 Regression output of Work index and logarithm of SF.

	Work index vs. Absolute selection function									
Size	Constant	X coeff.	r²	Err. of Y	Err. of Const.					
1.2 mm	-2.482	-0.142	0.968	0.167	0.018					
1.7 mm	-2.476	-0.116	0.964	0.144	0.016					
2.4 mm	-2.300	-0.100	0.956	0.138	0.015					
3.4 mm	-2.076	-0.091	0.895	0.201	0.022					
	Work index	vs. Normal	ized sel	ection funct	ion					
1.2 mm	-2.542	-0.142	0.945	0.222	0.242					
1.7 mm	-2.536	-0.117	0.933	0.202	0.022					
2.4 mm	-2.361	-0.100	0.901	0.216	0.024					
3.4 mm	-2:136	-0.091	0.821	0.276	0.030					

for the 1.2-1.7 mm, compared to  $b_1 = -1.152 \pm 0.295$  (a relative error of 25.6 %) for the 3.5-4.8 mm. This is not surprising, given that the finest size class has the lowest SF; hence, its breakage should be 'rate-limiting' (by analogy with a chemical reaction). This could indirectly support the Bond approach of characterising breakage with a single parameter, the GPR, which is the production rate of material finer than the finest size class (of the oversize).

#### 5.2 PHYSICO-MECHANICAL PROPERTIES

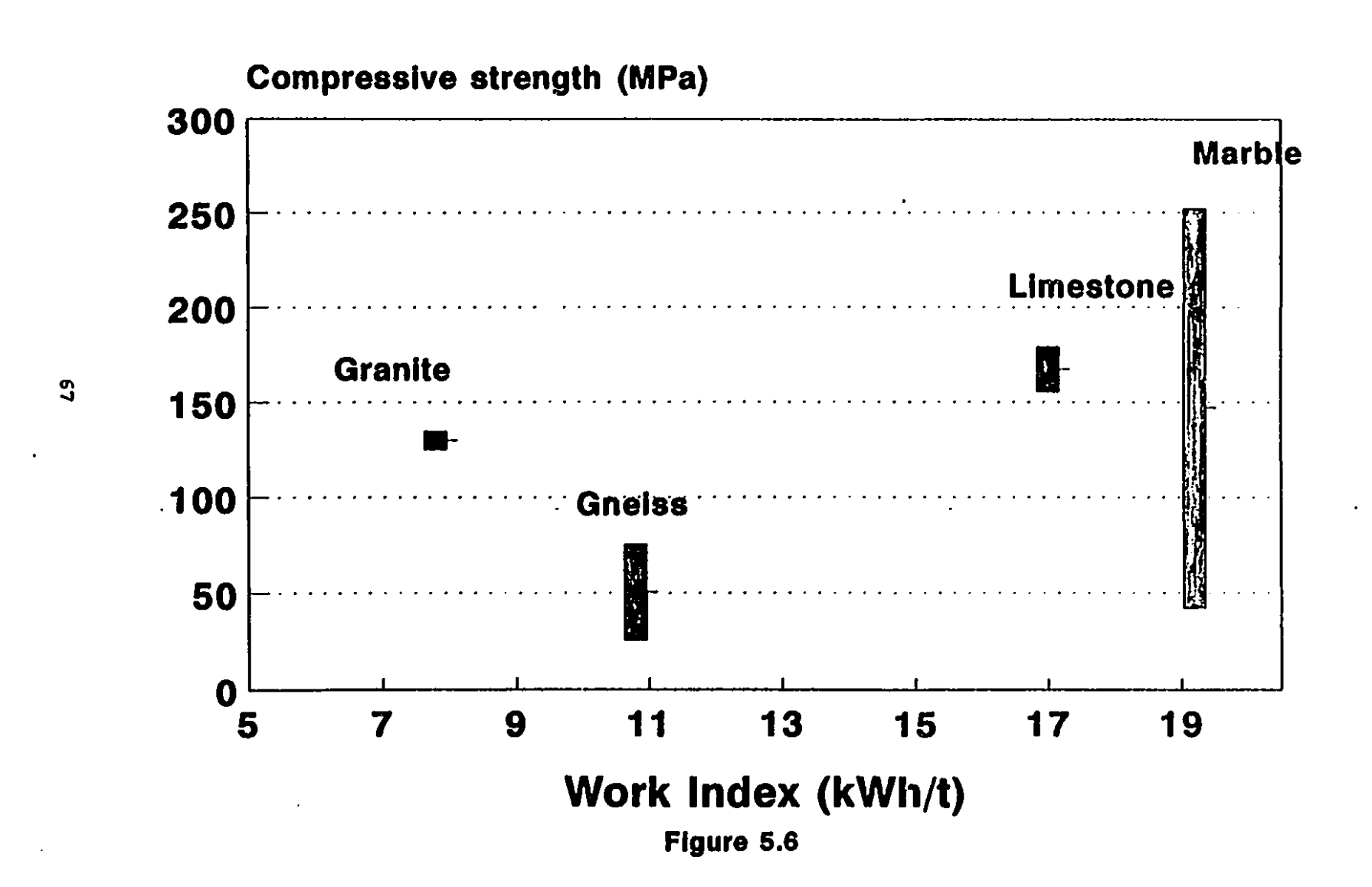
The physico-mechanical properties of the four rock types are shown in Table 5.6; the work index is also shown as a reference (these are plotted in Figure 5.6-5.15). The static properties are presented first, and

dynamic properties second. Errors are presented as  $\pm$  one standard deviation.

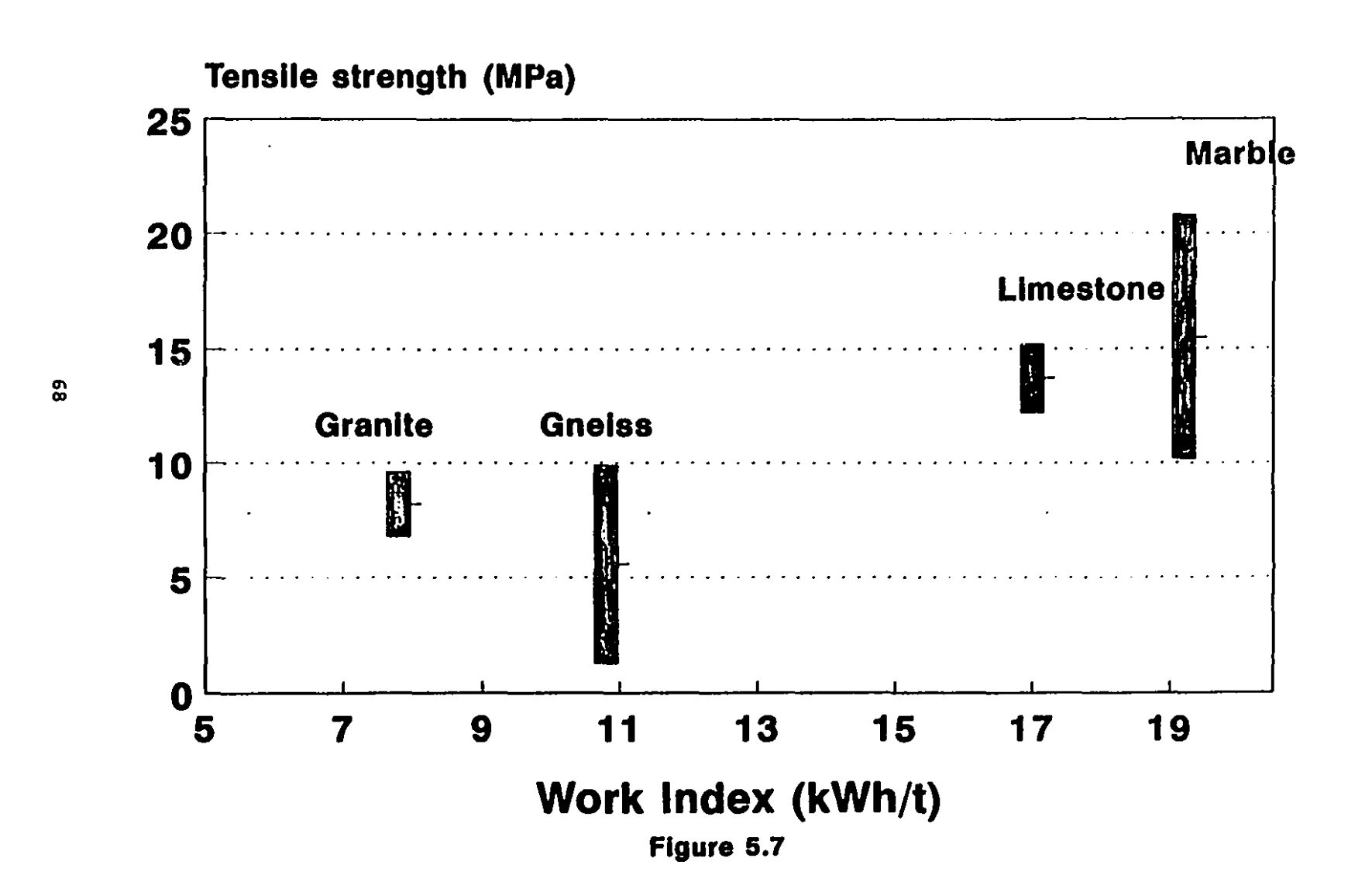
Table 5.6 Properties of rocks

Property	Unit	Granite	Gneiss	Limestone	Marble
Wi	MPa	7.8±0.1	10.8±0.1	17.0±0.2	19.2±0.2
σς	MPa	129.9±4.6	50.6±24.8	167.4±11.7	147.2±104.8
σι	MPa	8.2±1.4	5.6±4.3	13.7±1.5	15.5±5.3
P	kg/m³	2643±12	2789±24	2606±27	2864±28
C <sub>p</sub>	m/s	4170±100	4770±290	5300±318	5430±170
C,	m/s	2670±90	3080±110	3250±195	2830±85
Y	GPa	43.44±1.80	60.45±4.45	65.98±5.74	60.25±3.06
K	GPa	20.84±2.74	28.18±8.12	36.50±9.83	53.86±5.62
μ	GPa	18.84±1.27	26.46±1.90	27.52±3.32	22.94±1.40
ν	-	0.15±0.05	0.14±0.09	0.20±0.08	0.31±0.02

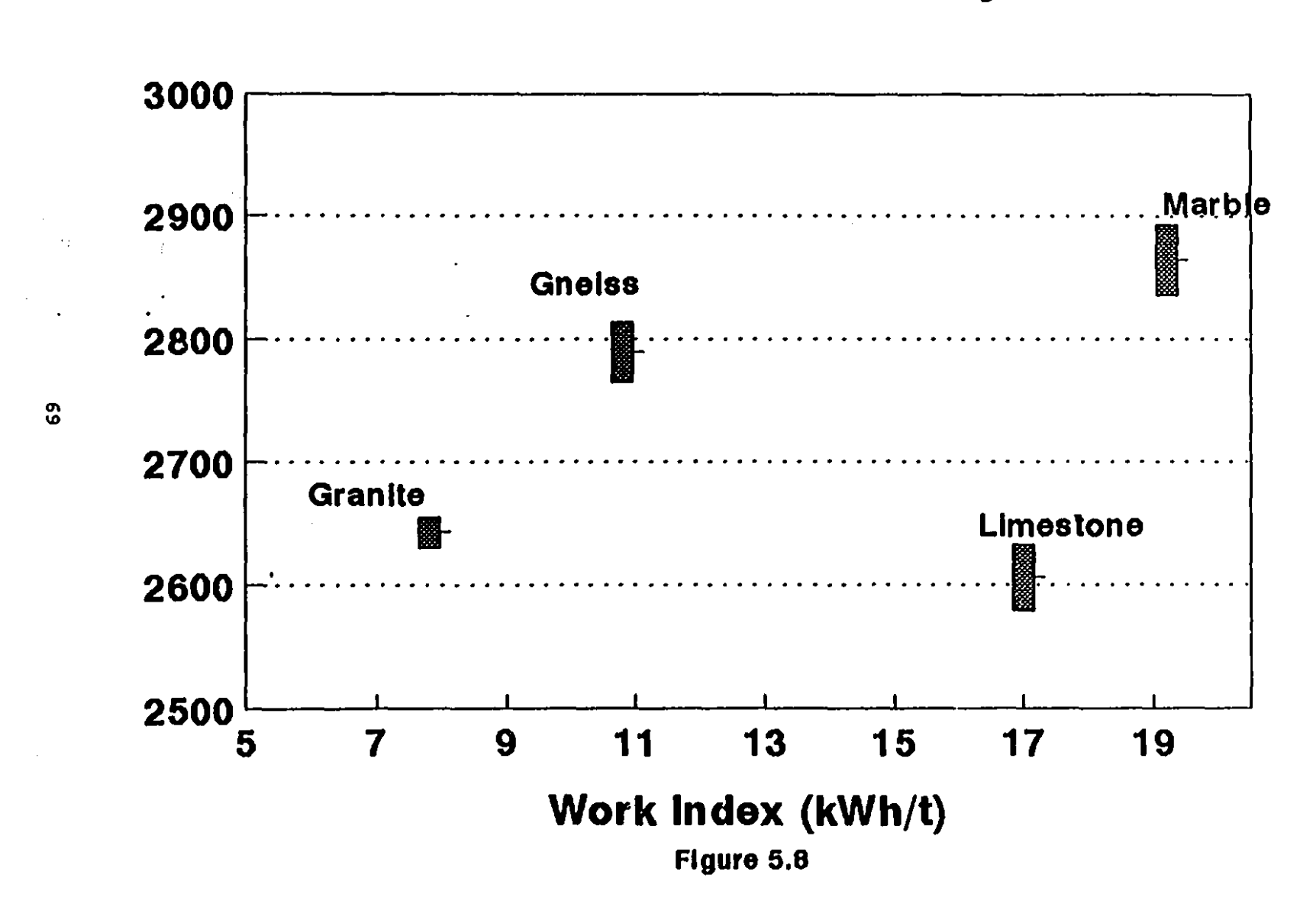
# WI and Compressive Strength



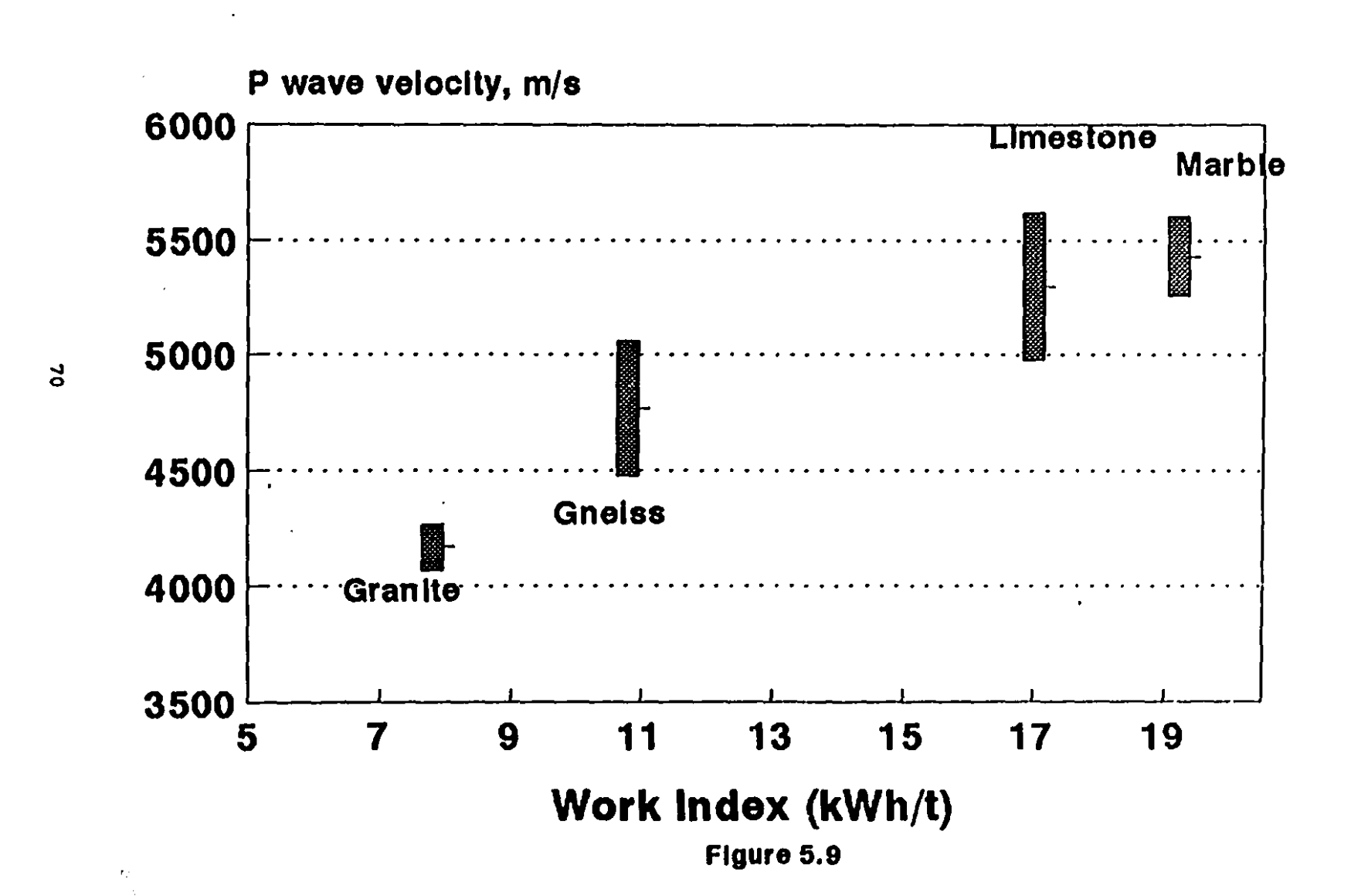
# WI and Tensile Strength



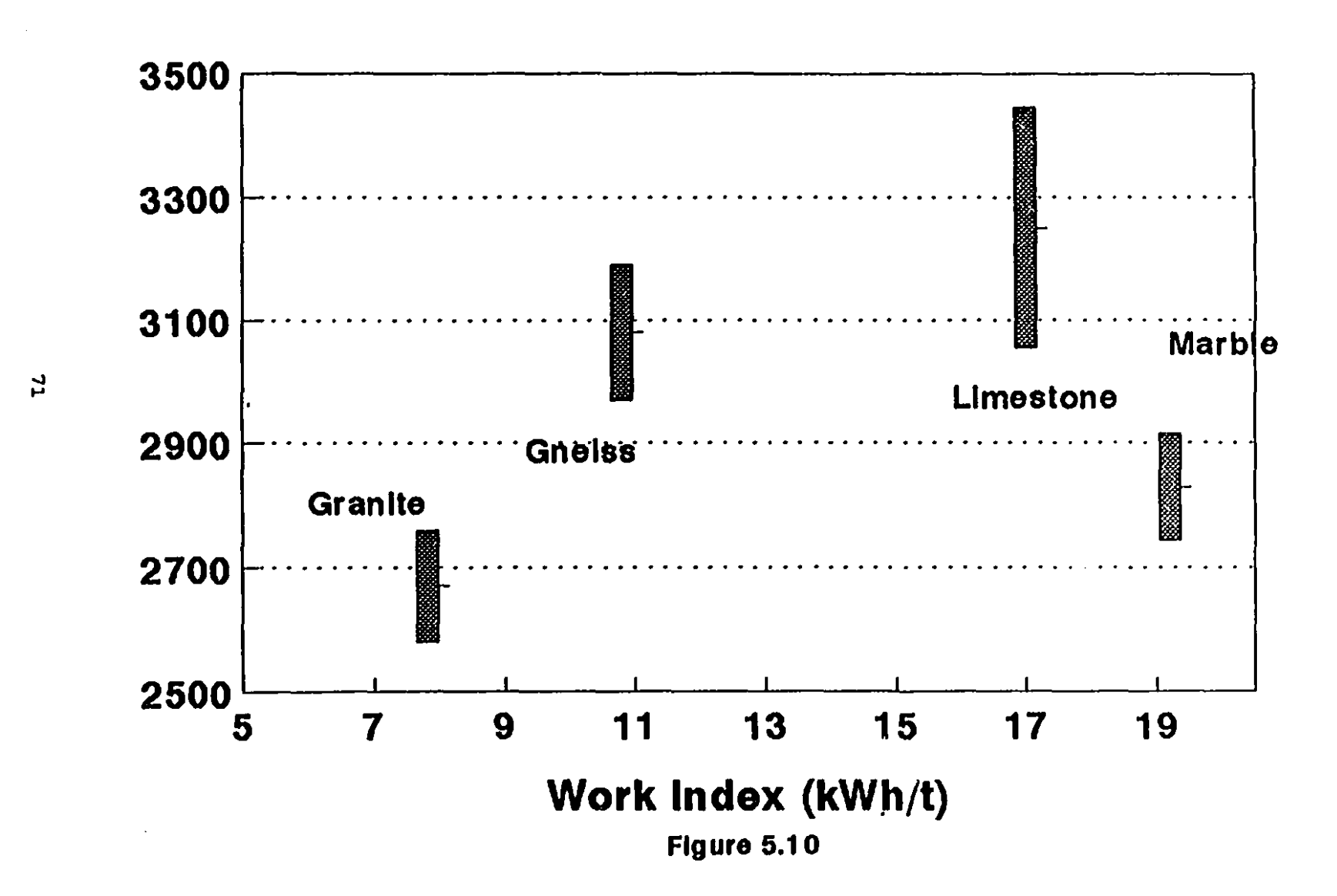
## WI and Bulk density



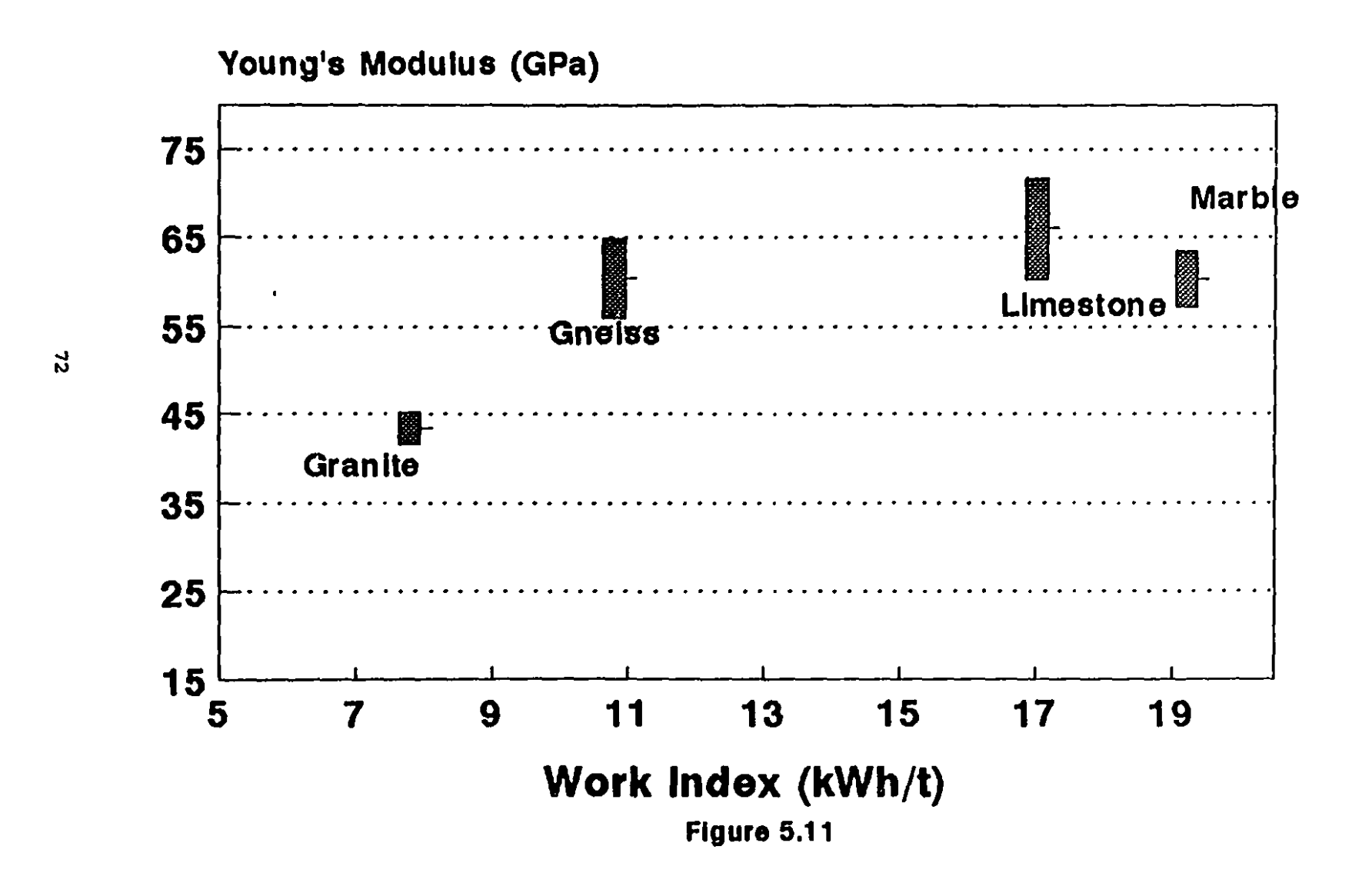
## WI and P wave velocity



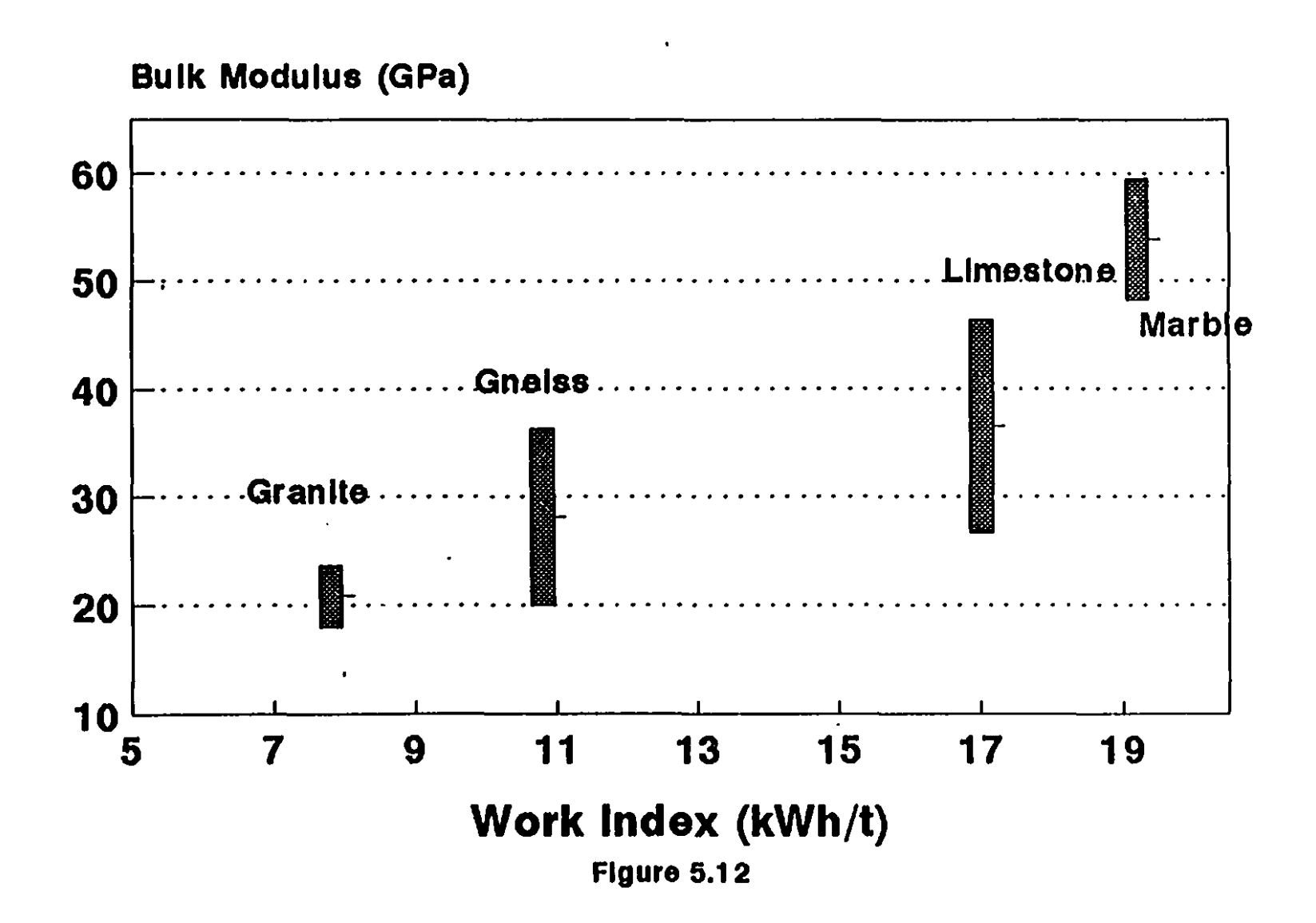
# WI and S wave velocity



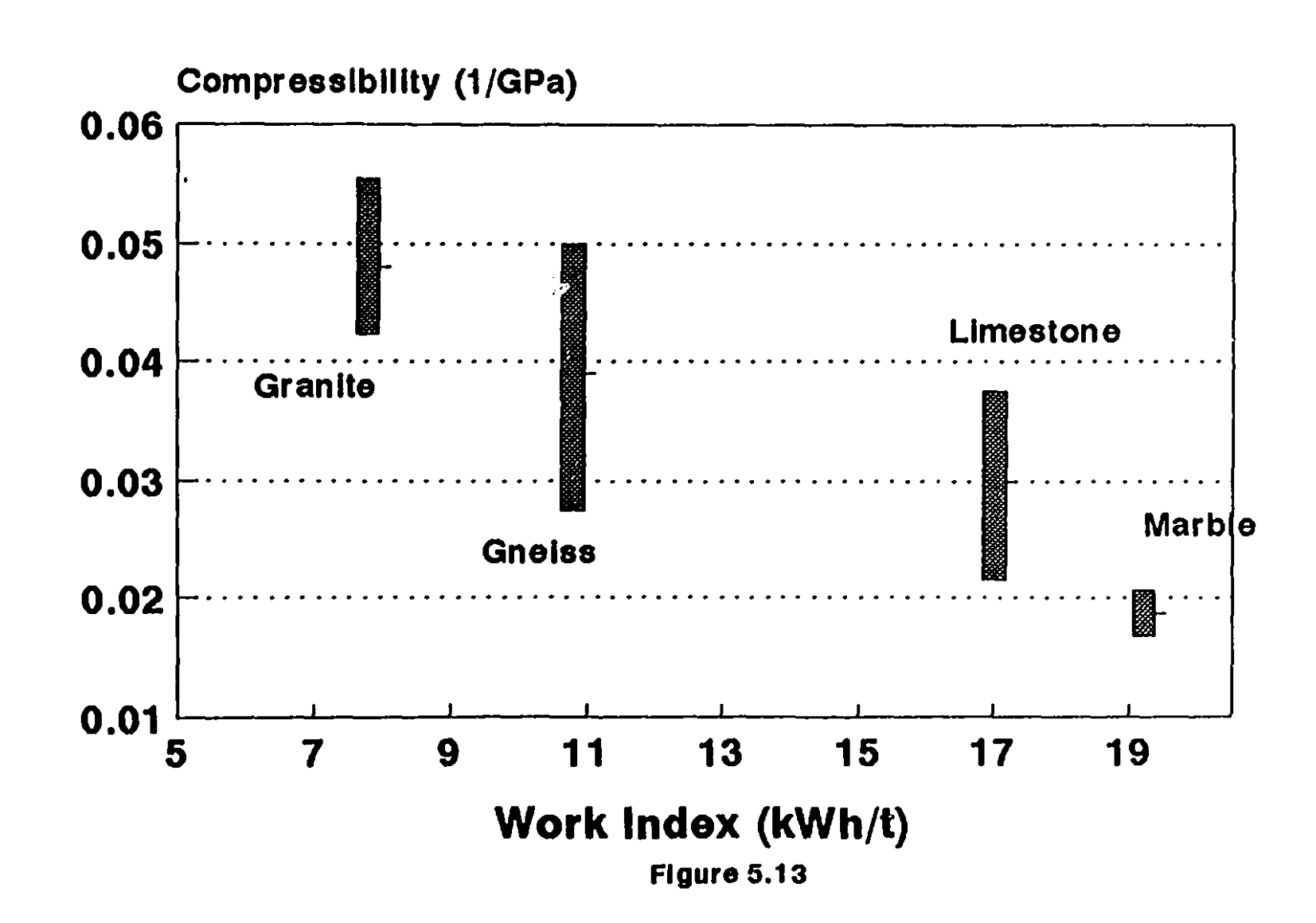
### WI and Dynamic Young's modulus



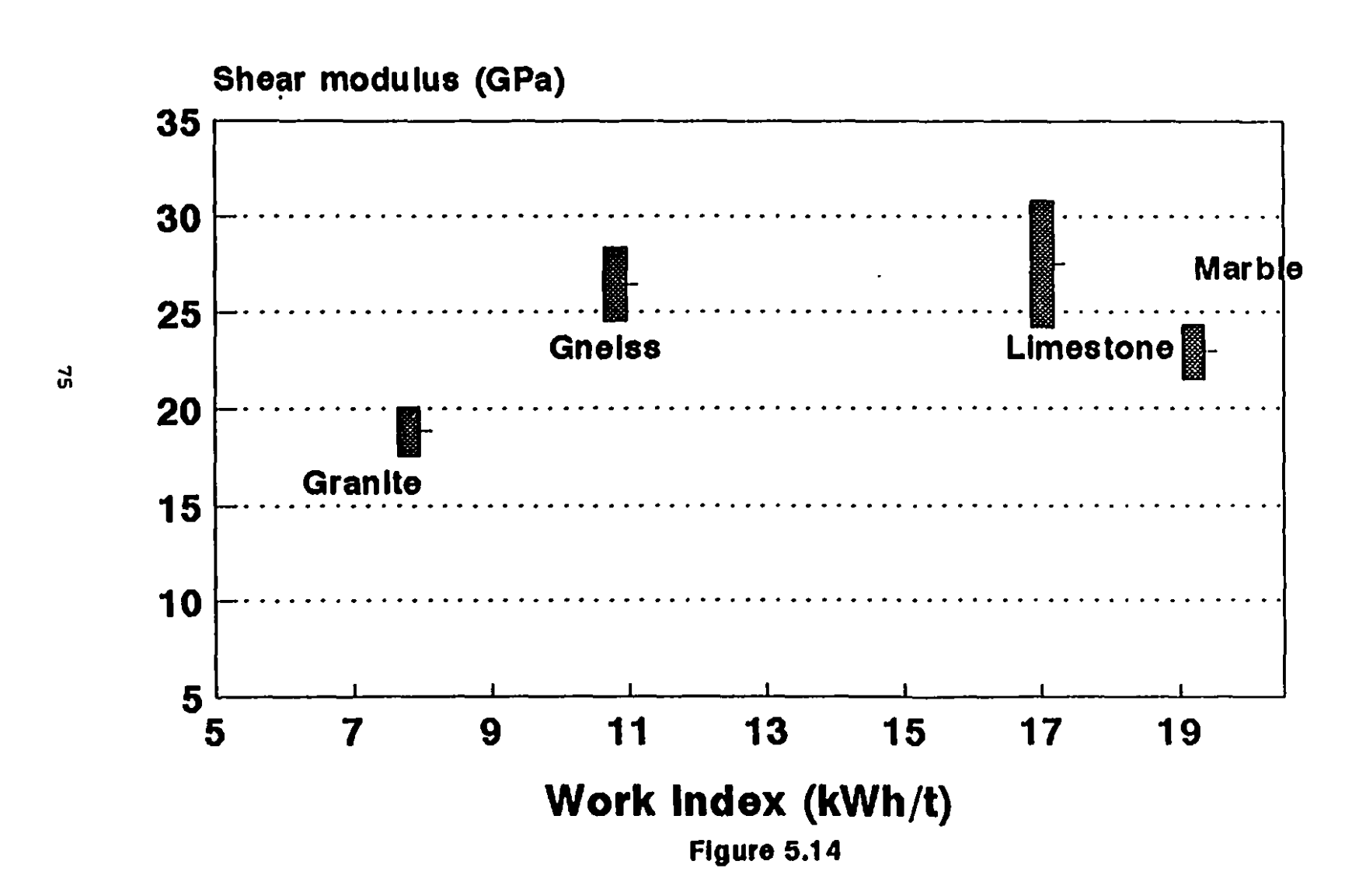
## WI and Dynamic bulk modulus



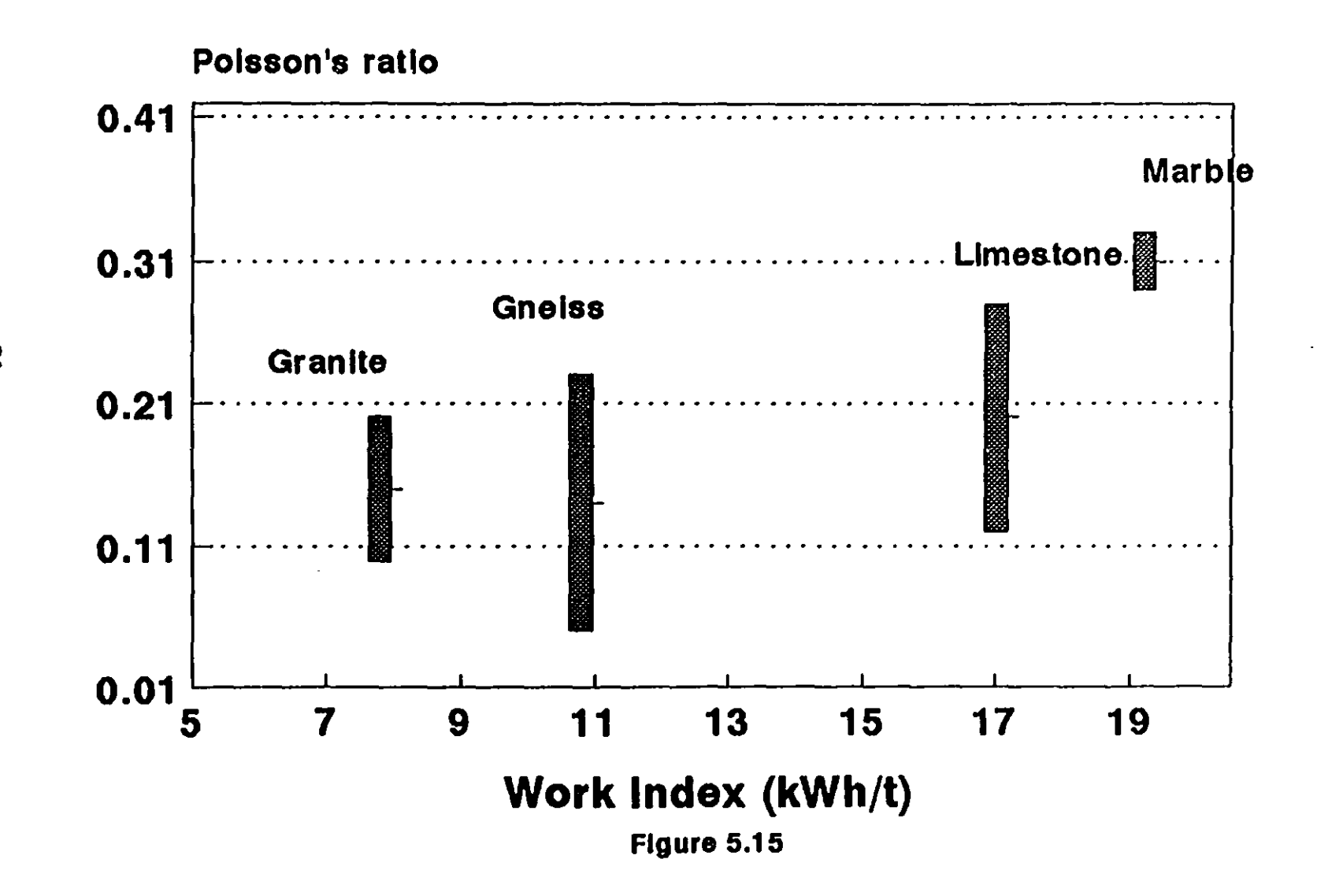
## WI and Compressibility



### WI and Shear modulus



### WI and Poisson's ratio



#### 6.0 DISCUSSION

#### 6.1 WORK INDEX

#### 6.1.1 Error Analysis

The effect of random error associated with sampling and actual test (screening and grinding) in the determination of work index has been analyzed by Laplante et al. [74]; they did not discuss if the error (standard deviation) is constant or proportional to the work index. However, for each type of error, this is self-evident. For example, the error associated with the number of revolution obviously has a constant absolute standard deviation. Table 5.6 shows the assumed errors for the four rock types.

The effect of the systematic error related to the weight used to perform the test and the size distribution of the fresh feed was determined for a quartzite sample from Baskatong (Québec) [64] (this is the sample with which the breakage function used for this work was determined). It was concluded that the mass used (determined as having a volume of 1250 cm³ in a graduated cylinder) had little impact on the calculated work index, as McIvor [75] had proposed. The effect of feed size distribution was negligible for  $F_{00}$  approximately above 9.5 mm, as were all four samples used for this work. Consequently, these errors were not considered in this work.

#### 6.1.2 Link to Population Balance Modelling

The use of PBMs to predict the required number of revolutions to achieve the target size distribution (i.e. 50% undersize) was particularly powerful, as the number of required cycles was reduced from the usual

<sup>&</sup>lt;sup>6</sup> As opposed to the relative standard deviation, equal to the absolute standard deviation divided by the corresponding measurement. In practice, the word 'absolute' is dropped, and we refer to it as the standard deviation vs. the relative standard deviation.

eight to four or five. However, the savings in time were largely lost to simulation; this could be avoided with a more user-friendly package that would incorporate not only the steps performed by BALLMILL and BALLDATA, but an automatic search of the required number of revolutions. Nevertheless, PBM still offers more advantages, such as a reduction in the required mass (because steady-state is achieved in fewer cycles), and an additional criterion to assess if steady-state was achieved (the selection function). This is illustrated in Figure 5.1; the selection function converges rapidly, even after only two cycles. For all four rock types the selection function of the two coarsest size classes shows more variability, as they hold little mass at the end of the cycle, and can be significantly affected by the accumulation of the material in the dead zones at the ends of the mill. However, these selection functions have a high value, and correspond to the coarsest size class; thus their content at the beginning of the cycle is rapidly ground into finer size classes. and impacts little on the predicted size distribution of the product.

Selection functions are inherently a measure of grindability (--i.e. in terms of grams per unit time per gram of material in each size class). The work index is itself a measure of grindability, as it is most affected by the GPR term in Equation 4.1 (i.e. for a given feed size, Fm, and size at which the work index is determined, p, the product size,  $P_{\mathbf{p}}$ , is remarkably constant for most materials). It follows, then, that the work index and the selection function of materials should be closely correlated (see Figure 5.3), especially if the selection function is corrected for mass (even the non-normalized selection functions display good correlation with the work index, Figure 5.2). This also suggests that the mill scaleup using the PBM should be possible, as postulated by Austin et al [62], Herbst & Rajamani [63] and Hodouin and Bérubé [57]. The work index remains the favoured method, not because it is more reliable (although it probably is as of today), but because it is far simpler, and generally proves adequate, the most famous exception to this rule being the

#### 6.2 PHYSICO-MECHANICAL PROPERTIES

Errors encountered during tests of physico-mechanical properties of rock are mainly associated with sample extraction, sample preparation and measurement. The errors incurred during destructive tests (unconfined compressive and tensile strength tests) are due to all the factors. However, for non-destructive tests (e.g. P and S wave velocity measurement), measurement errors can be minimized using a large number of repeats. For derived properties such as moduli of elasticity and Poisson's ratio, error propagation was estimated using first order Taylor series expansions.

Compressive Strength: The standard deviation of compressive 6.2.1 strength is highest for the marble and gneiss samples, due to the well defined and inclined weak planes in the former, and the large number of inclined foliation planes present in the latter. For the granite sample, reasonably homogenous and free from weak planes, the standard deviation is much lower. For the limestone sample, large bedding planes were present, but affected compressive strength little, as it was measured along the normal to the bedding planes. It can be concluded that the compressive strength depends only marginally on density and grain size. It is largely dependent on the structure of the sample and its orientation with respect to the direction of loading. No significant pattern was found between the work index and the compressive strength, as shown in Figure 5.6. regression output of work index with respect to compressive strength at different scale (linear-linear, linear-logarithmic, logarithmic and

<sup>&</sup>lt;sup>7</sup> It was then believed that the Bond approach would fail for large diameter mills [77]. A number of explanations were proposed [78]; amusingly, the problem did not arise again, and although academic interest for PBM as a scale-up approach survived, practitioners are still using the Bond approach today.

logarithmic-logarithmic) is shown in Table 6.1.

Table 6.1 Work index (kWh/t) and unconfined compressive strength (MPa)

Combinations	Const.	X Coeff.	r	Err of Y	Err Const.
WI-σ <sub>e</sub>	50.85	5.323	0.305	52.23	5.69
WI-ln(σ <sub>c</sub> )	4.034	0.051	0.242	0.58	0.06
ln(WI)-σ <sub>e</sub>	-30.29	60.29	0.240	54.59	75.77
$\ln(WI) - \ln(\sigma_e)$	3.316	0.552	0.178	0.605	0.84

Column 1 shows the different combination of X and Y axes using natural logarithm. The constants and the X coefficients are in column 2 and 3. The correlation coefficient  $(r^2)$ , standard error of Y-variable estimated and the error of the constants are shown in column 4, 5 and 6. No significant correlation is found, which confirms the lack of pattern of Fig. 5.6.

6.2.2 Tensile Strength: The measured tensile strength of the gneiss and marble samples displayed a high standard deviation. That of the limestone and granite samples was low. These differences are probably due to the same considerations as for the compressive strength test. The wide variation in the results could have been compensated by testing a very large number of samples, which was not practical. Figure 5.7 shows that work indices and the tensile strengths are slightly correlated for the four samples tested. As tensile strength depends on the weakest plane present in the rock rather than overall strength of the rock (grindability vis-a-vis work index in the present case), this result is very plausible.

Table 6.2 Work index (kWh/t) and tensile strength (MPa)

Combinations	Const.	X Coeff.	r <sup>2</sup>	Err of Y	Err Const.
WI-σ <sub>ι</sub>	0.005	0.785	0.805	2.511	0.273
WI-ln(σ <sub>ι</sub> )	1.27	0.075	0.714	0.308	0.033
ln(WI)-σ,	-13.53	9.503	0.726	2.975	4.130
ln(WI)-ln(σ <sub>i</sub> )	0.0001	0.899	0.631	0.350	0.486

The statistical analysis of WI and tensile strength for different combinations of logarithmic and direct regressions is shown in Table 6.2; it confirms the existence of a slight correlation.

6.2.3 Bulk Density: The low density of limestone, 2606 kg/m³, may be due to the presence of excessive weathered zone. The bulk densities measured were associated with the lowest standard deviations. In fact, the four rock samples have very similar bulk densities, to the extent that they can be considered virtually identical. Future work could incorporate it as an input variable, by using material such as iron ore or massive sulphides. As bulk density is not a mechanical property, it is almost independent of amount and orientation of weak planes present in the sample. However, the work index may be considered to be representative of physical as well as mechanical property. Thus, one would not expect a strong correlation between bulk density and work index (Figure 5.8). The regression output of WI and density plot is shown in Table 6.3, and confirm the absence of correlation.

**Table 6.3** Work index (kWh/t) and bulk density  $(kg/m^3)$ 

Combinations	Const.	X Coeff	L <sub>3</sub>	Err of Y	Err Const.
WI-p	2617.2	7.90	0.119	139.6	15.20
WI-ln(ρ)	7.87	0.003	0.113	0.051	0.006
ln(WI)-ρ	2469.1	100.3	0.118	139.7	193.9
ln(WI)-ln(p)	7.818	0.036	0.112	0.051	0.071

6.2.4 Seismic Velocity (P and S Waves): It was found that the velocities of seismic waves (especially P wave) are higher for fine grained rock (grain size is coarsest for granite, intermediate for gneiss, fine for limestone and finest for marble). These wave velocities vs. work indices plots are shown in Figures 5.9 and 5.10, respectively. The P wave velocity is almost linearly related with work index, but the S wave is not. This relationship does not appear to be affected by the presence of

Table 6.4 Work index (kWh/t) and P wave velocity (m/s)

Combinations	Const.	X Coeff.	r²	Err of Y	Err Const.
WI-C,	3469.06	105.73	0.953	152.50	16.60
WI-ln(C <sub>p</sub> )	8.194	0.022	0.938	0.037	0.004
ln(WI)-C,	1413.40	1371.23	0.986	82.56	114.61
ln(WI)-ln(C <sub>p</sub> )	7.764	0.286	0.977	0.022	0.031

discontinuities or weathering zones as it is present in gneiss and limestone (variations in velocity are significantly lower than variations

in mechanical properties). Correlation between P wave and WI would require more data for confirmation and to identify what is the nature of the actual relationship (log-log, semi-log, or linear). The regression output of the work index and P and S wave velocities correlationship is presented in Table 6.4 and 6.5.

Table 6.5 Work index (kWh/t) and S wave velocity (m/s)

Combinations	. Const.	X Coeff.	r²	Err of Y	Err Const.
WI-C,	2696.85	19.03	0.153	290.64	31.64
WI-ln(C,)	7.899	0.007	0.159	0.098	0.011
ln(WI)-C,	2204.65	1294.61	0.226	277.88	385.72
ln(WI)-ln(C,)	7.73	0.102	0.234	0.094	0.130

#### 6.2.5 Dynamic Elastic Properties

a) YOUNG'S MODULUS: The dynamic Young's modulus of elasticity, Y, for granite, gneiss, limestone and marble shows some correlation to the work index, as shown in Figure 5.11.

Table 6.6 Work index (kWh/t) and Young's modulus (GPa)

Combinations	Const.	X Coeff.	<u>r²</u>	Err of Y	Err Const.
WI-Y	38.44	1.39	0.573	7.827	0.851
WI-ln(Y)	3.68	0.026	0.575	0.147	0.016
ln(WI)-Y	8.36	19.24	0.672	6.85	9.51
ln(WI)-ln(Y)	. 3.11	0.363	0.674	0.129	0.179

The correlation, however, is weak: the dynamic Young's modulus of the gneiss, limestone and marble samples is similar, although their work index ranges from 11 to 19 kWh/t. It can be concluded that the dynamic Young's modulus is not truly representative of grindability or overall strength. The regression parameters obtained with various combination of WI and Young's modulus are shown in Table 6.6, and confirm the weak correlation.

b) BULK MODULUS: The bulk modulus of elasticity, K, shows better correlation with the work index, as shown in Figure 5.12. The inverse of bulk modulus --i.e. compressibility shows a linear decreasing trend with respect to work index (Figure 5.13). Inspection of Eq. 4.5 shows that K

Table 6.7 Work index (kWh/t) and bulk modulus (GPa)

Combinations	Const.	X Coeff.	r2	Err of Y	Err Const.
WI-K	0.417	2.513	0.881	6.00	0.654
WI-ln(K)	2.48	0.073	0.936	0.124	0.014
ln(WI)-K	-45.16	31.31	0.841	6.93	9.62
ln(WI)-ln(K)	1,117	0.929	0.920	0.139	0.193

is primarily dependent on  $C_p$  (because  $C_p$  is on an average 1.8 times higher than  $C_s$  for most homogenous rocks, which is similar to what was observed for the four rock type --Table 5.6). It is, therefore, not surprising that K is slightly less correlated with work index than  $C_p$ . A statistical analysis of the regression between the WI and the bulk modulus for different combinations of axes is shown in Table 6.7; correlation is high, but not as high as for the P wave velocity (Table 6.4).

c) SHEAR MODULUS (OR MODULUS OF RIGIDITY): The shear modulus or modulus of rigidity,  $\mu$ , shows the same relationship with the work index (Figure 5.14) as Young's modulus. Therefore, it also fails to represent grindability (as Young's modulus did). The statistical analysis presented in Table 6.8 confirms this observation.

Table 6.8 Work index (kWh/t) and shear modulus (GPa)

Combinations	Const.	X Coeff.	r²	Err of Y	Err Const.
WI-μ	19.22	0.345	0.217	4.251	0.463
WI-ln(μ)	2.95	0.016	0.244	0.183	0.20
ln(WI)-μ	10.61	5.21	0.306	4.003	5.56
ln(WI)-ln(μ)	2.55	0.239	0.336	0.171	0.237

d) POISSON'S RATIO: Poisson's ratio obtained by dynamic tests,  $\nu$ , vs. WI is plotted in Figure 5.15. Poisson's ratio shows some correlation with work index: the two lowest WIs correspond to the two lowest  $\nu$ s, but the order is reversed. The two highest WIs also yield the two highest  $\nu$ s but the difference between these two values of  $\nu$ , a relative 50 %, is much higher than the difference between the two values of  $W_i$ , a relative 15 %. The pattern looks to be opposite and a mirror image of the relation obtained in the case of Young's and the shear modulus. The poisson's ratio of marble is the highest and that of the granite is the lowest.

Again, the level of correlation can be explained by the dependence of  $\nu$  on  $C_p$  and  $C_s$ . Eq. 4.7 shows that the contribution of  $C_s$  is as important as that of  $C_p$  (contrary to K, where  $C_p$  was more important). This yields a poorer correlation between  $\nu$  and  $W_l$  than what was observed for K. The results of the regression analysis of WI and Poisson's ratio for different combinations of axes (linear, logarithmic or both) are

shown in Table 6.9.

Table 6.9 Work index (kWh/t) and Poisson's ratio

Combinations	Const.	X Coeff.	r²	Err of Y	Err Const.
WI-v	0.029	0.013	0.732	0.050	0.005
WI-ln(v)	-2.47	0.060	0.782	0.204	0.022
ln(WI)-v	-0.187	0.152	0.650	0.057	0.079
ln(WI)-ln(v)	-3.49	0.719	0.699	0.240	0.333

#### 6.2.6 Summary

Altogether nine different rock properties were compared to the work index. The density and the compressive strength were found to be independent of the work index (WI). The tensile strength was found to be slightly correlated with the WI. The WI is found to have an approximately linear trend with P wave velocity, and virtually no correlation with S wave velocity. The moduli of elasticity calculated from P and S wave velocities show correlation with the WI which depends on the extent of the mathematical dependence on P wave velocity. Physically, K characterizes the behaviour of rock under compressibility, which represents most the type of stress applied in tumbling mills. It may, therefore, not be surprising to observe a better correlation with the WI. In the following section the use of work index in blast energy calculation is discussed in detail.

#### 6.3 FRACMENT SIZE AND EMERGY UTILISATION IN BLASTING

#### 6.3.1 A case study:

To compare the fragment size and specific grinding energy (calculated from Bond's law) with respect to blast results and explosive energy, a blast conducted in a limestone quarry in southern Ontario was

selected as a case study [79]. This is the same quarry from which the sample of the limestone was selected for the determination of the work index and physico-mechanical properties. A brief description of the explosive types, blast geometry and the blast results are presented below.

The quarry employs a single bench and the blast consisted of 36 holes, initiated with short period detonators in a staggered 3throw pattern. The burden, spacing, collar length and the bench height were 2.4 m, 2.7 m, 1.2 m and 6.3 m, respectively. Each 75 mm diameter borehole with no subgrade contained on average 22 kg of 65 mm diameter detonatorsensitive plastic-wrapped explosive. The coupling ratio achieved was about 92 %. The explosive types used were emulsions with varying aluminum contents. The calculated and measured detonation properties of the explosives are shown in Table 6.10. The sum total of shock energy (capacity of doing work by high amplitude stress waves resulting from the detonation of the explosive), and bubble energy (capacity of doing work by highly pressurised expanding gas produced following the shock waves) gives rise to the total measured energy. The ratio of calculated 'ideal' energy (calculated from thermodynamic equations) to the total measured energy

Table 6.10 Parameters showing explosive properties [79].

Explosive	Emulsion #1 (0% Al)	Emulsion #2 (5% Al)
Density (kg/m²)	1120	1150
Bubble Energy (MJ/kg)	1.65	1.85
Shock Energy (MJ/kg)	1.11	1.24
Total measured energy (MJ/kg)	2.76	3.09
Calculated ideal energy (MJ/kg)	2.88	3.65
Energy efficiency (%)	96	85

denotes the 'efficiency' of the explosive energy release. This is in fact the 'actual' energy released by the explosive in that diameter. As an example the emulsion #2, of density 1150 kg/m³, has 1.85 and 1.24 MJ/kg of bubble energy and shock energy, respectively. The calculated ideal energy, 3.65 MJ/kg, results an efficiency of 85 % in such a small diameter of explosive.

The blast results were analyzed and quantified according to relevant parameters. These included the face velocity, ground vibration, height and throw of muck pile, backbreak and the fragmentation achieved. These parameters are shown in Table 6.11.

The size distributions from the resulting blasts were measured by photographic analysis by means of a 1.33 m  $\times$  1.83 m plastic grid (each grid measuring 0.61 m  $\times$  0.61 m), placed at random at numerous sites on the muck pile. A schematic layout of the blast pattern showing the initiation sequence of the boreholes, the profile of the muck pile obtained after the blast and the fragmentation characteristics of the blast is shown in Figures 6.1-6.3.

Table 6.11 Parameters showing blast results [79].

Explosive	Emulsion #1 (0 % Al)	Emulsion #1 (5 % Al)	
Maximum throw (m)	21.0	32.0	
Height of muck pile (m)	5.0	3.8	
Backbreak (m)	0.5	1.5	
Face velocity (m/s)	8.0	11.3	
Fragment size, P <sub>m</sub> (m)	0.92	0.66	
Vibration level (%)	100	125	

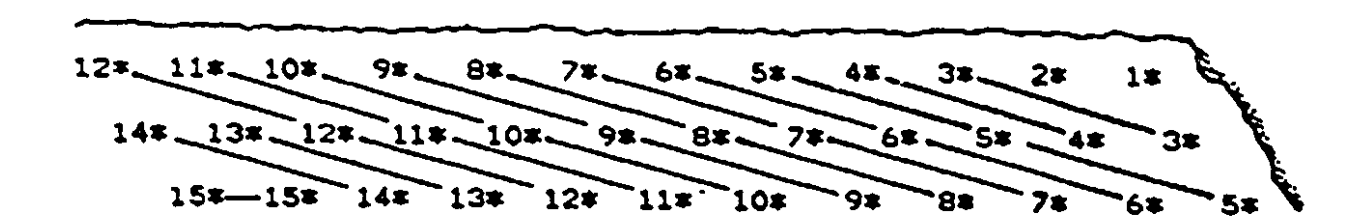


Figure 6.1: Typical blast pattern of the case study [79].

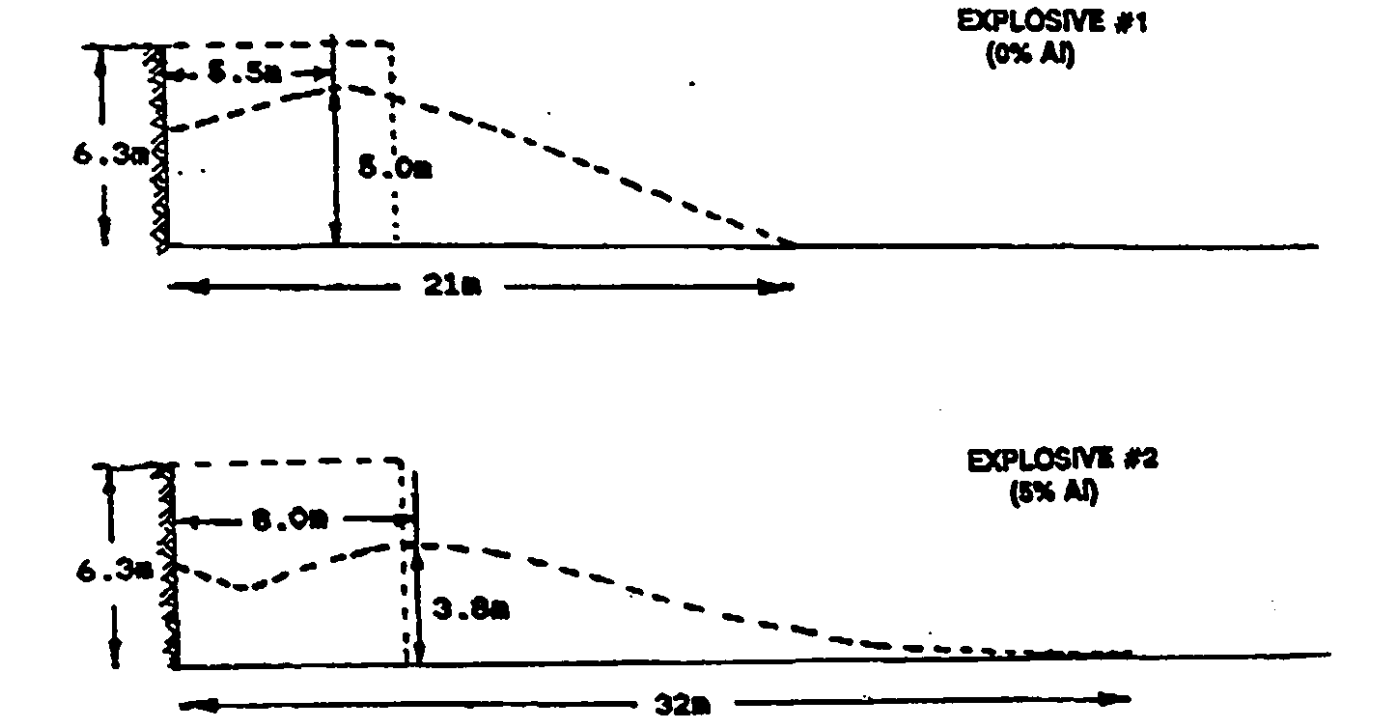


Figure 6.2: Profile of the muckpile after the blast [79].

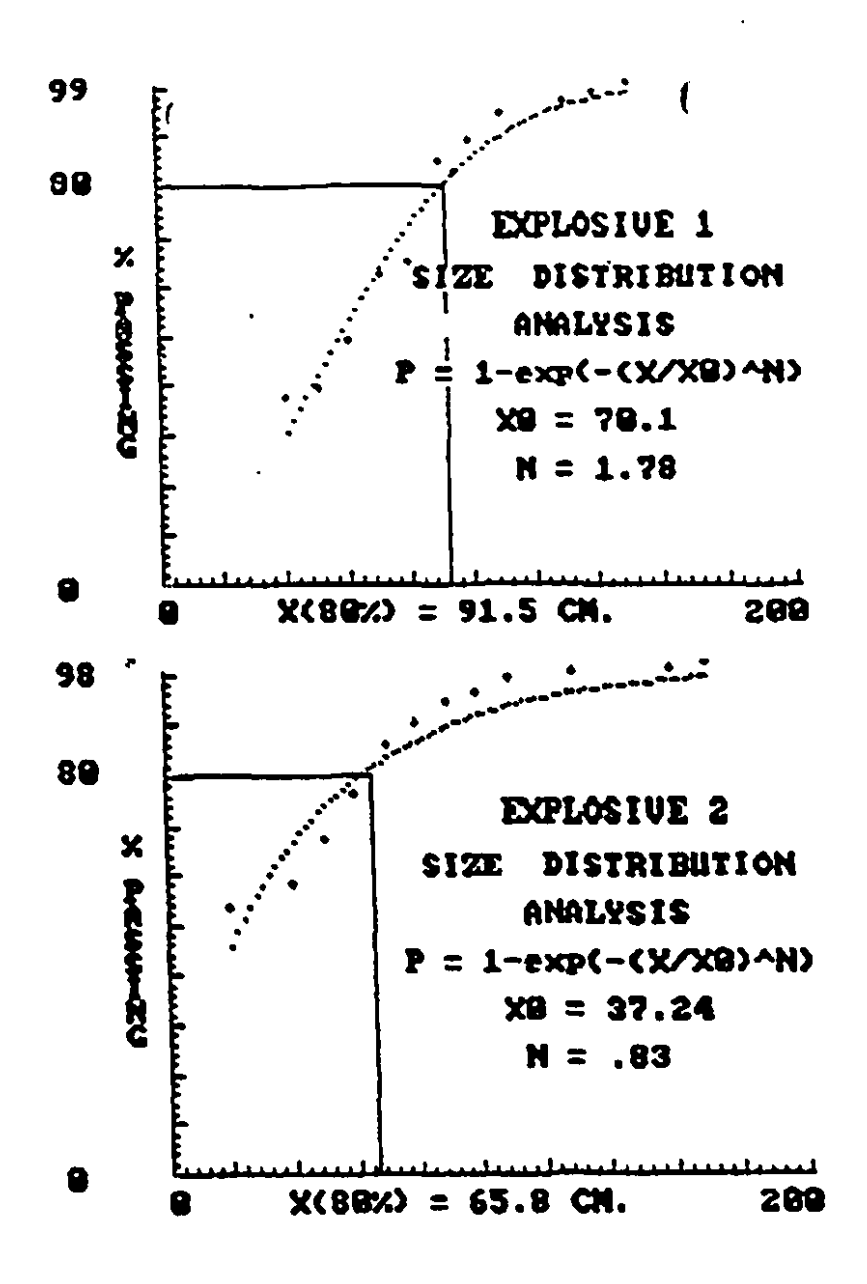


Figure 6.3: Fragmentation characteristics from the test blasts [79].

#### 6.3.2 Energy Utilisation in Blasting:

The energy breakdown of the test blasts in question is analyzed in terms of amount of explosive per borehole (kg), powder factor (kg/t), theoretical ideal energy (MJ/t) and actual measured energy (MJ/t). These parameters are shown in Table 6.12.

Table 6.12 Calculated parameters based on the present work.

Explosive	Emulsion #1 (0% Al)	Emulsion #2 (5% Al)
Explosive (kg/hole)	21.36	21.93
Rock blasted (v/hole)	106.3	106.3
Powder factor (kg/t)	0.20	0.21
Ideal energy (MU/n)	0.58	0.76
Actual energy (MUN)	0.55	0.64
(XWM)	(0.15)	(0.18)

Since the blast geometry is the same for both the explosives (106.3 t of rock blasted per borehole for both), the explosive content per hole differs very little as the two explosives have virtually the same density. As a result the powder factor (kilogram of explosive spent in blasting per unit weight of rock) is almost identical (0.20 and 0.21 kg/t). However, the ideal energy density (theoretical energy per unit weight of rock blasted) and the actual energy density (calculated from the measured energy in MJ/t) come out to be very different (energy densities of 0.55 vs. 0.64 MJ/t, because of the higher energy content in emulsion #2). It has to be noted that the explosive energy is responsible for the 'overall' blast results. These include, as Table 6.11 shows, fragmentation, heave, as well as blasting vibrations and air overpressure, in addition to

significant energy losses through heat and stemming ejection. Although, in a properly designed blast, a major fraction of the explosive energy is utilized in producing fragmentation, it is by no means the only usage of the explosive energy. In fact, a significant fraction of the energy is 'lost' through elasto-plastic deformation of rock, ground vibrations and air shock (from high velocity gases escaping through cracks and stemming ejection), and heating the surrounding rock.

The different energy densities result in smaller fragments ( $P_{\infty}$  of 0.92 vs. 0.66 m), larger throw, backbreak, face velocity and vibration, as shown in Table 6.11. Clearly specific energy, and not powder factor, should be the basic measure of energy input in blasting.

#### 6.3.3 Blast operating work indax:

In this section the concept of work index is applied to blasting for the prediction of the fragment size distribution (given a certain energy density) or the explosive energy required to achieve a given fragment size distribution. The operating work index calculated for either blast can be used to predict the fragment size (80 % passing) for the other blast by assuming the energy partitioning behaviour of the explosive to be the same. Similarly for the known operating work index of the blast the explosive energy requirement can be estimated for different product size and blast geometries. Further, as discussed in chapter 3, the ratio of operating work index to the laboratory determined work index can also be used in evaluating the efficiency of a blast. The operating work index (kWh/t) of a blast can be calculated by knowing total energy spent, W (kWh/t), the feed size,  $F_{80}$  ( $\mu$ m), and the product size,  $P_{80}$  ( $\mu$ m). The equation 4.1 follows,

$$W_{i \text{ operacing}} = \frac{W}{10 \ (\frac{1}{\sqrt{P_{80}}} - \frac{1}{\sqrt{F_{80}}})}$$
 6.1

This analysis depends on an accurate measure or estimate of feed

size. The assumption of feed size,  $F_{20}$ , as infinity [8,50] as well as that guided by drilling and firing pattern have been examined as possible approaches. In the first approach the operating work index for the two blasts is estimated at 13.4 kWh/t and 13.1 kWh/t, (the laboratory WI, 17 kWh/t, is approximately 30 % higher than the operating work index) and is in good agreement with earlier published blast work indices, one conducted at the Taconite iron ore quarry of the Mesabi range near Aurora, Minnesota [50], and the second at the underground Christmas mine of Inspiration Copper Company of Arizona [8].

In the second approach the  $F_{80}$  is assumed to be the arithmetic average of the effective burden and effective spacing. For the case studies in question, these are 0.9 m and 7.1 m, respectively. effective burden is taken to be 10 % larger than the actual distance between successive firing lines, perpendicular to the direction of throw. The additional amount is intended to incorporate the extent of backbreak behind the row of blast holes. The operating WI comes out to be 25.7 and 22 kWh/t for the two blasts, respectively (50 and 30 % higher than the laboratory rod mill work index, 17 kWh/t). At this stage of the investigation, it is not possible to state categorically that one approach is better then the other. Both approaches ('infinite' feed size vs. average of 'effective burden and spacing') show significant discrepancy between laboratory WI and actual blast WI. Although the results obtained with an infinite feed size are in good agreement with previous work, and the choice of infinite feed size has less built-in subjectivity, we know it to be incorrect as energy utilisation (and to some extent, fragmentation) would then be largely independent of actual blasting pattern and rock structure. The latter approach has the advantage of incorporating actual blasting pattern and joint spacing, but is somewhat subjective because it implies that there is actually a physical discontinuity in rock mass coincident with effective burden and spacing.

<sup>\*</sup> The effect of drilling pattern could be incorporated into the Bond approach with the ' $WL_{n}$ ' rather than  $F_{n}$ . This has been the choice of comminucation engineers when evaluating the impact of circuit efficiency.

Clearly, the proper choice probably lies somewhere in between. However, what is most encouraging and obvious is that both approaches are within reasonable range of energy use.

The differences in work indices raise question whether the blast operating work index is primarily a function of rock properties or blasting parameters. Much additional work involving full-scale blasting trials would be needed to establish a realistic feed size (if it exists) as a function of blast geometry and rock structure.

#### 6.3.4 Estimation of fragment size:

Based on the operating work index of emulsion #1, 13.4 kWh/t, the predicted product size for emulsion #2 (feed size of infinity, the total energy input, W, of 0.178 kWh/t are used as inputs in Eq. 6.1) comes out to be 0.69 m, as compared to the actual blast fragment size of 0.66 m. A similar agreement is achieved when performing the reverse operation (within the range of  $\pm$  5 % deviation than the measured size). This agreement is hardly surprising given that the operating WI is very similar for the two blasts. However, in the second approach of finite feed size, (Fm of 4.05 m) and the operating work index of emulsion #1, 25.7 kWh/t, results the product size of 0.79 m for emulsion #2. A similar agreement is achieved when performing the reverse operation (within the range of  $\pm$  18 % deviation from actual measured size). For the two explosive types, the measured and predicted fragment size, percent deviation and the work index used for both the approaches are shown in Table 6.13.

The noted discrepancy in measured and predicted size could be due not only to the absence of a proper method of calculating effective feed size in blasting (which may be some intermediate size between infinity and the average of the effective burden and spacing) but also due to the implicit assumption that the 'blasting' and 'comminution' work indices are

<sup>&</sup>lt;sup>9</sup> The reverse operation (work index of emulsion #2 as a reference) does not give an additional data set, but shows that either blast could have been used as a reference.

**Table 6.13** Prediction of fragment size,  $P_{10}$ , using the blast operating work index for different feed size,  $F_{10}$ .

Feed size, m	Explosive	WI used, kWh/t	P <sub>80</sub> predicted, m	% Deviation
Infinite	#1	13.1	0.88	-5
	#2	13.4	0.69	+5
Avg. of effective Burden+Specing	#1	22.0	0.78	-15
	#2	25.7	0.79	+20

exactly equivalent: in fact, Figure 3.3 suggests that the relationship between particle size and energy input should have an exponent closer to Kick's law than Bond's law. The much higher strain rates of blasting may also affect the nature of the relationship.

#### 6.3.5 Estimation of explosive energy:

In this section, a method is proposed to predict explosive energy requirements (in terms of MJ/t of rock blasted or kg of explosive per borehole) as a function of the operating work index of the blast. The explosive energy is calculated with reference to emulsion #2 by using its density and actual energy density factor as shown in Table 6.10. A finite feed size<sup>10</sup> equal to the average of the effective burden and spacing, 4.05 m, and an operating work index of 22 kWh/t calculated for second blast with emulsion #2 are used as inputs in Equation 6.1. Energy requirements in terms of kWh/t, MJ/t and kg/hole of emulsion #2 required for different product sizes, P<sub>20</sub>, of the limestone rock type are it shown in Table 6.14.

<sup>10</sup> The same exercise could be performed with an infinite feed size.

Table 6.14 Explosive energy requirement for different product sizes for limestone (feed size,  $F_{80}$  equal to 4.06 m,  $W_{i,constant}$  equal to 22 kWh/t).

Product pize, m	Energy, W (kWh/t) Energy, W (MJ/t)		Emulsion (kg/bole)
0.80	0.150	0.542	18.6
0.70	0.169	0.609	20.9
0.60	0.192	0.692	23.7
0.50	0.222	0.800	27.4

The required emulsion (kg/hole) shown in column 4 of the above table implies that the same blasting pattern (borehole diameter and burdenspacing) can not be employed for all desired product sizes (or, at constant product sizes, with rock types of different work index). It may be physically impossible to increase the charge weight in a borehole in a major way, as it is constrained by the borehole diameter and the bench height. In this case, one would have to recommend a larger borehole diameter or reduced burden and spacing, or a more energetic explosive. Of course, any change in explosive type or diameter may require modification to the energy balance shown in the Table 6.10. As discussed earlier, increasing borehole diameter leads more ideal behaviour from the explosive, which would affect the energy-size reduction.

Similar to the exercise shown in Table 6.14, the explosive energy (in terms of MJ/t or kg of emulsion per borehole) for a specific rock type (limestone in this case) and for a specified product size ( $P_{20}=0.66$  m) can also be calculated for different blast geometries (assuming the same firing sequence). The average of the effective burden and spacing (feed size,  $F_{20}$ ) for blast geometries of 2 m X 2.5 m, 2.4 m X 2.7 m, 4 m X 4 m, 6 m X 6 m comes out to be 3.4 m, 4.1 m, 6.6 m and 9.9 m, respectively.

The total energy required in terms of kWh/t, MJ/t and kg of explosives (emulsion #2 in the present case) is shown in Table 6.15.

Table 6.15 Explosive energy (MJ/t or kg of explosive/hole) for different feed sizes ( $F_m$ ) in limestone (product size,  $P_m$  equal to 0.66 m).

Feed size, Fe (m)	size, F <sub>6</sub> (m) W (kWh/t)		Emalsion (kg/hole)
3.4	0.129	0.600	20.6
4.1	0.137	0.640	21.9
6.6	0.158	0.733	25.1
9.9	0.171	0.795	27.3

The variation in explosive energy per borehole for the above two cases--i.e. with respect to product size,  $P_{10}$  and feed size,  $F_{20}$ , are shown in Figure 6.4.

Since the laboratory WI differs significantly from the operating work index, the laboratory WI alone cannot be used in predicting explosive energy requirement. Assuming the ratio of the operating WI of the second blast (calculated with  $F_{\infty}=4.05$  m) to the laboratory WI, 1.3 (the ratio might be due to the scale difference between laboratory WI and actual blasting WI), to be the same for all rock types, the energy requirement with reference to emulsion #2 can be calculated. Table 6.16 shows the required blasting energy for a product size of 0.66 m, for the other three rock types.

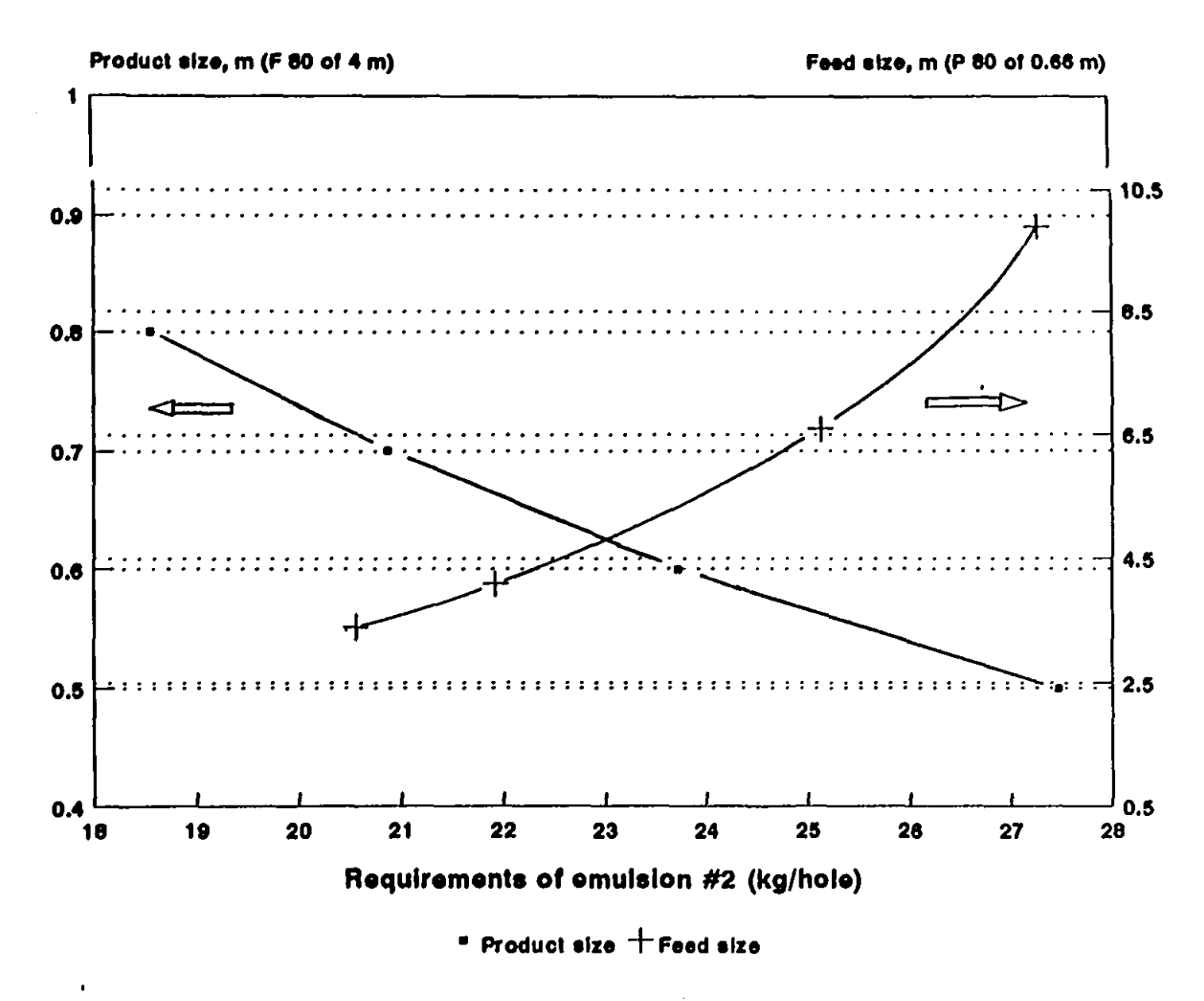


Figure 6.4: Explosive energy simulation with respect to feed size, F<sub>80</sub>, and product size, P<sub>80</sub>.

Table 6.16 Explosive energy requirements per borehole for different rock types  $(F_{\infty}=4.06 \text{ m}; P_{\infty}=0.66 \text{ m})$ .

ROCK TYPE	ROCK TYPE W, (EWbr)		W (MD/I)	Emilsion (kg/sole)
Granite	7.8	0.082	0.294	10.2
Gneiss	10.8	0.113	0.407	14.9
Limestone*	17.0	0.178	0.640	21.9
Marble	19.2	0.201	0.723	27.2

(\*: used as a reference)

#### 6.3.6 Comments:

The selection of feed size,  $F_{\infty}$ , in the above calculations is very critical. The  $F_{\infty}$  should take into account the macrostructure of the rock as well as the blast pattern. For this work, only the latter was considered, as no rock macrostructure information was available (nor is it known how this information would be used, if available). This should be the focus of future work.

An alternative to using a  $F_{80}$  strictly defined by burden/spacing is its back-calculation from Equation 4.1, using the laboratory work index,  $W_i$ , and specific blast energy input,  $W^{i1}$ . Equation 4.1 can be rewritten as:

$$F_{80}^{eff} = \frac{1}{(\frac{1}{\sqrt{P_{80}}} - \frac{W}{10W_4})^2}$$

This yields for the two blasts of the case study  $F_{80}^{eff}$  values of 21 m and

<sup>&</sup>lt;sup>11</sup> The implicit assumption is that the laboratory rod mill WI can be used for blasting WI, or conversely, that the difference between the two can be taken into account adequately in the  $F_{00}$  term—i.e. using the concept of 'effective feed size,'  $F_{00}^{eff}$ .

13 m, respectively, a value intermediate between infinity (i.e. the theoretical value) and the average of burden and spacing; this is the expected outcome, although it greatly exceeds the geometrical limit of the blast dimension.

The error in  $F_{m}^{eff}$  can be estimated from the errors in  $P_{m}$ , W and W<sub>i</sub> using Taylor series, the variance of  $F_{m}^{eff}$  is equal to:

$$\sigma^2$$
 of  $F_m^{eff} = (\partial F_m/\partial W)^2 \cdot \sigma(W)^2 + (\partial F_m/\partial W_i)^2 \cdot \sigma(W_i)^2 + (\partial F_m/\partial P_m)^2 \cdot \sigma(P_m)^2$ 

Whereas the standard deviation (SD) of the first two variables can be estimated quite readily, that of Wi raises an additional problem. The SD of the actual laboratory WI determination has been estimated at 0.14 kWh/t for a WI of 14.19 kWh/t by [74]. To the 'pure' laboratory error should be added a second error which relates more to differences between the laboratory rod mill WI and the operating blast WI. This second error is of course impossible to estimate at the present time, but is expected to exceed the first significantly. To estimate the SD of Fm we will use the same relative SD of 10 % for all three independent variables ( $P_{20}$ , W and  $W_i$ ). Table 6.17 shows how the error (or standard deviation) on  $W_i$  and  $P_{n}$  propagates into the standard deviation of  $P_{n}$ . The overall standard deviation in  $F_m$  is of the same order of magnitude as  $F_m$  itself (15 m vs. 13 m), and is largely a function of the standard deviations in total energy input, W or work index, W, (since both are linearly related the fractional errors shown in column 2 and 3 of the last row of the Table 6.17 are the same). The error in the  $P_{m}$  is clearly less critical.

Table 6.17  $F_{80}$  values, standard deviations and the error propagation with respect to energy factor, W, work index,  $W_i$ , and product size,  $P_{80}$ .

x	W, kWh/t	W <sub>i</sub> , kWh/t	P <sub>so</sub> , m	F <sub>ab</sub> err, m
Value	0.18	17.0	0.66	13
SD (σ)	± 0.02	± 1.7	± 0.07	± 15
(∂F <sub>80</sub> /∂X)²	25×10 <sup>16</sup>	25x10 <sup>12</sup>	0.7x10 <sup>4</sup>	1
$(\partial F_{\infty}/\partial X)^2 \cdot \sigma^2$ (in $m^2$ )	91	91	32	214

This observation is based on an extremely small data set, and would have to be validated by future work. What would be of particular value is an exploration of the relationship between  $F_{\mathbf{x}}^{\mathrm{eff}}$ , blast operating work index, blasting pattern and possibly rock macrostructure.

#### 7.0 CONCLUSIONS

The rod mill work index of four different rock types with very diverse lithological and mineralogical characteristics has been correlated with their strength and seismic properties.

It was found that the 'static' properties such as the unconfined compressive strength, were poorly correlated; the tensile strength was slightly correlated. In contrast, the 'dynamic' properties (e.g. seismic velocities and elastic moduli) had much better correlation. Of these the P-wave velocity and dynamic bulk modulus (or compressibility) were shown to have the best correlation with the work index. P-wave velocity and bulk modulus are more easily measured than the work index; in some applications work index measurements could therefore be replaced by P wave and dynamic compressibility measurements.

The work index determined in the laboratory has been further utilized to seek a quantitative correlation between size reduction achieved in laboratory grinding studies and that achieved in rock blasting. This has been carried out through a case study of two well-documented blasts, for which the energy characteristics of the explosives and rock properties (one of the four rock samples used in this work) were thoroughly quantified.

Direct comparison between the blasting operating work index and laboratory determined work index or, conversely, between actual blasting energy and comminution energy (calculated from the laboratory determined work index) showed the differences to be lower in the case of feed size of infinity (theoretical value) and higher in case of feed size defined by effective burden/spacing. In fact, choosing an intermediate feed size to calculate the blasting work index would yield a value equal to the rod mill work index, for this case study. Further it was found that the laboratory work index cannot be used alone in fragment size prediction

and/or explosive energy estimation unless corrected for the blasting work index. The correction factor may be applied to the laboratory work index (1.3 as shown in this study) when used with finite feed size, an average of effective burden and spacing, or, to the feed size<sup>12</sup> when used with laboratory work index.

The two main objectives of the investigation have thus been 'fulfilled,' albeit the first with only a limited data base, and the second in an illustrative rather than demonstrative manner with no systematic study of important variables such as rock macrostructure. This opens a potentially very useful venue, which would require an extensive data base to validate the concepts proposed by this thesis.

 $<sup>^{12}</sup>$  The effective feed size,  $F_{80}^{eff}$ , give good agreement with observed results, may greatly exceed the geometrical limit of the blast dimension, as shown in this study.

#### 8.0 FUTURE WORK

The correlation established in this investigation between the work index and dynamic properties such as P-wave velocity and compressibility on the one hand, and energy and size-reduction in blasting on the other, is based on limited data. Clearly much additional work needs to be carried out to achieve a more reliable correlation, and test its accuracy.

Rod mill grinding is only an approximation of the size reduction process inherent in blasting. The main differences are the widely different strain rates between the two processes and the scale of breakage. It is quite possible that work index obtained through explosion-induced fragmentation in rock at small scale (with strain rates closer to full scale blast) could serve as a better guide for predicting fragment size distribution and/or energy requirements in actual full-scale blasting.

So far most work index studies have been limited to low strain-rate system. The dependence of breakage energy requirements on strain rate is poorly understood at present. The first step in extending this work to the dynamic case would be through the use of a suitable 'pendulum apparatus' where both strain rate and energy input into the subject sample can be accurately controlled.

Establishing a more accurate correlation among the properties investigated in this thesis may not be sufficient to predict fragment size distribution in actual blasting to the required degree of precision. Determination and use of operating work indices (e.g. data obtained from blasts or a crusher at the quarry or mine in question) may be required. This would eliminate the scale-up problem and the problem of strain rate differences. In either case the investigation has opened up a challenging and potentially very useful avenue of research.

The above test work could be aimed at both underground and open pit operations. Intuitively, underground efforts should be at first the

easiest, because of the larger number of blasts, the better ability to determine fragment size and work index (blasts are on small scale). Underground applications could also reap greater benefits in terms of either improved productivity and reduction of oversize.

REFERENCES

- 1. Weiss, N. L., 1985; "Jaw crushers,", Mineral Processing Handbook, SME/AIME; vol. 1, pp. 3B-2, New York.
- 2. Schlitt, W. J. et al., 1992; "Mineral processing," Mining Engineering Handbook, SME/AIME; vol. 2, pp. 2184, New York.
- 3. Lacy, W. C. and Lacy, J. C., 1992; "History of mining," Mining Engineering Handbook, SME/AIME; vol. 1, pp. 10. New York.
- 4. Mular, A. L. & Jergensen, G. V. (Ed.), 1982; "Design and installation of comminution circuits," SME of AIME publications, New York.
- 5. <u>Comminution-Theory and Practice</u>, 1993; SME of AIME publications, S. K. Kawatra (Ed.), New York.
- 6. Barratt, D. J. and Sochocky, M. A., 1982; "Factors which influence selection of comminution circuits," Mular, A. L. & Jergensen, G. V. (Ed.), <u>Design and installation of comminution circuits</u>, SME of AIME; pp. 1-26, New York.
- 7. Bond F.C., 1961; "Crushing and Grinding Calculations, "British Chemical Engineering, 6(8), August, 1961, p 543.
- 8. Bond, F. C. and Whitney, B. B., 1959; "The work index in blasting," Ouart. of Colorado School of Mines, vol. 54, no. 3, third symp. on Rock Mechanics.
- 9. Kuznetsov, V. M., 1973; "The mean diameter of fragments formed by blasting rock," <u>Soviet Min. Sci.</u>, vol. 9, pp. 144-148.
- 10. Cunningham, ·C., 1983; \*The KUZ-RAM model for prediction of fragmentation from blasting, \* 1st Int. Symp. on Rock Fragmentation by Blasting, Lulea; Sweden, pp. 439-453.
- 11. Just, G. D., 1973; "The application of size distribution equation to breakage by explosives," <u>National Symp. on Rock Fragmentation</u>; Adelaide, pp. 18-23.
- 12. Da Gamma, C. D., 1971; "Size distribution general law of fragments resulting from rock blasting," <u>Trans AIME</u>, Dec'71, pp. 314-316.
- 13. Mohanty, B., 1988; "Parameters affecting explosives energy release-A case for realistic rating of commercial explosives", <u>Proc. 14 th Ann. Conf. on Explosives and Blasting Tech.</u>; Soc. of Expl. Eng., Anaheim.
- 14. Dowding, C. H. and Aimone, C. T., 1992; "Rock breakage: Explosives," <a href="mailto:SME\_Mining\_Engineering\_Handbook">SME\_Mining\_Engineering\_Handbook</a>, vol. 1, pp. 722-746.
- 15. Ash, R. L., 1963; "The mechanics of rock breakage", <u>Pit & Ouarry</u>, vol. 56, No. 2-5, Aug.-Nov. pp. 98-100; 112; 118-123; 126-131; 109-111; 114-118.
- 16. Puglise, J. M., 1973; "Designing blast patterns, using empirical formulas", <u>Pit & Ouarry</u>; vol. 66, No. 2, pp. 85-88.

- 17. Van Ormer, H. P., 1973; "7 Rules of thumb for blasting hard rock", Pit & quarry; vol. 66, No. 3, pp. 72-75.
- 18. Hagan, T. N., 1981; "Explosives and blasting-The next decade, Part II -rock properties and blastholes," <u>Australian Mining</u>; vol. 73, No. 8, pp. 33-40.
- 19. Dick, R. A. et al., 1983; "Explosives and blasting manual," Information Circular 8925, USBM, Washington, DC.
- 20. Langefors, U. & Kihlstrom, B., 1978; "The modern technique of rock blasting," John Wiley & Sons, pp. 18.
- 21. Atlas Powder Company, Field technical operations, 1987;, "Explosives and rock blasting," Dallas, Texas, USA, pp. 451.
- 22. Kutter, H. K. & Fairhurst, C., 1971; "On the fracture process in blasting," Int. J. Rock Mech. and Min. Sci., vol. 8, pp. 181-202.
- 23. Rinehart, J. S., 1959; "Quarterly of the Colorado Sch. of Mines", 3 rd Symp. on Rock Mechanics, vol. 54, No. 3.
- 24. Mohanty, B., 1985; "Characteristic crack patterns close to and exploding charge," Rock Breakage and Mechanical Excavation; P. Baumgartner, ed., Special vol. No 3, Canadian Institute of Mining & Metallurgy, pp. 32-36.
- 25. Porter, D.D. & Fairhurst, C., 1970; "A study of crack propagation produced by the sustained borehole pressure in blasting", <u>AIME</u>, pp. 497-515.
- 26. Hagan, T. N., 1977; "Good delay timing-perquisite of efficient bench blast", Proc. <u>Australasian Institute of Mining and Metallurgy</u>, No. 263, pp. 47-54.
- 27. Chiapetta, R. E. et al., 1983; "The use of high-speed motion picture photography in blast evaluation and design", <u>Proc. 9 th Conf. on Explosives and Blasting Tech.</u>, Soc. of Expl. Eng.; Solon, OH, pp. 258-309.
- 28. Touloukian, Y.S & Ho, C.Y., 1981; "Physical properties of rocks and minerals", McGraw Hill, pp. 47.
- 29. Fairhurst, C., 1962; "Rock Mechanics", <u>Proc. of 5 th Sym. on Rock mechanics</u>, held at University of Minnesota, May, Pergamon press 1963.
- 30. Lowrison, G. C., 1974; "Crushing and Grinding: The size reduction of solid materials," CRC Press Inc., Cleveland, Ohio; pp. 15.
- 31. Thomas et al., 1978; "Comparison of estimated versus actual capital cost and operating data for a copper concentrator," Mular, A. L. and Bhappu, R. B., (Ed.), <u>Mineral processing plant design</u>, SME of AIME, New York, pp. 101.
- 32. Lowrison, G. C., 1974; "Crushing and Grinding: The size reduction of solid materials," CRC Press Inc., Cleveland, Ohio; pp. 60.

- 33. Mineral processing handbook, 1985; vol. 1, SME/AIME, New York pp. 3A-12.
- 34. McIvor, R.E. & Finch J.A., 1986; "The effects of design & operating variables on rod mill performances", <u>CIM (mineral processing) Bulletin</u>, pp. 39, Nov., 1986.
- 35. McIvor et al., 1990; "Functional performances characteristics of ball milling", Mining Engineering, pp. 269, Mar., 1990.
- 36. Olaf Otte, 1988; "Grinding principles and Industrial application," The AusIMM Cobar branch, 3rd Mill operators conference, Cobar NSW, May 1988, pp. 131.
- 37. Wills, B. A and Atkinson, K., 1993; "Some observations on the fracture and liberation of mineral assemblies," <u>Minerals Engineering</u>, vol. 6, No. 7, pp. 697-706.
- 38. Wills, B. A., 1990; "Comminution in the minerals Industry," an overview; Minerals Engineering. vol. 3, No. 1-2, pp. 3-5.
- 39. Parekh, B. et al., 1984; "Novel comminution process uses electric and ultrasonic energy," Mining Engineering, vol. 36, pp. 1305.
- 40. Andres, U. T., 1977; "Liberation study of apatite-nepheline ore comminuted by penetrating electric discharges," <u>Int. J. of Min. Proc.</u>, vol. 4, pp. 33-38.
- 41. Chen, T. T. et al., 1984; "The relative transparency of minerals to microwave radiation," <u>Can. Met. Ouart.</u>, Vol. 23, No. 3, pp. 349.
- 42. Walkiewicz, J. W. et al., 1988; "Microwave heating characteristics of selected minerals and compounds," <u>Minerals and Met. proc.</u>, 39. February 88.
- 43. Jaeger J.C. & Cook, N.G.W., 1979; "Fundamentals of Rock mechanics" 3 rd edition, Chapman and Halls, London; pp. 517.
- 44. Austin, L. G., Klimpel, R. R. & Luckie, P. T., 1984; "Process Engineering", SME publication New York, pp. 28.
- 45. Bond, F.C., 1952; "The Third Theory of Comminution," <u>Trans. SME/AIME</u>; vol. 193, pp. 484-494.
- 46. Charles, R.J., 1957; "Energy-size relationship in comminution", <u>Trans. SME/AIME</u> vol. 208, pp. 80-88.
- 47. Hukki, R.T., 1961; "Proposal for a solomonic settlement between the theories of Von Rittinger, Kick and Bond," <u>Trans. SME/AIME</u>, Vol. 220, pp. 403-408.
- 48. Mineral processing handbook, 1985; vol. 1, SME/AIME, New York pp. 3A-20.

- 49. Rowlands, C. A., 1976; "The tools of power power: The Bond Work Index, a tool to measure Grinding efficiency," <u>AIME meeting</u>, Denver.
- 50. Bond, F. C., 1954; "Which is more efficient Rock Breaker?," Eng. Mining Journal; Vol. 155, No. 1, pp. 82.
- 51. Rowland, C. A., 1973; "Comparison of Work Indices calculated from operating data with those from laboratory test data," 10 th IMPC, London.
- 52. ASTM-D-409-51, 1952; "Annual book of ASTM Standards," Philadelphia, PA; vol. 5, pp. 840.
- 53. Brown, R. L., 1941; "Broken coal-III generalised law of size reduction", <u>J. of the Inst. of Fuel</u>, vol. 14, pp. 129-134, London.
- 54. Epstein, B., 1947; "The mathematical description of certain breakage mechanisms leading to log-normal distribution," <u>J. of the Franklin Institute</u>, vol. 244, pp. 471-477.
- 55. Weller, K. R., 1980; "Hold-up and residence time characteristics of full scale grinding circuits," <u>Third Symp. of IM3P of IFAC</u>, Montreal; Aug, 1980, pp. 303-309.
- 56. Narayanan, S.S., 1986; "Development of a laboratory single particle breakage technique and its application to ball mill modelling and scale-up. <u>PhD Thesis</u>, Univ. of Queensland, Australia.
- 57. Hodouin, M. A., Berube, and Everell, M. D., 1978; "Modelling industrial grinding circuits and application in design," <u>CIM Bull.</u>, sept. 1978, pp. 138-146.
- 58. Herbst, J. A. and Fuerstenau, D. W., 1968; "The zero order production of fine sizes and its implication in simulation," <a href="mailto:SME-AIME Trans.">SME-AIME Trans.</a>, vol.241, pp. 538.
- 59. Austin, L. G., Klimpel, R. R. & Luckie, P. T., 1984; "Process Engineering of size reduction: Ball milling, "SME publication New York, pp. 63.
- 60. Broadbent, S. R. and Callcott, T. G., 1956; "A matrix analysis of processes involving particle assemblies," <a href="Phil. Trans. Roy. Soc. of London">Phil. Trans. Roy. Soc. of London</a>; vol. A249, pp. 99-123.
- 61. Luckie, P. T. & Austin, L. G., 1972; "A review introduction to the solution of the grinding equations by digital computation," <u>Mineral Science and Engg.</u> 4, pp. 24.
- 62. Austin, L.G. et al., 1982; "Simulation of grinding circuits for design," <u>Design and Installation of Comminution Circuits</u>, Ed. Mular and Jergensen, II; New york pp. 301-324.
- 63. Herbst, J. A. & Rajamani, K., 1982; "Developing a simulator for ball mill scale-Up: A case study," <u>Design and Installation of Comminution Circuits</u>, Ed. Mular and Jergensen, II; New york pp.325-342.

- 64. Austin, L. G., Klimpel, R. R. & Luckie, P. T., 1984; "Process Engineering of size reduction; Ball milling," SME publication New York, pp. 82.
- 65. Austin, L. G., Klimpel, R. R. & Luckie, P. T., 1984; "Process engineering", SME publication New York, pp. 79-116.
- 66. Laplante, A. R., Prasad, U., McIvor, R. E. & Finch, J. A., 1993; "Error analysis for work index determinations. Part 2: A Phenomenological basis for analysis of systematic errors for the rod mill test," <u>Minerals Engineering</u>, vol. 6, no. 5, pp. 509-521.
- 67. ASTM-2938-86, 1988; "Annual book of ASTM Standards," Philadelphia, PA; vol. 4.08, pp. 345.
- 68. ISRM: "Suggested methods of Rock Characterization, Testing, and Monitoring," ISRM Commission on Testing Methods, E.T. Brown, Ed. (Pergamon, Oxford, 1981), pp. 211.
- 69. Duvall, W.I. & Obert, L., 1967; "Rock mechanics and the design of structures in rock," John Wiley & Sons Inc., pp. 275.
- 70. Wuerker G. R.; 1959; "Influence of stress rate and other factors on the strength and elastic properties of rocks," <u>Ouart. of Colorado Sch.of Mines</u>; vol.3, no. 54, pp. 3-33.
- 71. ASTM-3967-86, 1988; "Annual Book of ASTM Standard," Philadelphia, PA, vol. 4.08, pp. 504.
- 72. Jumikins, A.R., 1979; "Rock Mechanics," Trans tech publication, pp. 39.
- 73. ASTM-2845-83, 1988; "Annual Book of ASTM Standard," Philadelphia, PA, vol. 4.08, pp. 317.
- 74. Laplante, A. R. et al., 1988; "Error analysis for work index determinations. Part 1: Accuracy and reproducibility," <u>Minerals Engineering</u>, vol. 1, no. 2, pp. 113-125.
- 75. McIvor, A. R., 1988; "Technoeconomic analysis of plant grinding mills," <a href="PhD Thesis">PhD Thesis</a>, McGill University, Montreal.
- 76. Hively, E. E. and Wipf, E. H., 1983; "Flow criteria/retention as design limit to large mills," <u>SME/AIME Mini Symposium</u>, <u>Mill Design and Grinding Performance of Large Ball Mills I</u>; pp. 47-57, Salt Lake City, UT.
- 77. Burns, R. S. and Erskine, J. G., 1983; "Experience with large diameter ball mills at Bougainville Copper Limited," <u>SME/AIME Mini Symposium</u>, <u>Grinding Performance of Large Ball Mills II</u>, pp. 39-53, Salt Lake City, UT.
- 78. Herbst, J. A., Lo, Y. C., and Rajamani, K, 1983; "Population balance model Prediction of the performance of large-diameter mills," <u>SME/AIME Mini Symposium Grinding Performance of Large Ball Mills II</u>, pp. 1-6, Salt Lake city UT.

79. Mohanty, B., and Chung, S., 1990; "An integrated approach to evaluation of blasts- a case study," <u>Proc. 3 rd Int. Symp. on Rock Fragmentation by Blasting</u>, pp. 353-360, Brisbane, August 1990, Aust. Inst. of Min. & Met..

## **APPENDIX**

### STANSTEAD GRANITE

	Diam.	%SD	Cycle 1	Cycle 2	Cycle 3	Cycle 4	Cycle 5			
	(mm)	Rev.	50	24	31	30	28			
	9.5	21.63	0.23	1.33	0.37	0.86	0.45			
	6.7	19,37	0.36	3.12	0.96	0.78	0.85	Stanstead	granite	
	4.8	10.42	0.43	3.47	1.19	0.74	0.98			
	3.4	7.53	1.22	5.63	2.61	1.98	2.49	F80:	9740	micrometre
	2.4	5,87	3.17	7.79	5.93	5,06	5.56	P80:	930	micrometre
	1.7	5,01	7.49	12.73	13.36	12.45	13.06	GRP:	25,3	grammes per rev.
	1.2	5.26	13.42	20.02	24.55	26.91	28.21	P:	1180	micrometre
	-1.2	24.92	73.68	45.92	51.02	51.23	48.40	WI:	7.8	kWh/t
No.								Mass:	1980	grammes
<u>Pi</u>	Tot.	100.01	100.00	100.01	99.99	100.01	100.00			
	grammes pe	er rev.	19.31	22.74	25.28	25.42	25.20			
								Product si	ze	
	Diam.		selec.	selec.	selec.	selec.	selec.			
	(mm)		funct.	funct.	funct.	funct.	funct.	Diam.	Passing	passing
	•							(mm)	grammes	%
	9.5		0.0909	0.0104	0.1111	0.0861	0.1171			
	6.7		0.1216	0.1049	0.1184	0.1428	0.1403	0.9	127.61	25.12
	4.8		0.1503	0.1223	0.1439	0.1870	0.1721	0.6	91.92	18.09
	· 3.4		0.1085	0.0922	0.1100	0.1213	0.1153	0.4	74.17	14.60
	2.4		0.0798	0.0718	0.0753	0.0778	0.0759	0.3	56,68	11.16
	1.7		0.0523	0.0437	0.0435	0.0443	0.0414	-0.3	157.65	31.03
	1.2		0.0306	0.0243	0.0232	0.0221	0.0212	Total	508.03	100

## **GNEISS**

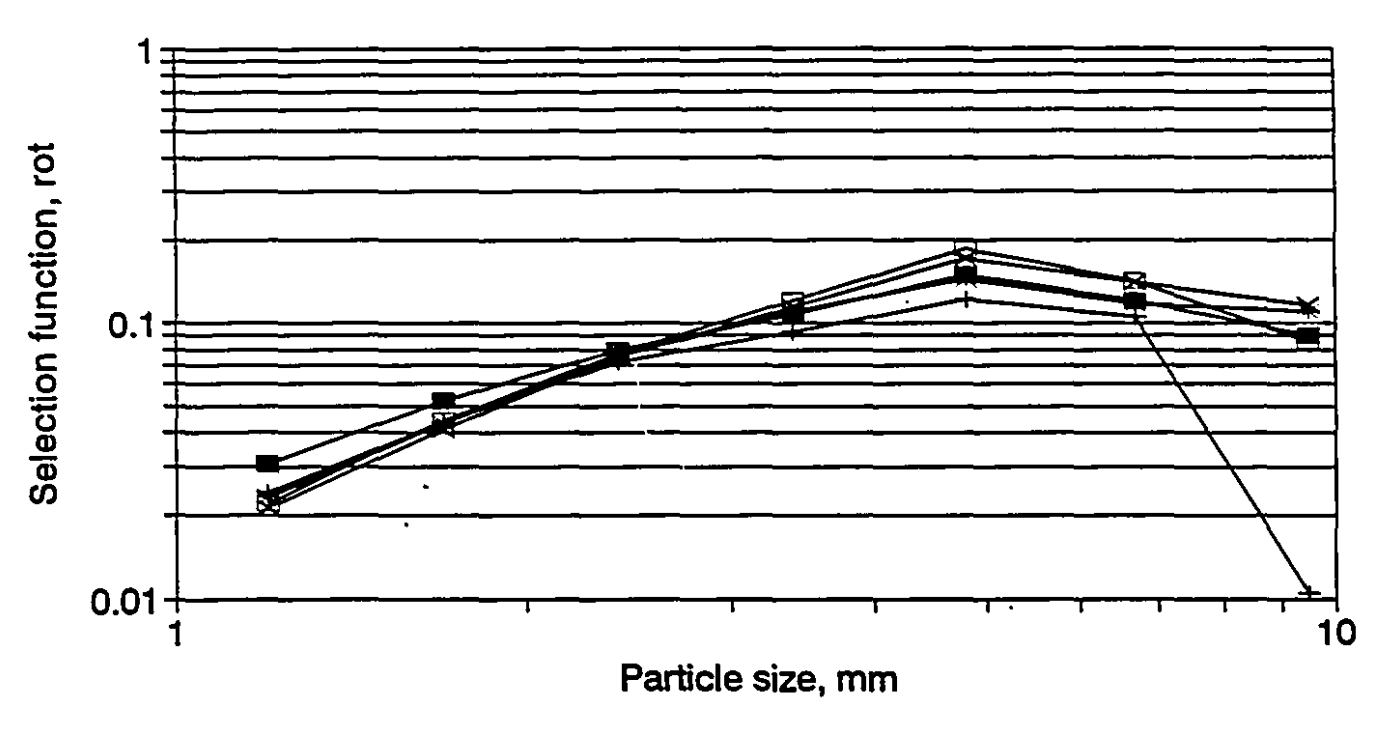
	Diam.	. %SD	Cycle 1	Cycle 2	Cycle 3	Cycle 4			
	(mm)	Rev.	80	55	60	57			
	9.5	11,49	0.00	0.43	0.22	0.32			
	6.7		0.53	2.29	1.24	0.5 <u>2</u> 0.66	Gneiss		
	4.8		1.49	3.91	2.08	1.64	Citoiss		
	3.4		4.02	6.70	5.19	4.16	F80;	8460	micrometre
	2.4		7.26	9.10	8.34	7.88	P80;	840	micrometre
	1.7		10.03	13.24	14.10	14.29	GRP:	14.31	
	1.7 1.2		10.03	15.19	18.13	20.03	P:	1180	grammes per rev. micrometre
	-1.2		66.18	49.14	50.70	51.02	WI:	10.8	kWh/t
	-1.2	21.10	00.10	45.14	30.70	31.02	Mass:	2190	grammes
i	ੈਂ Tot.	99.99	99.99	100.00	100.00	100.00	191055.	2190	grammos
	grammes		10.68	12.40	13.63	14.31			
	grammo	por lov.	10.00	12.40	10.00	14.01	Product s	78	
	Diam.		selec.	selec.	selec.	selec.	, rodust o		
	(mm)		funct.	funct.	funct.	funct.	Diam.	Passing	passing
	(11117)		idilot.	141101.	1011011	idilot,	(mm)	grammes	%
	9.5		0.0505	0.0522	0.0553	0.0515	(,	g, a	70
	6.7		0.0506	0.0442		0.0666	0.9	110.12	19.43
	4.8		0.0510	0.0433	0.0531	0.0587	0.6	67.85	11.97
	3.4		0.0389	0.0335	0.0367	0.0422	0.4	56.44	9.96
	2.4		0.0298	0.0281	0.0296	0.0307	0.3	50.31	8.88
	1.7			0.0205	0.0203	0.0205	-0.3	281.94	49.75
	1.2			0.0168	0.0157	0.0151	Total	566.66	100
			-,						

## MARBLE

	Diam.	%SD	Cycle 1	Cycle 2	Cycle 3	Cycle 4			
	(mm)	Rev.	80	200	150	139			
									•
	9.5	17.92	4.27	0.33	0.49	0.15			
	6.7	19.60	11.19	1.06	1.63	2.02	MARBLE		
	4.8	13.76	10.20	1.83	2.10	1.81			
	3.4	9.64	10.63	4.09	3.40	3,85	F80:	8200	micrometre
	2.4	7.20	9.47	7.72	6.91	7.22	P80:	910	micrometre
	1.7	5.61	8.63	12.81	12.87	12.85	GRP:	6.03	grammes per rev.
	1.2	5.81	8.75	17.01	20.47	22.48	P:	1180	micrometre
	-1.2	20.46	36.86	55.16	52.13	49.61	WI:	19.2	kWh/t
							Mass:	2150	grammes
	Tot.	100.00	100.00	100.01	100.00	99.99			
Æ	grammes pe	er rev.	4.41	5.12	5.86	6.03			
							Product si	ze	
	Diam.		selec.	selec.	selec.	selec.			
	(mm)		funct.	funct.	funct.	funct.	Diam.	Passing	passing
							(mm)	grammes	%
	9.5		0.0179	0.0175	0.0203	0.0301			
	6.7		0.0132	0.0186	0.0191	0.0176	0.9	123.16	23.71
	4.8		0.0153	0.0201	0.0224	0.0263	0.6	84.83	16.33
	3.4		.0.0132	0.0161	0.0199	0.019	0.4	63.9	12.30
	2.4		0.0129	0.0124	0.0139	0.0137	0.3	46.88	9.03
	1.7		0.0088	0.0088	0.0094	0.0094	-0.3	200.62	38.63
	1.2		0.0061	0.0061	0.0061	0.0058	Total	519.39	100

# Selection function

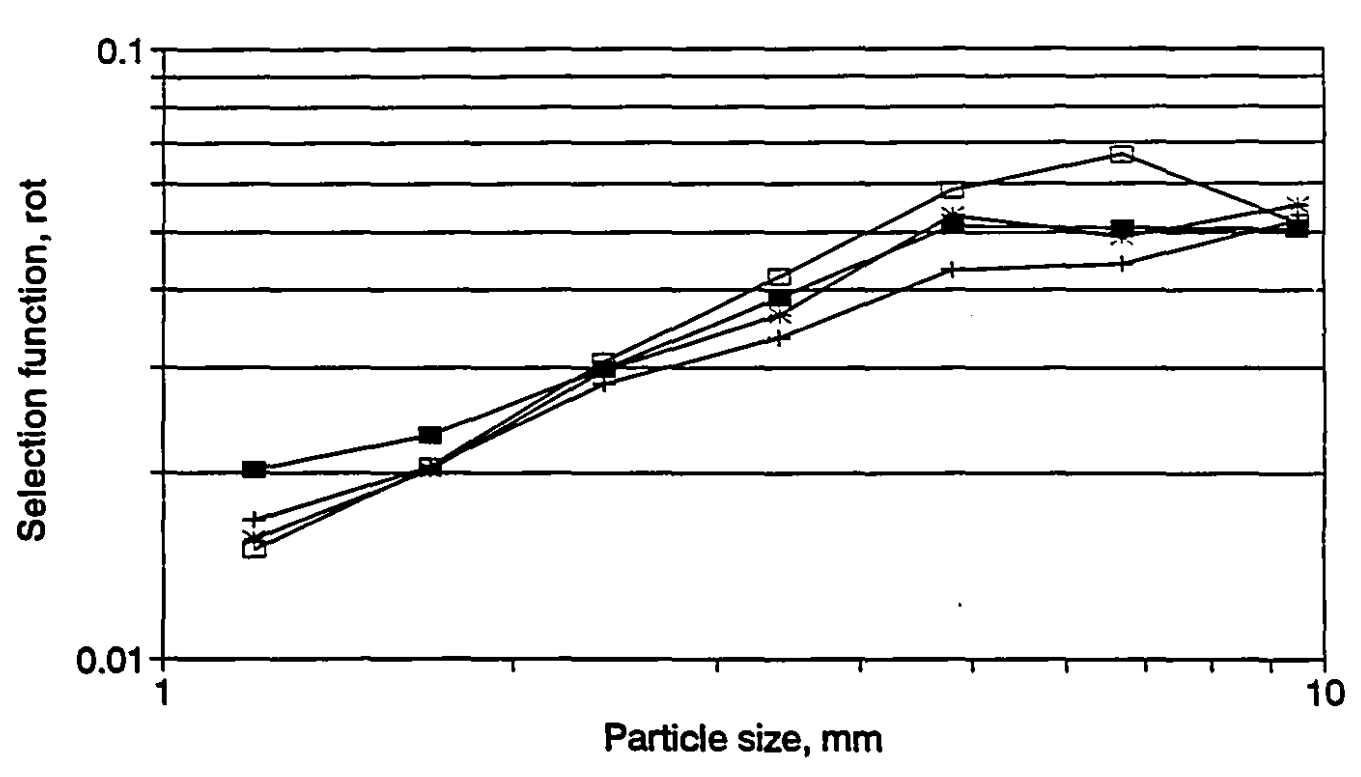
Granite



-- 1st cycle -- 2nd cycle -- 3rd cycle -- 4th cycle -- 5th cycle

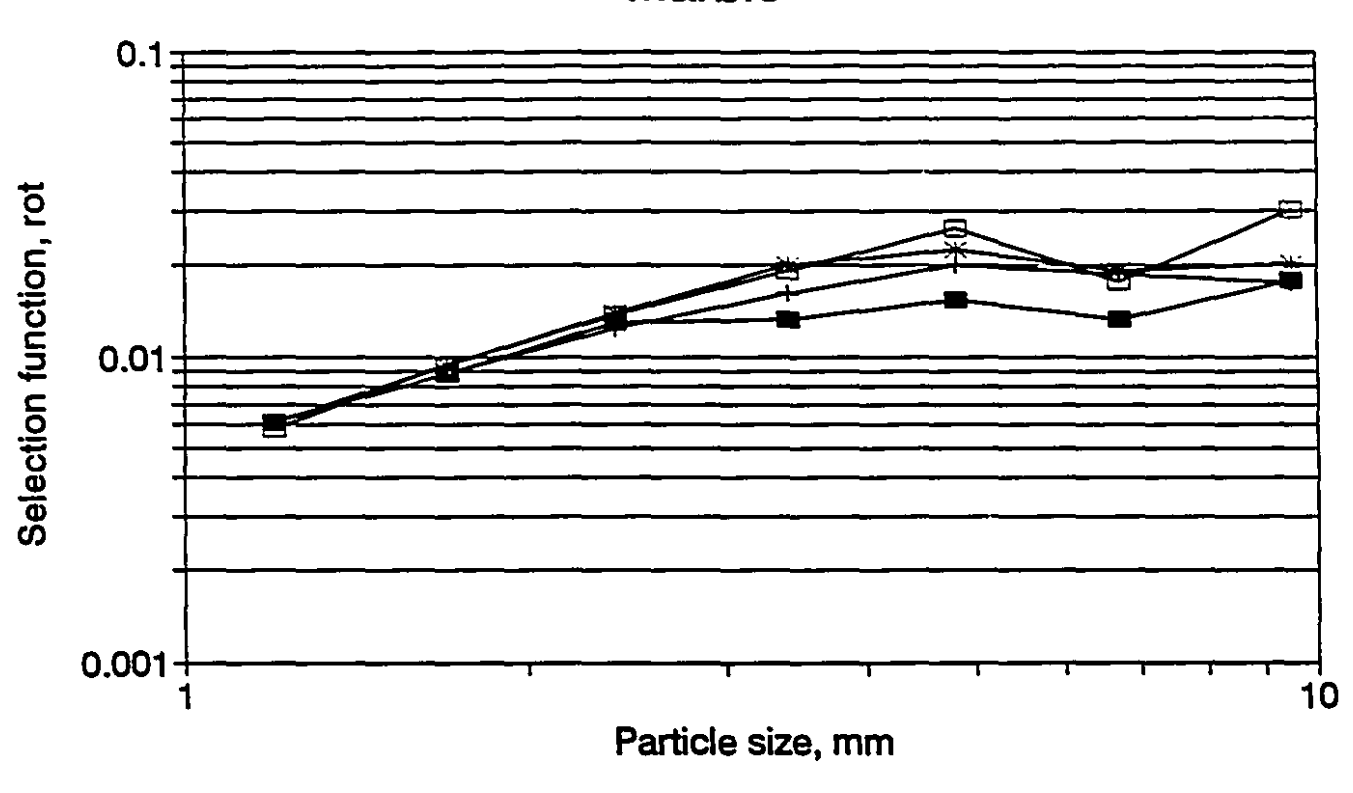
# Selection function

**Gneiss** 



1st cycle --- 2nd cycle --- 3rd cycle --- 4th cycle

## Selection function Marble



-■ 1st cycle --- 2nd cycle --- 3rd cycle --- 4th cycle